Terms and Conditions of Use of Digitised Theses from Trinity College Library Dublin

Copyright statement

All material supplied by Trinity College Library is protected by copyright (under the Copyright and Related Rights Act, 2000 as amended) and other relevant Intellectual Property Rights. By accessing and using a Digitised Thesis from Trinity College Library you acknowledge that all Intellectual Property Rights in any Works supplied are the sole and exclusive property of the copyright and/or other IPR holder. Specific copyright holders may not be explicitly identified. Use of materials from other sources within a thesis should not be construed as a claim over them.

A non-exclusive, non-transferable licence is hereby granted to those using or reproducing, in whole or in part, the material for valid purposes, providing the copyright owners are acknowledged using the normal conventions. Where specific permission to use material is required, this is identified and such permission must be sought from the copyright holder or agency cited.

Liability statement

By using a Digitised Thesis, I accept that Trinity College Dublin bears no legal responsibility for the accuracy, legality or comprehensiveness of materials contained within the thesis, and that Trinity College Dublin accepts no liability for indirect, consequential, or incidental, damages or losses arising from use of the thesis for whatever reason. Information located in a thesis may be subject to specific use constraints, details of which may not be explicitly described. It is the responsibility of potential and actual users to be aware of such constraints and to abide by them. By making use of material from a digitised thesis, you accept these copyright and disclaimer provisions. Where it is brought to the attention of Trinity College Library that there may be a breach of copyright or other restraint, it is the policy to withdraw or take down access to a thesis while the issue is being resolved.

Access Agreement

By using a Digitised Thesis from Trinity College Library you are bound by the following Terms & Conditions. Please read them carefully.

I have read and I understand the following statement: All material supplied via a Digitised Thesis from Trinity College Library is protected by copyright and other intellectual property rights, and duplication or sale of all or part of any of a thesis is not permitted, except that material may be duplicated by you for your research use or for educational purposes in electronic or print form providing the copyright owners are acknowledged using the normal conventions. You must obtain permission for any other use. Electronic or print copies may not be offered, whether for sale or otherwise to anyone. This copy has been supplied on the understanding that it is copyright material and that no quotation from the thesis may be published without proper acknowledgement.

Stress Concentrations in Bone Cement:

A Critical Distance Approach

David Hoey, B.A., B.A.I.

A thesis submitted to the University of Dublin in partial fulfilment of the requirements for the degree of

Doctor in Philosophy

October 2008

Supervisor

Prof. David Taylor

External Examiner

Prof. John F. Orr

Internal Examiner

Dr. Kevin O'Kelly

Declaration

I declare that I am the sole author of this thesis and that the work presented in it, unless otherwise referenced, is entirely my own. I also declare that the work has not been submitted, in whole or in part, to any other University as an exercise for a degree or other qualification.

I agree that the library of Trinity College Dublin may lend or copy this thesis upon request.

David Hoey

October 2008

Abstract

Bone cement is a biomaterial which is used in the fixation of orthopaedic implants. Despite its extensive use it is regarded as the 'weak link' in cemented arthroplasties, fatigue failure of the cement mantle being a major cause of aseptic loosening, leading to revision. The cement mantle contains stress concentrations in the form of the metallic stem, protruding bone and from defects, including porosity (trapped air/monomer) and casting defects (incomplete filling, laminations), all of which have been shown to initiate fatigue failure *in vivo*. The aim of this thesis was to investigate the role of these stress concentrations in the fatigue strength of bone cement.

A series of experimental tests and computational models were designed. Various defects (notches, holes, hemispheres) were introduced into uniaxial samples, which also contained naturally occurring porosity. These types of stress concentration would be similar to casting defects and/or protruding bone in the cement mantle. It was demonstrated that these defects had a significant effect on the fatigue strength of the material, particularly when their stress concentration factor (K_t) was greater than approximately 2.4. Stress concentrations in the form of the stem were also investigated in a more realistic experimental model and were found to be the major source of fatigue crack initiation in the cement mantle. The effect of naturally occurring porosity was investigated in plain uniaxial samples. Porosity in the form of large pores and pores in close proximity were found to be the main contributors to failure in these specimens. Also the level of porosity plays a major role in failure, as an increased level of porosity increases the probability of getting a large pore or cluster of pores.

Despite the damaging effects of porosity it was demonstrated that once bone cement contains a stress concentration with a K_t>2.4 i.e. more damaging than porosity, the porosity did not influence fatigue failure in any form. This finding puts forward a

possible explanation for why removing porosity from the cement mantle is not resulting in an increased fatigue life in cemented implants, as high stress concentrations do arise *in vivo* in the form of the stem. Given the negligible damaging effects of porosity, it is proposed that porosity should not be removed from the cement mantle. This would reintroduce the beneficial effects of porosity (i.e. improved drug dispersion, bone ingrowth and as a method of blunting cracks) which are lost when modern mixing techniques are used.

All data collected in this study were analysed using the Theory of Critical Distances (TCD). The TCD involves using a characteristic distance and stress to describe fatigue failure in a material. The TCD was found to predict the effect of all introduced stress concentrations in the form of notches and design features such as the stem with good accuracy. The TCD was also developed to predict the role of pore size and pore clustering and was incorporated into a virtual model of porous bone cement allowing the scatter associated with porous specimens to be predicted. This is the first time the TCD has been used to predict fatigue failure in any polymer and as such should prove to be a simple yet powerful tool in the future design and development of cemented artificial joints.

Acknowledgements

I would like to start by acknowledging my supervisor David Taylor to which I am eternally grateful. Not only did he give me the opportunity of this PhD, he supervised my work with patience, brilliance and sense of humour and to top it off, he paid for it. I would also like to thank David for introducing me to everything Italian and of course the world of mai thai's. Thank you David.

I would also like to thank the man who knows how everything works, Peter O'Reilly for all his help, which was extensive. Nothing would have been done without him showing me first. Thank you Peter. Thank you also to the students who have helped me over the past three years: Mick Penston, Didier Carette and Daniel Biro. Thank you also to all the technicians in the workshop for putting up with endless requests for specimens and moulds. Thank you J.J., Sean, Gabriel, Mick, Tom and Danny. I would also like to thank Joan Gillen and Sheena Brown for helping me my whenever it was needed.

Much appreciation is given to my fellow postgrads for their support and banter over the past three years: in particular Emmet (bad jokes), Paul (coffee), Peter (pro-ev), Darren (tea), Saeid (stories) and Daniella (cake). Thank you also to all my friends for their support and encouragement.

A very special thank you goes to my parents, Jim and Marie. Their endless support and encouragement has helped me get to where I am now. They are ultimately the people that made this happen. Thank you very much. Thank you also to my brother Brian and two sisters Cliodhna and Marie-Claire. Thank you to Tony and Cathy for their support and bags of food over the past seven dark years of student life. Last but not least, a sincere thank you to Lisa. Her willingness to listen to me going on about bone cement and the TCD was simple astonishing. I'm sure this thesis could have been better written by her. Thank you for everything.

Publications

Work from this thesis has been published as follows:

Hoey, D., Taylor, D., "Quantitative analysis of the effect of porosity on the fatigue strength of bone cement" Acta Biomaterialia, doi:10.1016/j.actbio.2008.08.024.

Hoey, D., Taylor, D., "Fatigue in porous PMMA: the effect of stress concentrations" International journal of fatigue, **30 (6):** 989-995.

Hoey, D., Taylor, D., "Comparison of the fatigue behaviour of two different forms of PMMA" Fatigue and Fracture of Engineering Materials and Structures, In Review.

Hoey, D., Taylor, D., "Study findings show potential for healthcare improvements" Engineers Journal, **62 (6):** 354-356.
Reprinted in: BEAI Spectrum: Biomedical and Clinical Engineering, 19-20, Autumn 2008: **ISSN 2009-0714**,

Work from this thesis has been presented at the following national and international conferences:

Hoey, D., O'Reilly, P., Taylor, D., "Fatigue in PMMA: the effect of notches and pores predicted using the TCD" In: *Proceedings of European Conference of Fracture,* Brno 2008

Hoey, D., Carette, D., O'Reilly, P., Taylor, D., "The role of stress concentrations in the bone cement mantle" In: *Proceedings of the ASME Bioengineering Division 2008 Summer Bioengineering Conference*, Florida 2008.

Hoey, D., Taylor, D., "The role of stress concentrations in the fatigue strength of a porous bone cement mantle" 2008 Engineers Ireland Biomedical Research Medal, Dublin 2008.

Hoey, D., O'Reilly, P., Taylor, D., "Fatigue behaviour of PMMA vs PMMA based bone cement" In: *Proceedings of the 14th Annual Conference of the section of Bioengineering of the Royal Academy of Medicine in Ireland*, Sligo 2008.

Hoey, D., Taylor, D., "The role of porosity in the fatigue strength of bone cement: the importance of pore size and pore distribution" In: *Proceedings of the Second International Conference on the Mechanics of Biomaterials and Tissues.* Hawaii, 2007.

Hoey, D., Taylor, D., "Using the Theory of Critical Distances with FEA to predict Fatigue Failure in Bone Cement" In: *Proceedings of the European Society of Biomechanics Workshop,* Dublin 2007

Hoey, D., "The role of stress concentrations in the fatigue strength of porous PMMA" In: *Proceedings of 10th annual Sir Bernard Crossland Symposium,* Galway 2007.

Hoey, D., O'Reilly, P., Taylor, D., "The role of defects in the fatigue strength of bone cement" In: *Proceedings of the 13th Annual Conference of the section of Bioengineering of the Royal Academy of Medicine in Ireland*, Fermanagh 2007.

Hoey, D., O'Reilly, P., Taylor, D., "Predicting fatigue failure in bone cement" In: *Proceedings of the 12th Annual Conference of the section of Bioengineering of the Royal Academy of Medicine in Ireland*, Galway 2006.

Taylor, D., Hoey, D., Sanz, L., O'Reilly, P., "Fracture and fatigue of bone and bone cement: The critical distance approach" In: *Proceedings of European Conference of Fracture,* Alexandroupolis 2006.

Awards

Awards and honours arising from this work are as follows:

Awarded 1st prize in the PhD Student Poster competition at the American Society of Mechanical Engineers (ASME) Bioengineering Division Summer Conference, Marco Island, Florida (2008).

Awarded the Engineers Ireland Biomedical Research Medal (2008) for making a significant contribution to the field of biomedical engineering research in Ireland.

Invited to write article for Engineers Ireland Journal (2008)
Hoey, D., Taylor, D., "Study findings show potential for healthcare improvements" Engineers Journal, ***62 (6):*** *354-356.*
Reprinted in: BEAI Spectrum: Biomedical and Clinical Engineering, 19-20, Autumn 2008: **ISSN 2009-0714**,

Awarded 1st place at the Sir Bernard Crossland Symposium (2007) for demonstrating excellence in research in the mechanical engineering field in Ireland.

"A theory is something nobody believes, except the person who made it. An experiment is something everybody believes, except the person who made it."

Albert Einstein

Contents

Nomenclature

2-D	2-Dimensional
3-D	3-Dimensional
a	Crack length
DBC	Distance between centres
DBS	Distance between surfaces
D	Notch depth
E	Young's Modulus
F	Notch geometry correction factor
Hz	Hertz
K_t	Stress concentration factor
K_c	Fracture toughness
ΔK_{th}	Stress intensity threshold
L	Characteristic length
Log	Logarithm to the base 10
m	Metre
cm	Centimetre ($x10^{-2}$)
mm	Millimetre ($x10^{-3}$)
µm	Micrometre/micron ($x10^{-6}$)
nm	Nanometre ($x10^{-9}$)
cm^2	Centimetres squared
mm^2	Millimetres squared
N_f	Number of cycles to failure
NS	Not significant
N	Newton
kN	Kilonewton
N.m.	Newton metre

P	Probability
Pa	Pascal
MPa	Megapascal ($x10^6$)
GPa	Gigapascal ($x10^9$)
R	Radius
r_c	Critical distance
^oC	Degrees Celsius

σ	Stress (MPa)
σ_0	Fracture strength of plain unnotched specimen
σ_{ts}	Tensile Strength
σ_y	Yield Strength
$\Delta\sigma_u$	Fatigue limit for defect free specimen
$\Delta\sigma_0$	Fatigue limit for plain unnotched specimen
$\Delta\sigma_{0n}$	Fatigue limit for notched specimen
∞	Infinity
π	Pi constant
Ø	Diameter

List of Figures

List of Tables

Chapter 1

Introduction

1.1. Introduction

Bone cement is a biomaterial which was first introduced into orthopaedics during the 1960's through the pioneering efforts of Charnley (Charnley 1960). Its purpose was to create a mechanical bond between an artificial implant and the surrounding tissue, smoothly transferring the load from one to the other. Bone cement achieves this bond by filling the gap between the prosthesis and the bone and interlocks the two through interdigitation. It was first used in the fixation of hip implants but is now routinely used in the fixation of a range of other artificial joints such as the knee, elbow, shoulder, wrist and finger. It has also found a use in the repair of pathological fractures, vertebrae compression fractures and in the repair of bone defects. Bone cement has been a great success at fulfilling these tasks and is still the sole material used in the fixation of artificial implants (Lewis 1997).

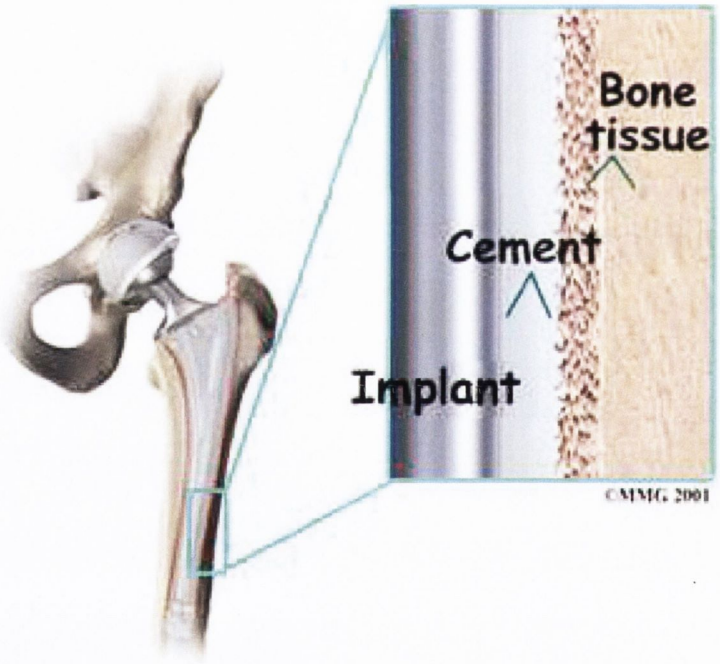

Figure 1.1: Illustration of cemented hip replacement (www.jointreplacement.com 2005).

Orthopaedic implants can also be fixated without cement by so-called 'cementless fixation'. This fixation technique relies on bone ingrowth into the surface of the implant. This type of fixation is more common with younger patients, as successful

bone ingrowth is more likely. However, given that the majority of patients that require joint replacements tend to be elderly, the cemented replacement is generally preferred, with recent studies showing 88% of hip replacements being secured through cementation (Karrholm 2006). These trends are represented in table 1.1. In addition, the improvements in mixing techniques and surgical practices has generally increased the survival rates of cemented implants, while no such improvements have been reported for cementless implants (Havelin 2000; Lucht 2000; Karrholm 2006).

Type of Fixation	< 50 years		50-59 years		60-75 years		> 75 years		Total	Share
Cemented	3,288	40.7%	14,545	64.5%	80,303	93.6%	52,448	98.7%	150,584	88.8%
Hybrid	1,723	21.3%	3,292	14.6%	2,810	3.3%	363	0.7%	8,188	4.8%
Uncemented	2,377	29.4%	3,254	14.4%	1,587	1.8%	75	0.1%	7,293	4.3%
Reversed Hybrid	644	8.0%	1,419	6.3%	1,024	1.2%	134	0.3%	3,221	1.9%
(missing)	48	0.6%	42	0.2%	106	0.1%	141	0.3%	337	0.2%
Total	8,080	100%	22,552	100%	85,830	100%	53,161	100%	169,623	100%

Table 1.1: Number of primary total hip replacements (THR) per type of fixation and age, (1992-2006) (Karrholm 2006).

Due to the worlds aging population and the increasing wave of individuals with degenerative joint disease, the number of joint replacements being performed is increasing rapidly. This trend is reflected in figure 1.2 (left) where the number of total hip replacements (THR) in Sweden has been increasing progressively over the past 30 years. Another trend is reflected in figure 1.2 (right) where it is clear that the average age of the patient is gradually decreasing. This corresponds to a younger, more active patient, which means higher stressed joints. Despite the continued improvement in the lifetimes of artificial joint replacements, the increasing number of replacements being conducted means there are still an increasing number of revisions. The US in 2003 performed 36,000 revisions at a cost of $1.6 billion (Burns 2006). This figure is set to rise due to the trends of an aging population and younger, more active patients. Therefore, for both medical and economic reasons, a deeper understanding of the failure process of cemented arthroplasties is needed, with an aim to reduce the incidence of revision.

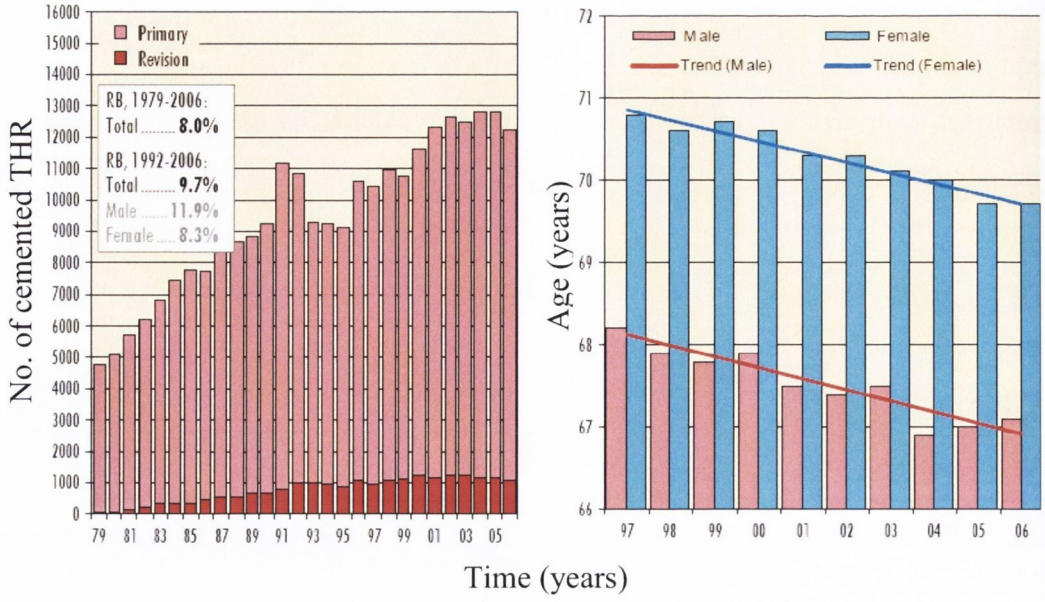

Figure 1.2: Number of total hip replacements (THR) with cemented implants from 1979-2006 (left). The average age of a patient over the last ten years (right) (Karrholm 2006).

1.2. Fatigue failure of bone cement

Despite the great success of bone cement, it is not without its drawbacks and it has become known as the 'weak link' in cemented arthroplasties (Jasty 1991). The loading pattern of the cement mantle *in vivo* is cyclic in nature and so it is not surprising that fatigue failure of the bone cement, leading to implant/cement/tissue interface failure and eventual complete failure of the cement mantle, has been proposed as the primary mechanism of aseptic loosening (Topoleski 1990; Jasty 1991; Culleton 1993), which is in turn the primary cause of revision surgery (Karrholm 2006).

The magnitude of stresses predicted in a total hip arthroplasty (THA) are small in comparison to the fatigue strength of bone cement (Harrigan 1992), however failure still occurs. Therefore it is evident that the role of defects and/or stress concentrations in the cement mantle is a key area of concern. Bone cement is based on a brittle polymer polymethylmethacrylate (PMMA) and as a consequence its strength can be greatly affected by defects or stress concentrations found within the

mantle. Bone cement is mixed in disposable apparatus during surgery and, as a result, it frequently contains defects which can be conveniently classified as: (i) porosity and; (ii) casting defects. Even in the absence of defects, stress concentrations arise in the complex geometry of orthopaedic implants. Also agglomerations of $BaSO_4$ or ZrO_2 (radiopaque additives) and protruding trabeculae have been shown to concentrate stress in the cement mantle (Jasty 1991; Ginebra 2002).

1.2.1. Porosity

Despite the multiple forms of stress concentration in the cement mantle, porosity is by far the most common associated with failure. It has been shown from many studies that pores act as fatigue crack initiation sites (Topoleski 1990; Topoleski 1993; Lewis 1997; McCormack 1999a; Dunne 2003) and so the current consensus is that porosity reduction is necessary. Much effort has been expended to try to reduce the incidence of porosity and other defects as a way of improving the fatigue strength of the material. Techniques such as the application of a vacuum or centrifugation have been developed, and a positive pressure can help to prevent incomplete filling. On the other hand it has been suggested that the presence of pores could have a beneficial effect. Topoleski suggested that pores may have the effect of 'blunting' a propagating crack (Topoleski 1993), thereby increasing the life of the arthroplasty. This line of thought has originated from publications stating that there is no increase in the clinical life of a cemented arthroplasty when these new mixing techniques are used (Ling 1998; Hernigou 1999; Geiger 2001). In other words, a reduction in porosity does not necessarily result in increased life. These conflicting findings have added much confusion over the true role of porosity in the fatigue strength of bone cement.

1.3. The Theory of Critical Distances (TCD)

The theory of critical distances (TCD) is a collection of methods for predicting the effect of stress concentrations on both the static and fatigue behaviour of a range of materials. Each method uses a material property with units of length, the so-called

critical distance. The TCD is by no means a new theory; it was first developed in the 1950's, being applied to the problem of notch fatigue in metallic materials (Neuber 1958; Peterson 1959). Despite the TCD's initial success, it did not become widely used and was relatively forgotten. This was primarily due to its main requirement: an accurate estimation of the stresses in the material.

Over the years the TCD has been reinvented by many authors studying different materials in different fields (Whitney 1974; Kinloch 1980; Tanaka 1983; Taylor 1999). However, despite the repeated discoveries of the theory it is only in the past decade or so that the theory has begun to thrive. This is largely due to development in stress analysis software such as finite element analysis (FEA) and the increase in computing power. These new techniques can achieve an accurate estimation of stresses in real life components allowing the TCD to reach its full potential. Over the past decade, extensive research has been conducted on the TCD, applying the theory to a very wide range of materials, loading conditions and geometric features (Taylor 2000a; Susmel 2003; Susmel 2008) including engineering components of complex shape (Taylor 2005a; Taylor 2008). This extensive research has resulted in a book which was recently published on the theory (Taylor 2007).

Apart from the early work by Kinloch and Williams (Kinloch 1980) and a recent paper by Taylor *et al* (Taylor 2004a) on applying the TCD to predict static failure in polymers, little has been done on this class of material. Indeed, to date the TCD has never been applied to predict fatigue failure in any polymer. Ultimately, the next step in the development of this theory would involve applying the TCD to predict fatigue failure in polymers and given the problem of fatigue in bone cement, to use the TCD to predict fatigue failure in this material.

1.4. Open questions

It has been repeatedly proposed that fatigue failure of the cement mantle *in vivo* is the primary cause of aseptic loosening, leading to revision surgery. Therefore, given that the stresses predicted in the mantle are less than the fatigue strength of bone

cement it is fair to assume that stress concentrations or defects are playing a role in the failure of the mantle. Therefore the main focus of this thesis is to investigate the role of stress concentrations in the fatigue strength of PMMA based bone cement. In particular, to find answers to the following open questions:

- How damaging are stress concentrations such as casting defects and protruding bone on the fatigue strength of bone cement? Also, what is the effect of stem design on stress concentration in the cement mantle and is this a major factor in the fatigue failure of cemented implants?

- What is the true role of porosity in the fatigue strength of bone cement? Are the damaging effects of porosity simply a matter of porosity volume or do other factors such as pore size or pore distribution come into play? Also, despite the damaging effect of porosity, can porosity play a beneficial role in the fatigue life of bone cement?

- Why does a reduction in porosity, using modern mixing techniques, increase the fatigue strength of simple laboratory specimens but does not increase the fatigue strength of cemented artificial hip implants?

As important as investigating the role of stress concentrations is, it is experimentally impossible to investigate the role of all forms of stress concentration. It is therefore important to have a tool capable of predicting their role. The theory of critical distances is one such tool. Therefore the second major aim of this thesis was to develop the TCD to predict the role of stress concentrations in the fatigue strength of polymers and in particular, PMMA based bone cement. The development of this theory would provide a useful tool in the future design and development of cemented artificial joint replacements.

Chapter 2

PMMA based Bone Cement

2.1. Poly(methyl methacrylate)

Poly(methyl methacrylate) or PMMA is an acrylic plastic, which is sold under the brand names of Perspex, Lucite, Plexiglas, and Crystallite. PMMA is a tough, highly transparent material with excellent resistance to ultraviolet radiation and weathering. It can be coloured, moulded, cut, drilled, and formed. These properties make it ideal for many applications including airplane windshields, skylights, automobile taillights and outdoor signs.

Acrylic acid was first prepared in 1843. Meth acrylic acid, which is a derivative of acrylic acid, was formulated in 1865. When meth acrylic acid is reacted with methyl alcohol, it results in an ester known as methyl methacrylate (MMA). The polymerisation process to turn methyl methacrylate into poly(methyl methacrylate) was discovered by the German chemists Fittig and Paul in 1877, but it was not until 1936 that the process was used to produce sheets of acrylic safety glass commercially (www.enotes.com 2008).

Methyl methacrylate is the basic molecule, or monomer, from which poly(methyl methacrylate) is formed (see figure 2.1(a)). The chemical notation for this material is $CH_2=C(CH_3)(COOCH_3)$. It is written in this format, rather than the more common chemical notation $C_5H_8O_2$, to show the double bond (=) between the two carbon atoms is in the middle. PMMA is produced by reacting the monomer, MMA, with a catalyst under higher temperatures and pressures. During polymerisation, one leg of this double bond breaks and links up with the middle carbon atom of another methyl methacrylate molecule to start a chain. This process repeats itself until the final polymer is formed (www.enotes.com 2008)

2.2. Bone Cement

In 1936 it was discovered that mixing ground PMMA with a monomer produced a dough like substance that could be manipulated and moulded. This material became one of the earliest biomaterials. It was initially used in dentistry for the fabrication

of denture bases. It was then in 1960 that Charnley, through his connections with the dental school at the University of Manchester, saw the material's potential in orthopaedics. Charnley was the first to use it in the fixation of a femoral head prosthesis to the femoral bone (Charnley 1960). Today, bone cement is still the sole material used in the anchoring of a cemented arthroplasty (Lewis 1997). A reported 23 million doses of Simplex P type cement have been implanted over the past 40 years (www.stryker.com 2008) and this only accounts for 24% of the market. Since its first use in the 1950s the interest in bone cement and its uses has been immense. Currently there are roughly 40 different types of bone cement on the market (Kühn 2000).

2.2.1. Components

Acrylic bone cement consists of two main components, a powder component (polymethylmethacrylate, PMMA) and a liquid monomer (methyl methacrylate, MMA). The powder component consists of:

i. Pre-polymerised PMMA beads.
ii. An initiator, benzoyl peroxide, to catalyze the polymerisation process.
iii. A radiopacifying agent, usually barium sulphate ($BaSO_4$) or zirconium dioxide (ZrO_2), which allows the cement to be seen radiographically.

The liquid monomer consists of,

i. An inhibitor, hydroquinone, which prevents premature polymerisation.
ii. A promoter, N-N dimethyl-p-toluidine (DPT), to break down the catalyst on the powder and initiate free radicals.

Other additives can include an antibiotic, such as gentamicin, which is most commonly used in septic revision surgeries. Also some formulations add a colorant such as chlorophyll to act as contrast agent to aid in the removal of a cement mantle during a revision arthroplasty (Lewis 1997).

2.2.2. Preparation

Bone cement is prepared in the operating theatre during surgery. Once the two components are mixed, a self-polymerising exothermic reaction takes place. The

polymerisation of MMA to PMMA is a free radical polymerisation that can be split up into three different chemical reactions (Kjellson 2005),

i. **Initiation** - During this stage, free radicals are generated when the benzoyl peroxide undergoes cleavage of the peroxy bond. This forms two free benzoyloxy radicals (see figure 2.1(b)). These radicals add to the monomer molecule creating a monomer ended macromolecule (see figure 2.1(c)).

ii. **Propagation** - This stage involves the successive addition of monomer units to the active radicals already produced in the initiation phase (see figure 2.1(c)).

iii. **Termination** - This final stage involves the termination of the cycle of monomer addition. This occurs by mutual annihilation of two free radicals which generally happens by combination (joining together of two chains forming a paired electron bond (see figure 2.2(a)) and/or disproportionation (two radicals form chain molecules by the transferral of a hydrogen atom (see figure 2.2(b)).

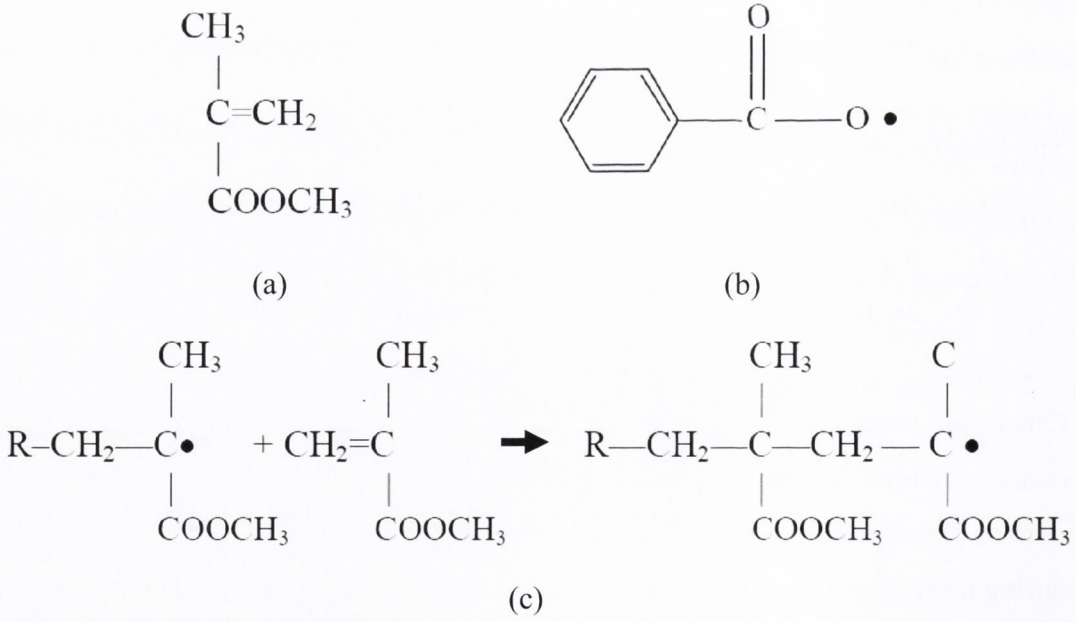

Figure 2.1: (a) The repeating unit of the monomer, MMA. (b) A benzoyloxy radical, the initiator. (c) The process of free radical addition in PMMA.

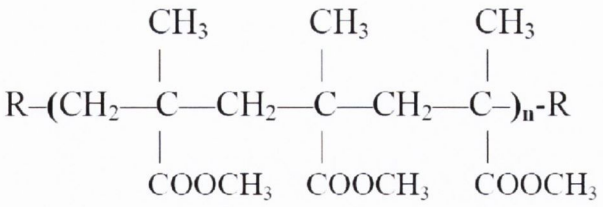

(a)

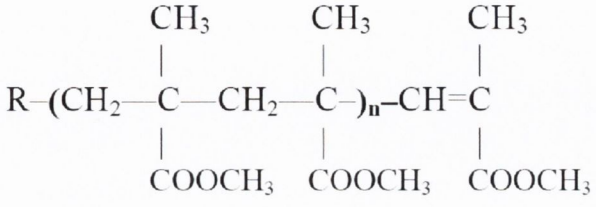

(b)

Figure 2.2: (a) A terminated macromolecule of PMMA composing of n MMA molecules, termination in this case is caused by combination. (b) A macromolecule of PMMA; propagation has been stopped by hydrogen transfer (Murphy 2001b).

On complete polymerisation, the polymer consists of a matrix of pre-polymerised beads locked inside a PMMA matrix. The curing period of PMMA can be described in three different time periods (see figure 2.3).

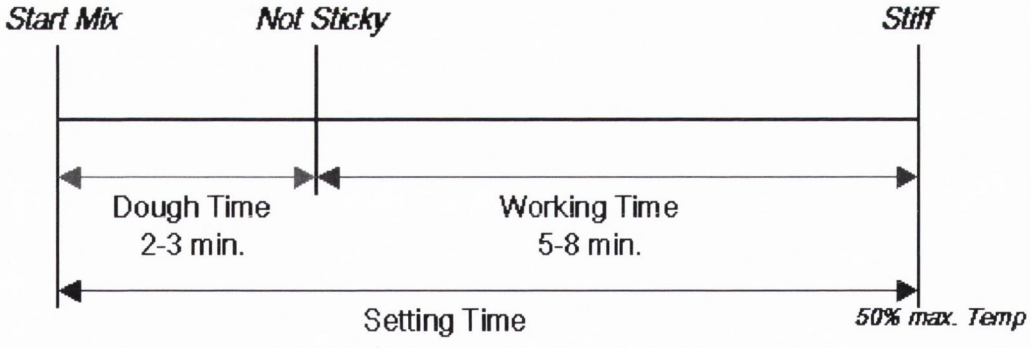

Figure 2.3: Curing Period of PMMA (www.orthoteers.co.uk 2005)

i. **Dough Time** - This begins from the start of mixing and continues until the cement mixture will not stick to an unpowdered surgical glove (~2-3min).

ii. **Working Time** - This starts from the end of dough time and continues until the mixture is too stiff to manipulate (~5-8min).

iii. **Setting Time** - This is the sum of the dough and working time periods. It is measured from the beginning of the mixture until the surface temperature of the dough mass is one half its maximum value (~8-10min).

2.3. Failure of a cemented prosthesis

Failure of a cemented prosthesis results in a re-operation or revision surgery. There are many reasons for failure *in vivo* (see table 2.1) but the number one cause of failure is aseptic loosening of the implant. The Swedish hip register reports that out of 21,519 primary hip replacements over a 27 year period 74.9% of revision surgeries were due to aseptic loosening (Karrholm 2006). Aseptic loosening can be considered as a mechanical failure of the reconstruction. Although there is some debate as to the causes of aseptic loosening, it has been frequently argued that fatigue failure of the bone cement mantle, leading to implant/cement/tissue interface failure and eventual complete failure of the cement mantle is the primary mechanism of aseptic loosening (Topoleski 1990; Jasty 1991; Lewis 1997). Other proposed mechanisms of loosening include the production of wear particles which can migrate to the bone/cement interface causing bone resorption (osteolysis) (Jacobs 2001; Oparaugo 2001).

Reason for revision	1979-2001	2002	2003	2004	2005	2006	Total	Share
Aseptic loosening	11,820	952	908	804	822	822	16,128	74.9%
Dislocation	944	123	125	168	133	140	1,633	7.6%
Deep infection	1,165	86	90	79	83	68	1,571	7.3%
Fracture	811	74	95	94	94	97	1,265	5.9%
Technical error	432	8	6	10	8	6	470	2.2%
Implant fracture	244	12	21	16	16	15	324	1.5%
Pain only	49	5	5	5	3	7	74	0.3%
Miscellaneous	38	0	1	7	5	3	54	0.3%
Total	15,503	1,260	1,251	1,183	1,164	1,158	21,519	100%

Table 2.1: Number of Revisions per Reason and Year of Revision; primary Total Hip Revisions 1979-2006 (Karrholm 2006)

The initial sign of failure in a cemented hip implant is the deterioration of the stem-cement bond. However the rate of this debonding is strongly dependant on the surface roughness of the implant, with rougher stems remaining bonded for longer periods of time. Once debonded these stems tend to have an increased wear rate. Debonding of the cement-bone interface can also occur but the likelihood of this type of interface failure has dramatically reduced due to modern bone bed preparation and surgical techniques. Debonding of the stem has numerous consequences. However, the main outcome of debonding is an increase in the stresses in the cement mantle (Verdonschot 1996). This increase in stress increases the likelihood of fatigue micro-crack nucleation from the stem/cement interface and also from defects found within the mantle. Jasty *et al* (Jasty 1991) examined 16 retrieved cement mantles and found debonding of the cement from the stem to be the most common early feature of failure. Specimens which had been in place for longer periods of time were found to have circumferential cracks in the cement, near the cement/stem interface and radial cracks extending from the stem into the cement (see figure 2.4), with some cracks extending to the cement/bone interface. Cracks were also found initiating from cavities and pores within the mantle. This multiple crack nucleation decreases the mechanical stability of the cement mantle, resulting in loosening of the hip implant.

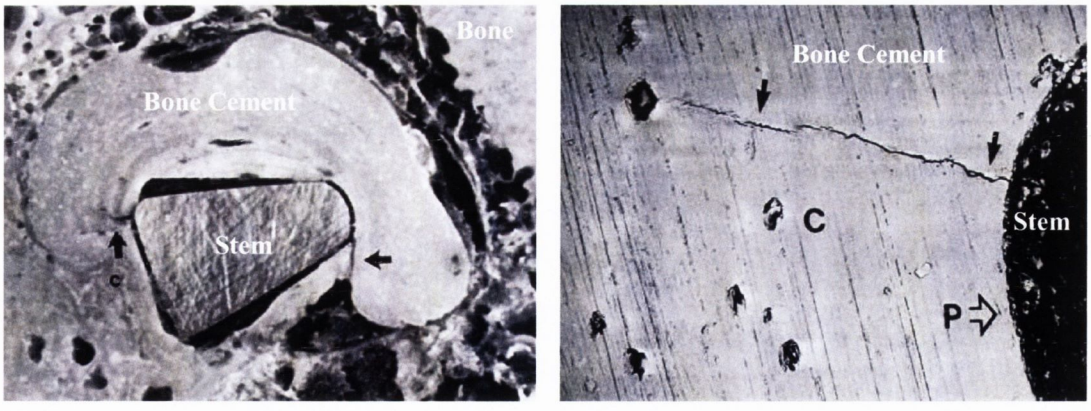

Figure 2.4: (left) Fractures through a cement mantle at 13 years. (right) SEM of incomplete fracture through the cement mantle. The prosthesis had loosened from the cement mantle and had been removed from the section (Jasty 1991). Black arrows indicate the location of cracks.

As mentioned above, another mechanism of aseptic loosening is the production of wear particles resulting in osteolysis. In a cemented hip replacement, the two surfaces most common to wear are the metallic surface of the implant and ultra high molecular weight polyethlene (UHMWPE) surface of the acetabular component. The wear debris volume consists of approximately 80% PE particles. The remaining debris consists of bone cement particles, Co and Ti alloys particles, silicates, stainless steel, and bone. These particles can gain access to the articulating surfaces accelerating the PE wear through third body mechanisms (Jacobs 2001). Prosthetic wear is a significant factor influencing osteolysis with clinical evidence relating wear rate to the degree of bone resorption (Oparaugo 2001).

Stresses within the cement in the *in vivo* loading situation have been predicted to be low, one third of the fatigue strength of bone cement (Prendergast 1989; Harrigan 1992). Nonetheless failure still occurs. A possible explanation for this may be due to the presence of defects or stress concentrations found within the mantle. As mentioned previously, the stem initially becomes debonded, resulting in an increase in the stresses in the cement (Verdonschot 1996). This increase in stress results in multiple fatigue crack formation from stress concentrations in the cement, such as defects and the corners of the stem. As time progresses these cracks propagate and eventually form through-mantle cracks (Topoleski 1990; Jasty 1991) linking the stem/cement/bone interfaces, decreasing the mechanical stability of the mantle. Simultaneously, wear particles generated at the implant/acetabulum interface can freely migrate along the debonded cement/stem interface. The generation of through mantle cracks gives these particles a transportation network to reach the bone/cement interface initiating osteolysis. In a long-term follow-up study by Müller (Muller 1997) the number of osteolytic sites was found to correlate with cement cracks. Similarly, Maloney *et al* (Maloney 1990) examined post mortem retrieved, well-fixed femoral components and found that the area of osteolysis corresponded to either a defect in the cement mantle or an area of thin cement.

It is clear from the literature that fatigue crack nucleation and propagation from defects or stress concentrations is a major concern regarding the mechanical stability of the bone cement mantle. It is also clear that fatigue crack propagation creates a pathway for wear debris to reach the bone surface initiating osteolysis.

Therefore in order to improve the longevity of cemented artificial replacements it is necessary to understand the role that stress concentrations play in fatigue strength of bone cement.

2.4. The role of Stress Concentrations

A stress concentration is a location in a body where the stress is localised or concentrated. Geometric discontinuities cause an object to experience a local increase in the intensity of the stress field. This increase in stress can cause the object to fail at a quicker rate, particularly through fatigue. Understanding the role of stress concentrations in the fatigue strength of bone cement is the major focus of this thesis. Examples that cause stress concentration in bone cement are as follows:

2.4.1. Porosity

One of the main forms of stress concentration associated with the failure of bone cement is porosity. As bone cement is prepared *in situ* under suboptimal conditions, it tends to contain pores of various sizes. Large pores (macropores) with diameters greater than 1mm occur due to entrapment of air during the mixing process and insertion of the cement into the bone cavity. Smaller pores (micropores) with diameters less than 1mm can arise from evaporation of the monomer component (see figure 2.5). A third source of porosity arises from polymerisation shrinkage, which can lead to gap formation and clusters of pores particularly at the stem/cement interface (Gilbert 2000; Messick 2007) (see figure 2.10).

The role of porosity in the fatigue strength of bone cement is somewhat controversial. Numerous laboratory studies have demonstrated pores acting as fatigue crack initiation sites (McCormack 1999a; Cristofolini 2000; Ishihara 2000; Dunne 2003)(see figure 2.6). The findings from such studies have prompted the development of modern mixing techniques to reduce porosity, such as vacuum-mixing and mixing followed by centrifugation (see section 2.5). These techniques have been very successful in reducing porosity and have resulted in increased fatigue life in laboratory specimens (James 1992a; Dunne 2003). Other important

parameters apart from the overall level of porosity are the average size of individual pores and the distribution of pores. Ishihara *et al* (Ishihara 2000) along with Cristofolini *et al* (Cristofolini 2000) concluded that fatigue life decreases with increasing pore size, especially when the pore diameter becomes greater than 1mm. Murphy *et al* (Murphy 2000) noted that fatigue failure may initiate by cracking between two or more pores in close proximity and Jeffers *et al* (Jeffers 2005) when modelling porosity in laboratory specimens found early failure in specimens containing pores in close proximity, highlighting the importance of pore distribution. It is understandable then, that the general consensus is that porosity should be eliminated from the cement mantle.

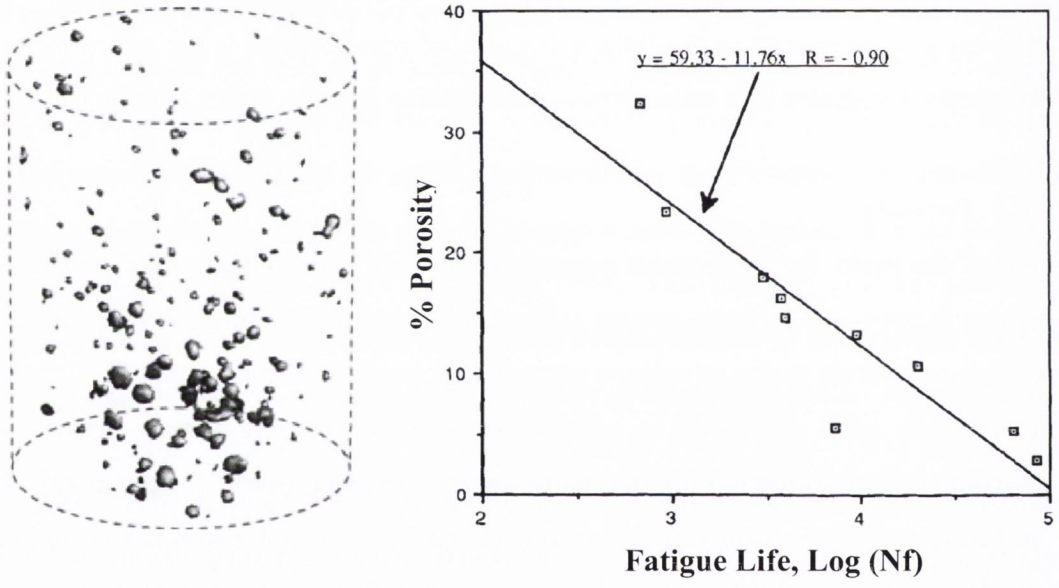

Figure 2.5: (left) Inverted μ-CT image of bone cement cylinder (6mm Ø, 12mm height), illustrating the extent of porosity, the size of pores and phenomenon of pore clustering (Cox 2006). (right) 2D porosity on fatigue fracture surfaces of laboratory specimens versus cycles to failure with least squares fit (James 1992a).

The controversy arises, however, in studies showing no increase in the lifetime of cemented arthroplasties when using these modern mixing techniques to reduce porosity (Malchau 1994; Ling 1998; Hernigou 1999; Geiger 2001). Recent studies have suggested that the lack of clinical improvement could be due to two reasons. Firstly, the cement could be failing from other more damaging stress concentrations found within the cement mantle, such as the corners of the stem, agglomerations of

radiopacifiers or protruding trabeculae (Ginebra 2002; Janssen 2005b). Secondly, a recent study has shown that porosity does not decrease in the cement mantle despite using a modern vacuum mixing technique (Messick 2007). This unexpected pore formation was attributed to polymerisation shrinkage.

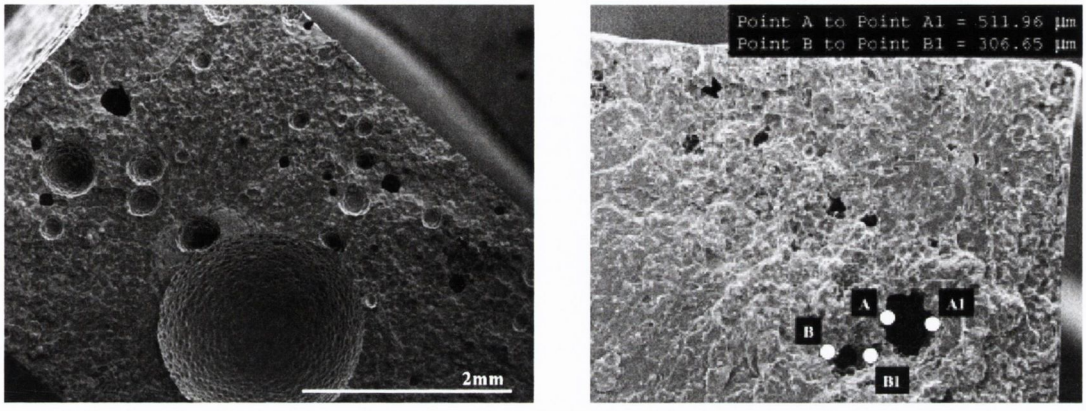

Figure 2.6: SEM images of a fracture surface of hand-mixed bone cement sample which failed from a pore, (left) (Murphy 2001b) (right) (Dunne 2003).

Despite the well documented damaging effects of porosity in laboratory specimens, porosity has also been associated with beneficial effects. Antibiotics are commonly added to bone cement for the treatment and prevention of infection in orthopaedics. The release of the antibiotics from the cement requires penetration of dissolution fluids into the polymer matrix, which requires a certain porosity (Baker 1988; van de Belt 2000). In addition, it has been proposed that porosity and pore size play a critical role in bone formation when using bone cement. Pores give the bone the opportunity to grow in, resulting in a better fixation of the prostheses (Bruens 2003; Karageorgiou 2005). Also Topoleski *et al* (Topoleski 1993) has suggested that due to the micro-crack nucleation effect of porosity, the energy at the crack tip may be dispersed forming a larger damage zone, effectively blunting the propagating crack. Due to these beneficial effects and the confusion over the true effect of porosity many surgeons are still hesitant to use modern mixing techniques.

2.4.2. Casting defects

There are three forms of stress concentration which can be considered as a casting defect. The most damaging defect arises due to incomplete filling of the bone cavity, which results in large defects of varying shape. A study by Culleton *et al*

(Culleton 1993) of a retrieved cement mantle found two casting related defects, a vertical slit (18mm long by 0.5mm wide) and a elliptical defect with a major axis of 10mm. These defects were found to initiate fatigue failure *in vivo*. A second form of casting defect arises due to premature solidification of the cement, resulting in laminations. This creates weak regions in the mantle which can result in an increased likelihood of failure. A third form of stress concentration which may be considered as a casting defect include trapped debris such as bone, blood and fat. Trapped debris behaves very similar to voids or pores in the cement but with the added stress concentration effect of an irregular shape.

2.4.3. Additives

Various additives are incorporated into the cement. Radiopacifiers are commonly added to the material to allow visualisation of the cement mantle radiographically. Numerous systematic studies have been conducted on the effect of radiopacifiers on the fatigue strength of bone cement; all concluding that the addition of a radiopacifier increases the fatigue performance of the cement (Freitag 1977; Ginebra 2002). Ginebra *et al* (Ginebra 2002) concluded that the radiopacifier $BaSO_4$ resulted in a decrease in the tensile strength of the material but also decreased the fatigue crack propagation rate. As the $BaSO_4$ particles tend to agglomerate, these form sites of stress concentration which decrease the tensile strength of the material. However, as these particles are only found in the interbead matrix, this results in preferential fatigue crack propagation through the matrix, which results in a longer crack path, decreasing the propagation rate.

Antibiotics are also added to the cement to prevent against infection, particularly during a revision surgery where the risk of infection is greater. Davies *et al* (Davies 1989) and Dunne *et al* (Dunne 2008) demonstrated that the presence of the antibiotic, gentimacin, resulted in a reduction in the mean fatigue strength of the cement.

2.4.4. Implant design

The geometry of the implant can play a major role in stress concentration *in vivo*. Several features such as overall shape (straight or anatomical), the cross-section (oval or square), the presence of a collar, the shape of the tip of the stem, the length

of the stem and whether the edges are rounded to a greater or lesser degree all contribute to stress concentration (Scheerlinck 2006).

The cross-sectional shape particularly influences the stress distribution within the cement mantle. It also influences the rotational stability of the implant and the distribution of cement within the femoral canal. Stems with a square or rectangular cross-section offer more rotational stability than an oval stem (Kedgley 2007). However, sharp edges create peak stresses in the cement, which could lead to fatigue crack initiation at the stem corners. McCormack *et al* (McCormack 1999b) and Hertzler *et al* (Hertzler 2002) both experimentally investigated the effect of the torsional loading component of the stem on the cement and found cracks initiating and propagating from the corners of the stem. Kim *et al* (Kim 2008) calculated, based on a finite-element model, that optimal rotational stability with acceptable peak stresses in the cement was obtained when the corners of the stem had a fillet radius of 2mm on an oval cross-section. Also, Janssen *et al* (Janssen 2005b), using a damage mechanics approach in a computer simulation of a cross-section of a cemented hip implant, found cracks to initiate from the corners of the stem, despite porosity also being simulated in the model, indicating that the stem is the greatest contributor to failure in the cement (see figure 2.7).

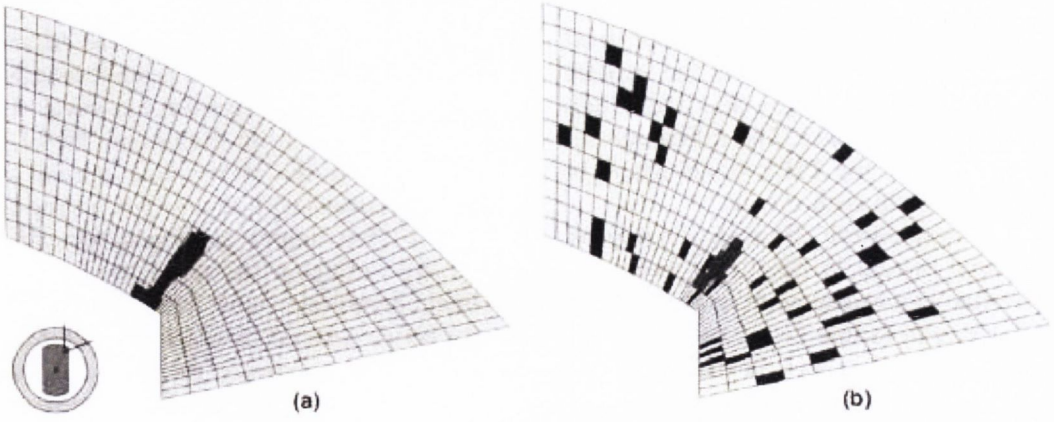

Figure 2.7: Crack in the cement mantle after two million cycles of loading in (a) the pore-free model and in (b) the transverse slice model with a porosity level of 9%. The dark gray area represents the crack in the cement; the porotic elements are coloured black (Janssen 2005b).

Several retrieval studies have also witnessed cracks emanating from the corners of the stem. Topoleski et al (Topoleski 1990), Jasty *et al* (Jasty 1991) and Cristofolini *et al* (Cristofolini 2007) all reported fatigue cracks initiating from the stem/cement interface, particularly from the corners of the stem (see figure 2.4 and 2.8). Several of these cracks were found to propagate through the mantle linking the stem/cement interface with the bone/cement interface. These findings agree strongly with the experimental and computational evidence discussed earlier and strongly indicate that the stem plays a major role in the fatigue failure of the cement mantle *in vivo*.

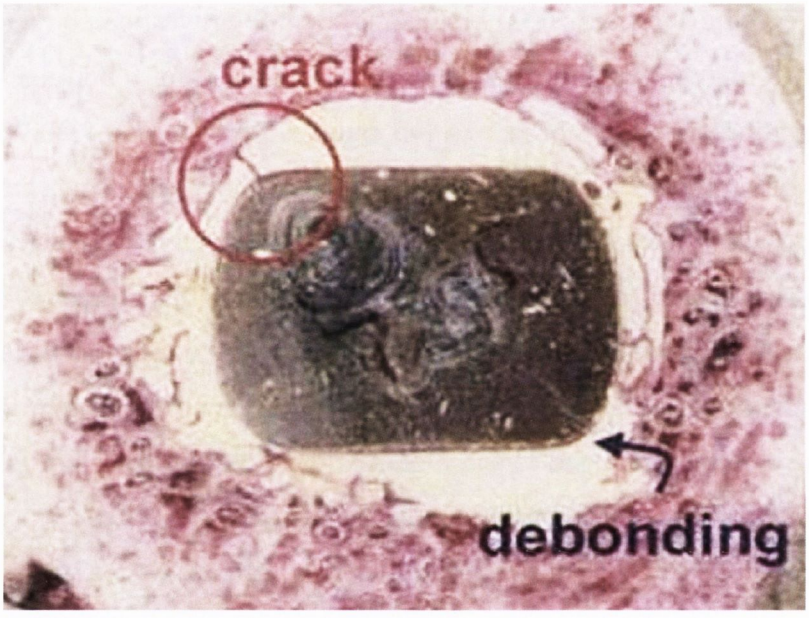

Figure 2.8: Cross sectional view of a retrieved specimen showing stem cement debonding and cracking at the corner of the stem (Breusch 2005).

2.4.5. Tissue preparation

Another form of stress concentration arises from the protrusion of bone into the cement mantle. A certain degree of interdigitation is required in order to achieve a mechanical interlock between the cement and the surrounding tissue. However this protruding bone can act as a site of stress concentration which can lead to crack initiation (Gardiner 1994; Cristofolini 2007). Examples of protruding bone can be seen in figure 2.4 and 2.8.

2.4.6. Pre-polymerised beads

Polymerised bone cement consists of pre-polymerised beads locked inside a PMMA matrix. The pre-polymerised beads act as polymerisation sites and influence the rate of the polymerisation process (Lewis 1997). Recent studies have suggested that these beads may act as a stress concentration in the body of the material, particularly at the surface of a pore, where the beads become embedded in the surface (see figure 2.6) (Murphy 2000). Recent work in this area has focused on changing the composition of bone cement by removing these beads. Lewis *et al* (Lewis 2007) compared the properties of a cement containing beads against that of a cement where the beads had been removed. No significant difference was found in the fatigue strength and an increase in the compressive strength was noted. These conclusions led the authors to suggest that the beads should be removed from future cements. However, other studies have demonstrated large beads acting as obstacles or barriers to crack growth (Bhambri 1995; Murphy 2001a; Sinnett-Jones 2005) indicating that the beads may act to improve the fatigue performance of the cement.

2.5. Improved surgical techniques

The strength of a cemented joint replacement is greatly affected by the method in which it is implanted. Over the past 60 years, extensive research has been conducted on the method of bone preparation, cement preparation and cement insertion. This has resulted in an evolution of surgical techniques and corresponding increase in the lifetime of cemented arthroplasties. Malchau and Herberts (Malchau 1993; Gardiner 1994) showed an increase of 7% in survival rates at 16 years post operation using modern surgical techniques. The improvement in techniques is summarised in table 2.2 illustrating the evolution of surgical practices from first generation through to the modern third generation techniques.

Generation	First	Second	Third
Bone bed Preparation	Rasp only / Leave cancellous bone	More aggressive rasp / Brushing Pulsative lavage	More aggressive rasp / Brushing Pulsative lavage
Mixing Technique	Hand-mixed	Hand-mixed	Vacuum mix / Centrifugation
Insertion	Manual insertion with finger packing	Cement gun with distal canal plug	Cement gun with pressure / Distal canal plug
Centralisation	None	Early distal centraliser	Proximal and distal centraliser

Table 2.2: Evolution of surgical techniques from first to third generation.

2.5.1. Bone bed preparation

Bone bed preparation is critical for the long-term survivorship of a cemented implant. The aim is to provide a clean, stable, bony bed for cement interdigitation into the remaining cancellous bone and to maintain a stable interface (Majkowski 1993). First generation techniques involved very little bone bed preparation. This had numerous consequences. Firstly, large volumes of loose cancellous bone were left within the femur. This resulted in abundant sites of stress concentration with the bone struts having a similar effect to a notch in the cement mantle. Secondly, this loose bone did not supply adequate interface strength resulting in loosening of the bone/cement interface. Thirdly, the bone bed was not cleaned which resulted in large quantities of debris such as bone, blood and fat which would then become trapped in the cement mantle, resulting in further sites of stress concentration (Majkowski 1993).

The issue of proper bone bed preparation was quickly realised and modern techniques were developed. These included aggressive rasping of the cancellous bone, removing all loose struts but leaving the dense bone nearest the cortex to enhance interdigitation. This technique decreased the number of loose struts protruding into the cement and significantly increasing the shear strength of this interface (Majkowski 1993). Cleaning of the bone bed was also introduced through a pulsative lavage which has decreased the levels of trapped debris.

2.5.2. Mixing technique

Bone cement was originally mixed by hand during surgery. This resulted in a large distribution of pores with average porosity levels ranging from 4-13% (Lewis 1997). As discussed in section 2.4.1, porosity is heavily associated with failure in bone cement. This association prompted the development of modern mixing techniques to reduce porosity with the aim of improving the longevity of cemented joint replacements. The two main techniques which emerged were mixing of the cement followed by centrifugation (Burke 1984) and mixing the cement under a vacuum (Demarest 1983).

Numerous studies have been conducted to determine the validity of these techniques at reducing the extent of porosity (Davies 1989; Linden 1989; James 1992a; Murphy 2000; Macaulay 2002; Dunne 2003). Linden and Gillquist (Linden 1989) compared the porosity level of cement prepared using different techniques and found the porosity levels to decrease when using modern techniques with mechanical mixing (see figure 2.9). Both Jasty *et al* (Jasty 1990) and Dunne *et al* (Dunne 2003) investigated the effect of centrifugation and vacuum mixing respectively and also found a decrease in the level of porosity. They also determined that the size and distribution of pores changed. It was concluded by Jasty *et al* that centrifugation reduced the mean pore size but also increased the number of pores/cm^2 in comparison to hand-mixing. Another worrying feature of centrifugation was the distribution of pores. It was concluded that pores tended to concentrate in one part of the cement. This would lead to pore clustering which has been highlighted as a potential hazard in bone cement. Dunne *et al* concluded that vacuum-mixing resulted in an increase in the mean pore size but significantly reduced the number of pores/cm^2 in comparison to hand-mixing (see table 2.3).

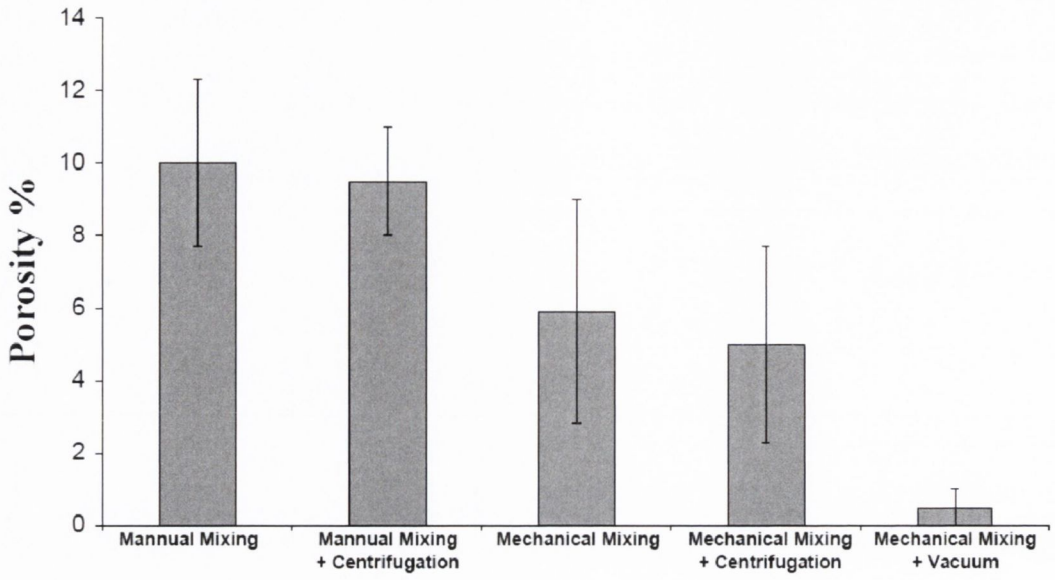

Figure 2.9: Porosity results from Linden and Guillquist (1989) showing that the introduction of modern mixing techniques results in a reduction in overall porosity levels.

Mixing system	Reduced pressure (kPa)	Pore area (mm^2)		Number of pores		Porosity (%)	
		x	σ	x	σ	x	σ
Hand Mix	Atmospheric pressure	0.4324	0.2599	5	3	2.47	1.49
DePuy Johnson & Johnson Ultramix®	−59	0.6827	0.5725	2	1	3.90	3.27
Summit Hivac Bowl®	−72	0.7651	0.3319	3	2	4.37	1.90
Summit Hivac Syringe®	−72	0.5693	0.3657	4	2	3.25	2.09
Mitab Optivac®	−86	0.5352	0.3722	2	1	3.06	2.13
Cemvac®	−92	0.6436	0.5178	2	1	3.68	3.53

Table 2.3: Summary of pore sizes and numbers, and percentage area porosities on fractured surfaces of bone cement prepared using different vacuum-mixing systems (Dunne 2003)

The introduction of modern mixing techniques has resulted in an increase in the fatigue strength of laboratory specimens. Davies and Harris (Davies 1988) investigated the fatigue life of cement prepared using three different vacuum mixing systems and also cement prepared by centrifugation. Figure 2.10 demonstrates that the modern mixing techniques resulted in an increase in the fatigue strength of the material. However regarding the vacuum-mixed cement there was no significant difference due to the severity of scatter in the results. This was attributed to the occurrence of large singular pores frequently found in the vacuum-mixed material.

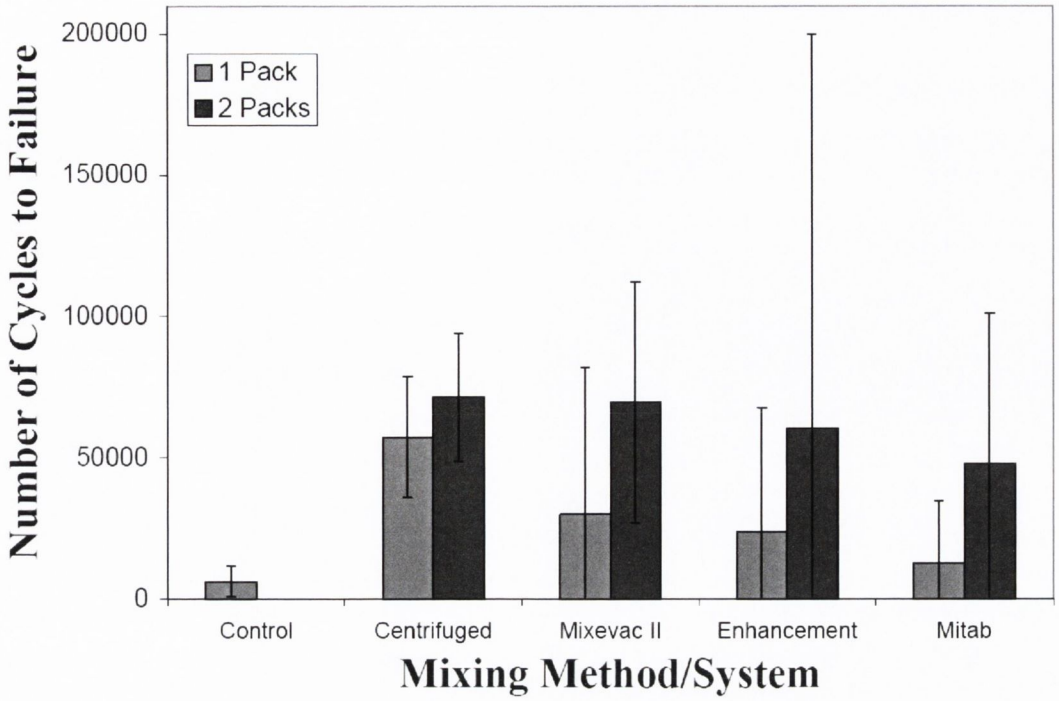

Figure 2.10: Fatigue results from Davies and Harris. Taken from Murphy (Murphy 2001b).

Despite the success of these techniques *in vitro*, there is some controversy over the success of these techniques *in vivo*. Recent studies have suggested that the porosity may not actually be decreasing *in vivo*. Messick *et al* (Messick 2007) compared the porosity levels of two cement mantles, one prepared by hand-mixing, the other by a vacuum mixing system and found no significant difference in the porosity level (see figure 2.11). Despite the pores being removed prior to insertion, further pores developed post-insertion, particularly at the stem/cement interface as a consequence of polymerisation shrinkage. The pore distribution also changed, with the evenly distributed small pores formed by hand-mixing being replaced by large singular pores close to the stem/cement interface. As this interface has been highlighted as a weak zone in the hip construct, the occurrence of pore clustering in this area should be a major concern.

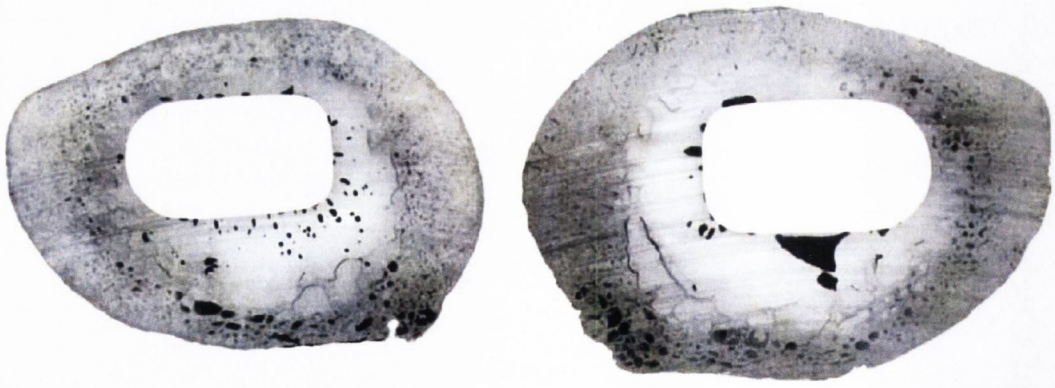

Figure 2.11: Cross sections of a cemented hip implant illustrating the porosity distribution in hand-mixing (left) and vacuum-mixed (right) cement (Messick 2007)

2.5.3. Insertion

Initially the mixed cement was inserted into the bone cavity manually and was then finger packed into place. This resulted in poor interdigitation and production of large casting defects due to incomplete filling of space. One of the first advances in insertion was the introduction of a distal plug. This allowed the cement to be pressurised on insertion and reduced the size and extent of the stem column (Heisel 2003; Dunne 2004). A cement gun was then developed which achieved a more uniform, pressurised distribution of cement through the filling of the cavity in a retrograde fashion. Various cones can be added to the tip of the cement gun to improve pressurisation during cement insertion. The introduction of the distal plug and cement gun has significantly improved interdigitation and dramatically reduced the number and size of casting defects (McCaskie 1997).

2.5.4. Centralisation

The thickness of the cement also plays a role in the integrity of the mantle. Although the ideal thickness is the subject of debate, it has been shown that stems with a 2-5mm cement mantle demonstrate the superior survival rates (Ebramzadeh 1994). The occurrence of a thin cement mantle has been associated with fast fracture (Hertzler 2002) resulting in reduced mechanical stability and an increase in osteolysis (Maloney 1990). Modern centralisers have been developed to aid the surgeon during insertion of the stem to obtain an acceptable uniform mantle thickness (Yousef 2006).

2.6. Fatigue of Bone Cement

If a component or structure is subjected to repeated stress cycles, i.e. the cement mantle in an artificial hip joint, it may fail at stresses well below the tensile strength σ_{ts}, and often below the yield strength σ_y, of the material. The processes leading to this failure are termed 'Fatigue' (Ashby 1980). The insidious feature of fatigue failure is that there is no obvious warning; a crack forms without appreciable deformation of the structure making it difficult to detect the presence of growing cracks. Fractures usually start from small nicks, scratches, or fillets that cause a localized concentration of stress.

The average person takes 1,000,000 steps in a year, hence in the hip joint, of the order of 1,000,000 fatigue cycles per year are applied to the bone cement (Ishihara 2000). Recent studies have shown a body of fractographic evidence that indicates fatigue failure and fatigue crack propagation as the primary cement failure mechanism. Culleton *et al* witnessed striations and areas of wear on a retrieved cement mantle, both of which are indicative of fatigue (Culleton 1993). Topoleski *et al* compared fracture surfaces of samples which failed *in vivo* with fracture surfaces created *in vitro*. This study revealed remarkable similarities between the *in vitro* and *in vivo* fatigue failure surfaces, further emphasising that fatigue failure is the primary failure mechanism (Topoleski 1990). All fatigue data collected pre-1987 was reviewed by Krause and Mathis (Krause 1988). Data collected post-1987 was reviewed by Lewis (Lewis 1997; Lewis 2002). However despite the volume of data collected on the fatigue behaviour of bone cement it is difficult to compare studies. This is mainly due to the differences in the testing environment, loading conditions, loading frequency, specimen shape and preparation method.

2.6.1. Testing Environment

The environment in which a polymer is tested can greatly affect the outcome of the test. When investigating the fatigue behaviour of bone cement it is clearly desirable to conduct the tests in an environment as similar to an *in vivo* environment as possible. One of the major environmental conditions associated with the body is an

increased temperature, i.e. body temperature (37°C). There are many possible methods to test at this elevated temperature. The most common are given below,

- Air
- Saline solution
- Simulated physiological environment
- Water bath
- Ringer's solution

Very few studies have been conducted on the effect of temperature on the fatigue strength of PMMA. Johnson *et al* (Johnson 1989) demonstrated an increase in the fatigue performance of bone cement at 37°C in comparison to 24°C. Out of the five methods of testing at elevated temperature, a water bath is the most common and is the method used in this study (Carter 1982; Davies 1988; James 1992a; Murphy 2000).

2.6.2. Loading conditions

There are two main modes in which an experimental test can be conducted; under load/stress control (force on the specimen remains constant and does not fall off) and under displacement/strain control (force on the specimen falls off due to creep and crack extension and thus the stress decreases as the test proceeds). Soltesz (Soltesz 1994) verified that the fatigue strength of bone cement obtained under load control was significantly weaker than that obtained under displacement control. Testing under load/stress control will draw attention to weaker cements and is therefore the preferred choice of loading condition. As bone cement is weakest in tension (Lewis 1997), a fatigue test generally incorporates tension into its loading cycle.

2.6.3. Loading frequency

Three systematic studies have been conducted on the effect of frequency on the fatigue strength of bone cement. Johnson *et al.* (Johnson 1989), Ishihara *et al* (Ishihara 2000) and Lewis *et al* (Lewis 2003) all concluded that an increase in test frequency resulted in an increase in the fatigue strength. As the test frequency is increased in the testing of a polymer, fatigue crack propagation rate decreases due to crack blunting caused by local hysteretic heating (Hertzberg 1980).

2.6.4. Specimen preparation and shape

There are two forms of specimen preparation; moulding of the cement to the desired shape, i.e. no machining; and moulding of the cement into a plate or a rod, followed by machining of the specimen to the desired shape. One systematic study has been conducted to date on the effect of specimen preparation. Paravic *et al* (Paravic 1999) found the fatigue life of the machined specimens to be weaker by a factor of three. This decrease in fatigue life was attributed to an increased level of porosity on the surface of the specimen. Also it has been shown that machined thermoplastic specimens are weaker than moulded specimens, as the machining process removes a skin layer which is different in structure to the bulk of the material (Crawford 1978).

Various specimen shapes and sizes have been used in previous research. These mainly consist of cylindrical and dog-bone shaped specimens. Dog-bone shaped specimens tend to be used in tensile loading tests, while cylindrical specimens are used in mechanical tests which involve a compressive load (Lewis 1997). No study has been conducted on the effect of specimen shape or size.

2.7. Summary

This chapter has presented a review of the literature on PMMA based bone cement. It is clear that despite the success of bone cement, fatigue failure of the cement mantle resulting in revision surgery is still a major concern. It can also be concluded that stress concentrations certainly play a role in the failure of the mantle. Despite the extent of research on this material, the role of stress concentrations in the fatigue failure of bone cement is still relatively unknown. This is reflected in the confusion over the effect of porosity. The main focus of this thesis is to investigate the role of stress concentrations in bone cement, allowing a deeper understanding of the failure process of a cemented artificial implant. Also an understanding of the role of defects could allow more efficient and effective surgical techniques to be developed.

Chapter 3

Theory of Critical Distances

3.1. History

The Theory of Critical Distances (TCD) is a name given to a group of methods which can be used to predict fracture and fatigue in materials containing stress concentrations. For a full discussion on the theory and its applications, see a recently published book on the subject (Taylor 2007). Each of the methods uses a linear elastic analysis along with a constant characteristic length which can be denoted L. There are four methods in total and the methods can be split into stress-based methods and energy based methods. The four methods are as follows:

1) Point Method (PM)
2) Line Method (LM)

} Stress-based

3) Imaginary Crack Method (ICM)
4) Finite Fracture Mechanics (FFM)

} Energy-based

3.1.1. Stress-based methods

The history of the stress-based TCD begins in the 1930's where two researchers, Neuber in Germany and Peterson in the United States, were working on the problem of predicting fatigue failure in metallic components containing notches. Neuber developed the method which is now referred to as the Line Method. This method involves averaging the elastic stresses over a critical distance from the notch root, where the critical distance corresponds to 2L (Neuber 1958). Peterson, aware of Neuber's work, developed a different approach and decided to look at the stresses at a particular point instead of averaging the stresses (Peterson 1959). The point in which he refers to is L/2 away from the notch root. This became known as the Point Method (PM). Both researchers faced two main problems; how to determine the characteristic length for a particular material and also how to determine the stresses surrounding real components?

In 1974, two researchers, Whitney and Nuismer, unaware of Neuber and Peterson developed theories identical to the PM and LM but with one important difference, they made the link to linear elastic fracture mechanics (LEFM) (see equation 3.1).

This allowed the critical distance to be expressed as a function of fracture toughness, K_c and the fracture strength of the material as measured using plain unnotched specimens, σ_0. They made this discovery while studying monotonic brittle failure of fibre composite materials (Whitney 1974).

$$L = \frac{1}{\pi}\left(\frac{K_c}{\sigma_o}\right)^2 \tag{3.1}$$

The link to fatigue was not made until 1983 but was largely ignored due to a lack of experimental verification (Tanaka 1983). This link was then rediscovered only recently by various authors and verified (Lazzarin 1997; Taylor 2000a). The critical distance for fatigue can be found in very much the same way as for static failure, replacing the static properties such as K_c and σ_o with the corresponding fatigue properties, ΔK_{th} and $\Delta\sigma_o$ (see equation 3.2).

$$L = \frac{1}{\pi}\left(\frac{\Delta K_{th}}{\Delta\sigma_o}\right)^2 \tag{3.2}$$

Given that the characteristic length could now be determined using the above equations, the only other problem faced by the pioneers of this theory was the determination of the elastic stresses in the vicinity of a defect. Elegant analytical solutions are and were available to the likes of Neuber and Peterson but these were only available for the simplest of geometries. It is only in the last few decades with the development of finite element stress analysis software (FEA) that the stresses surrounding more complex notches and real life components can now be easily determined allowing the TCD to reach its full potential.

3.1.1. Energy-based methods

The history of the energy-based TCD begins in the 1970's with Waddoups *et al* (Waddoups 1971) and El Haddad *et al* (El Haddad 1979). Both researchers developed a method in which a crack is imagined to be present at the root of the notch. This imaginary crack is then assumed to obey linear elastic fracture

mechanics (LEFM). This method is known as the Imaginary Crack Method (ICM) and an equation for the length of the imaginary crack is shown below.

$$a_0 = \frac{1}{\pi}\left(\frac{K_c}{F\sigma_0}\right)^2 \tag{3.3}$$

As can be seen by comparing equation 3.1 with 3.3, the length of the imaginary crack is practically identical to the critical distance; it only differs by the parameter F^2, where F is dependent on the notch geometry. For the case of a central, through-crack in a large plate, where F is unity, the imaginary crack is the same length as the critical distance.

Another method which is similar to the imaginary crack method is Finite Fracture Mechanics (FFM). This method was developed only recently by Taylor *et al* (Taylor 2005b). In this method failure will occur if there is sufficient energy available to allow a finite amount of crack growth where the finite amount of crack growth is a material constant. It can be shown that FFM, for a sharp crack at least, gives an identical prediction to that from the ICM and the LM. For further discussions on the comparison of the four methods, see for example (Taylor 2007).

As shown, the TCD consists of four methods which have much in common, mainly they all use a critical distance which is related to L and they use a linear elastic analysis. A formal definition of the TCD was given by Taylor (Taylor 2007).

> *'We can say that it is the name given to a group of methods, all of which use linear elastic analysis and a constant critical distance. Two of these methods – the PM and the LM – calculate a stress value and equate it to a characteristic strength for the material; the other two methods – the ICM and FFM – use energy concepts to consider the propagation of a crack of finite size, and thus use the material parameters of G_c or K_c'*

3.2. The Point Method

The Point Method (PM) is a stress based approach which was pioneered by Peterson and is the method used in this study. Despite this method being the simplest realisation of the TCD it has been shown to be the most accurate for predicting the effect of stress concentrations in the area of high cycle fatigue. The PM predicts that failure will occur if the stress at a distance L/2 from the notch root is equal to the plain strength of the material. The same applies for fatigue, replacing the stress with a stress range and the plain strength with the plain fatigue strength. This is illustrated in figure 3.1.

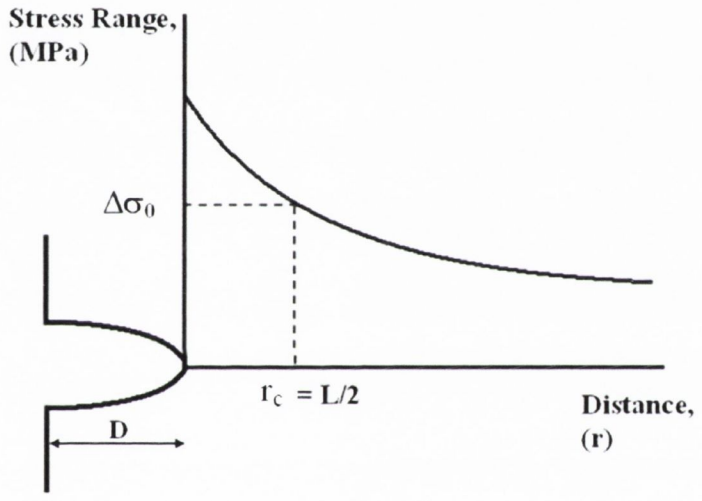

Figure 3.1: Illustration of the TCD (Point Method), using a plot of elastic stress as a function of distance from the stress-concentration feature. The fatigue strength of plain specimens $\Delta\sigma_0$ occurs at a critical distance L/2.

The PM is used to predict fatigue failure in the following way. The material is assumed to possess a characteristic material length parameter, L. The value of L can be calculated using two material properties, $\Delta\sigma_0$ and the crack-propagation threshold ΔK_{th}, using equation 3.2. $\Delta\sigma_0$ is the fatigue strength of plain (i.e. unnotched) specimens of the material, defined as the range of stress (i.e. the difference between the maximum and minimum stress in the cycle) at which failure occurs in a specified number of cycles. Once the critical parameters (L/2 and $\Delta\sigma_0$) are known, fatigue failure of a specimen containing a stress concentration feature is

estimated by examining the stresses along a path drawn normal to the underlying surface at the point of maximum stress concentration. The relevant stress parameter is the maximum principal stress. If the stress at a distance L/2 along this path is greater than the critical stress i.e. plain strength of the material, the PM predicts that a crack will propagate from that defect and the body will fail. This is illustrated in figure 3.1 for a notch of length D. A more detailed description of the application of the PM is given in chapter 5.

3.3. Polymers

The use of polymers in load bearing applications has increased dramatically in recent time. Modern production techniques have allowed stiff, strong and light polymers to be developed which are ideal for various load bearing applications. The two polymers studied in this thesis are based on the brittle polymer poly(methyl methacrylate) (PMMA). Polymers can be considered as relatively new materials and as a result there is still a lot of work to do in order to fully understand the mechanical behaviour of this class of material. For example, when searching the literature for information on the effects on stress concentrations on the fatigue behaviour of polymers, only one paper was found on the subject due to Gotham (Gotham 1973). In fact, to date, the TCD has never been applied to predict fatigue failure in any polymer. Therefore this section deals with the application of the TCD to static failure in polymers.

The TCD has been applied to brittle fracture in a number of polymers. Initially the same approach as described in section 3.2 was applied to the material, where the critical distance was determined using equation 3.1 and the critical stress was taken to be the fracture strength of the material determined from plain specimens. However this resulted in significant errors. It was discovered by Kinloch *et al* that the critical stress is actually considerably higher for polymers (Kinloch 1983). In order to determine the correct value Kinloch *et al* had to vary the critical stress in their calculations until they achieved a best fit to experimental data.

To determine the correct critical parameters, a new approach was devised by Taylor *et al* (Taylor 2004a). In this approach only two different notch geometries are required. Finite element models are created of each defect and the corresponding experimentally determined failure load is applied to the model. This allowed the maximum principal stresses to be determined in the vicinity of the defect. Stress/distance curves are then drawn along a path perpendicular to the point of maximum stress concentration, similar to that shown in figure 3.1. Plotting the two curves on the same axes, the point at which they intersect corresponds to the values of L/2 and σ_o. This is illustrated in figure 3.2 for a PMMA (Perspex) material. The curve corresponding to the plain specimen is also drawn which is represented as a straight line. As can be seen from figure 3.2 the critical point is considerably higher than that of the fracture strength, σ_u. Table 3.1 shows the values for L and σ_o for Polystyrene (PS), Polymethylmethacrylate (PMMA) and bone cement. Also shown are the values for L_u determined using equation 3.1 and the experimentally recorded σ_u. The critical stress is only slighter higher than σ_u for PS but is higher by a factor of approximately 2 for the two forms of PMMA.

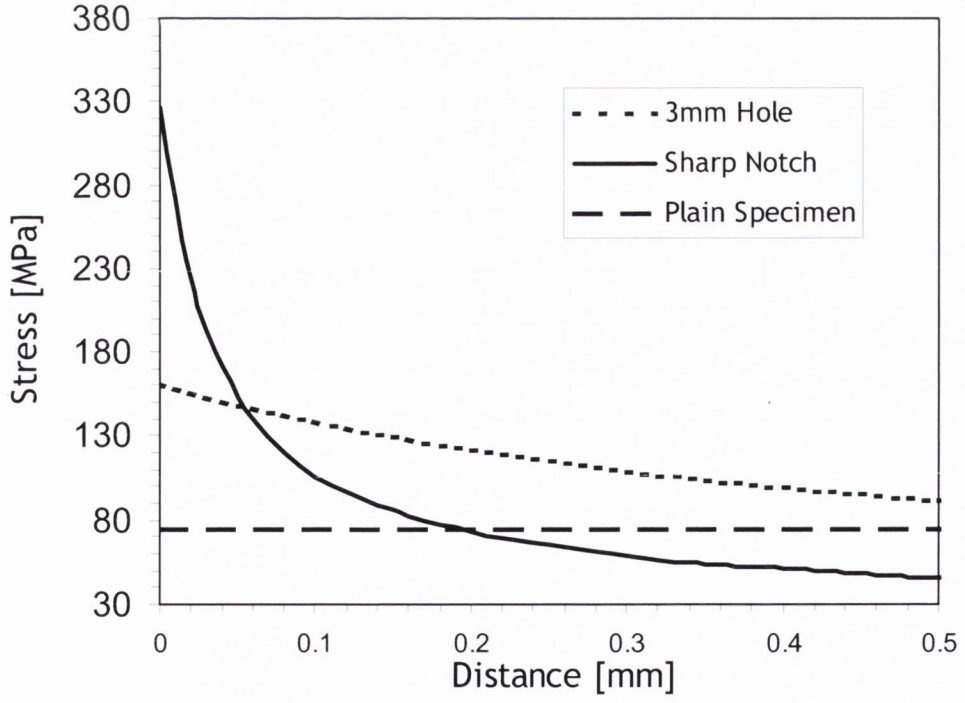

Figure 3.2: Stress-distance curves corresponding to the failure loads for three specimens. The values of L and σ_0 are found at the point of intersection of the lines for the 3mm hole and the sharp notch. Taken from Taylor *et al* (Taylor 2004a).

Using the modified approach discussed above has been shown to be very successful at predicting static failure in polymers (Kinloch 1983; Taylor 2004a). However, a value of σ_o greater than σ_u results in an interesting phenomenon. If a defect has a K_t factor less than σ_o/σ_u, then, due to the small stress gradient, the TCD will predict a fracture strength which will be greater than the plain strength of the material. As this is clearly impossible, it implies that the defect is non-damaging. These types of defect will concentrate stress but will have no effect on the strength of the material. This phenomenon is discussed in more detail in section 3.5. It is obviously very useful to be able to identify features of this type when they occur, since the designer can use them with no fear that their presence will compromise the strength of the component. This factor for static failure was found to be 2.04 for PMMA and 2.0 for bone cement.

Material	K_c (MPa(m)$^{1/2}$)	σ_u (MPa)	L_u (mm)	σ_0 (MPa)	L (mm)
PS	1.8	41.9	0.59	57.6	0.42
PMMA	2.23	71.5	0.31	146	0.107
Bone Cement	1.6	52	0.30	104	0.154

Table 3.1: Results for L and σ_0 for static failure for three different polymers. Taken from Taylor (Taylor 2007)

3.4. Fatigue

Fatigue is by far the most common cause of mechanical failure in engineering components and has been heavily linked as the main mechanism of failure in the cement mantle of artificial implants. Fatigue cracks usually initiate from stress concentrations. It is therefore essential that predictive methods are available to prevent against such failures.

As mentioned above, the TCD was pioneered by Neuber and Peterson in the 1930's while working on the problem of predicting fatigue failure in metallic components containing notches. Since then, the TCD has been used extensively to predict fatigue in metallic components (Lazzarin 1997; Taylor 2000b; Susmel 2005). The critical distance can be determined using equation 3.2 and the critical stress simply corresponds to the plain fatigue strength of the material. This approach has found to be very successful. Figure 3.3 shows data for 0.15% carbon steel taken from Frost *et al* (Frost 1974) along with predictions made using the Point method and the Line method taken from Taylor *et al* (Taylor 2007). As can be seen in figure 3.3 both predictions agree strongly with the experimental findings but it is the PM which is the most accurate. The PM was found to be the most accurate form of the TCD at predicting the effect of stress concentrations in high-cycle fatigue.

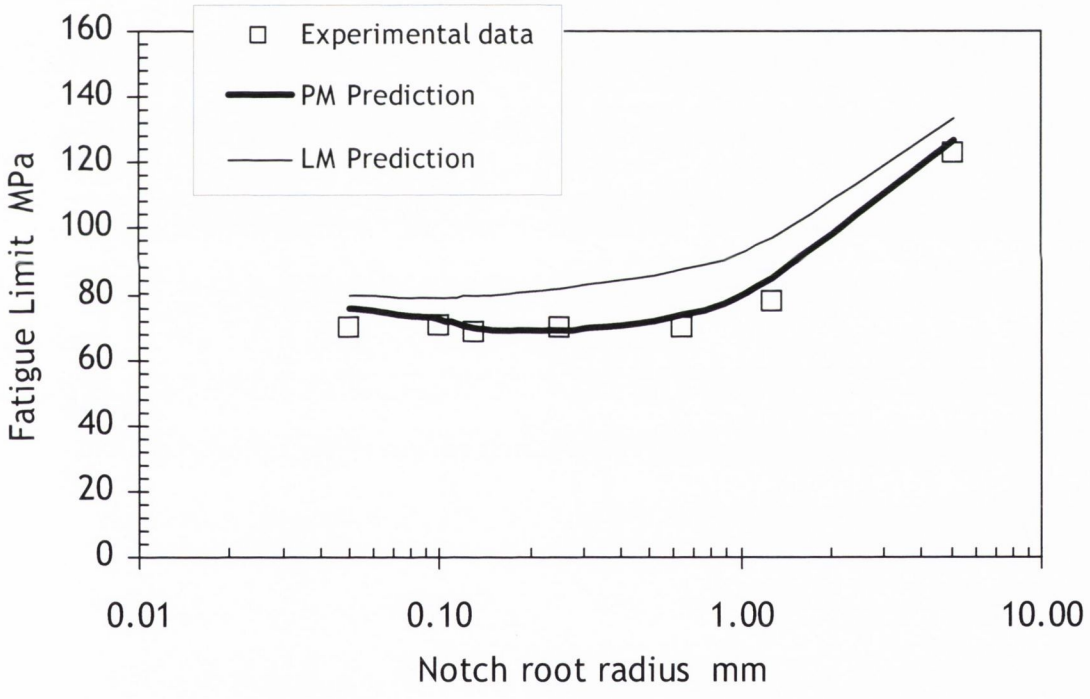

Figure 3.3: Data on the effect of notch radius on fatigue limit (Frost 1974) for carbon steel tested at R=-1; predictions using the PM and LM (Taylor 2007).

Not only is the TCD very successful at predicting the fatigue behaviour of materials, it also performs better than other more established approaches. A well known approach for the prediction of high-cycle fatigue in notched components was

developed by Smith and Miller some 30 years ago (Smith 1978). They found that the fatigue limit of low K_t notches could be predicted using the following equation:

$$\Delta\sigma_{on} = \frac{\Delta\sigma_o}{K_t} \tag{3.4}$$

Here the effect of the notch is simply to reduce the fatigue limit of the material $\Delta\sigma_o$ (measured using plain specimens) by the factor K_t. However, for high Kt notches the fatigue limit becomes constant, equal to that of a sharp crack of the same length, therefore the standard Linear Elastic Fracture Mechanics (LEFM) equation applies:

$$\Delta\sigma_{on} = \frac{\Delta K_{th}}{F\sqrt{\pi D}} \tag{3.5}$$

Here F is the geometry correction factor for the particular crack. The Smith & Miller approach is not exact; it tends to underestimate the fatigue limit in some cases, especially close to the transition of low to high K_t. Figure 3.4 shows the same data presented in figure 3.3 rearranged to represent the effect of K_t factor on the fatigue limit. Predictions based on the Smith and Miller approach are shown along with a prediction made by the TCD. As figure 3.4 shows, the overall prediction using these two equations is very accurate. However the data points fall slightly below the LEFM line implying that notches of finite size are slightly worse than cracks; this small effect is predicted by the PM.

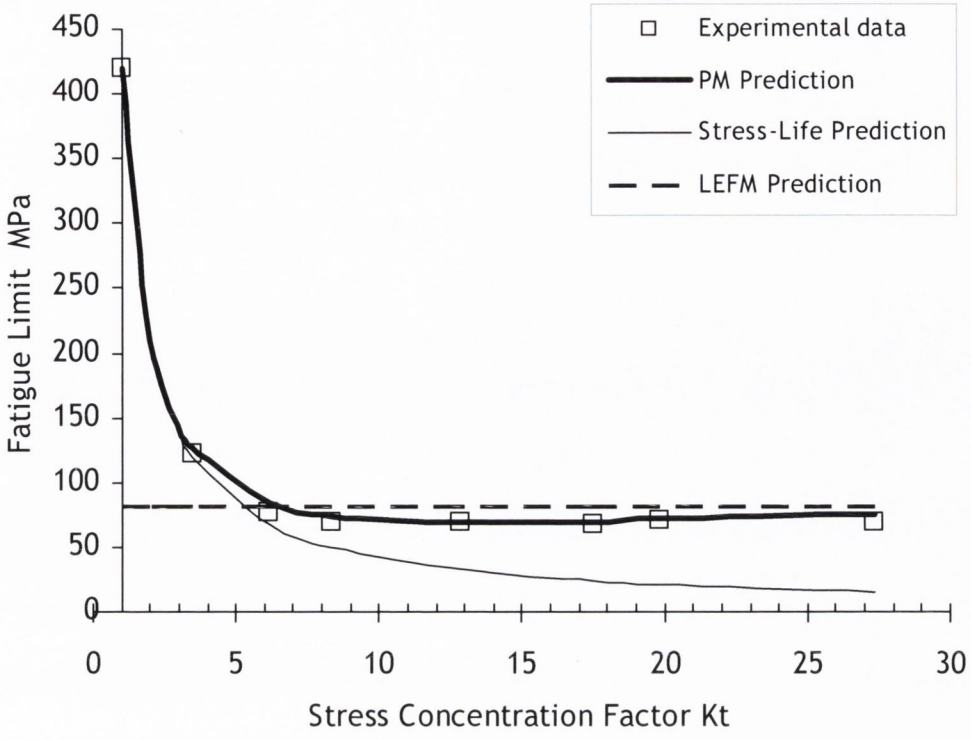

Figure 3.4: The same data and predictions as in figure 3.3 (plus the plain-specimen data) replotted using the notch K_t factor. Predictions using the PM, LEFM and stress-life methods.

3.5. Other aspects

The theory of critical distances is very much based on continuum mechanics and so assumes the material is a homogenous continuum with certain mechanical properties such as Young's modulus and Fracture toughness. Continuum mechanics theories are typified by Linear Elastic Fracture Mechanics (LEFM). The advantage that the TCD has over LEFM is that it includes a single length scale parameter which represents the existence of mechanisms at the microstructural level. It therefore can be considered as a modification of LEFM.

Although the TCD assumes the material is a homogeneous continuum, it is interesting to compare the length scale parameter L, to microstructural features. It has been shown that small values of L can be related to the grain size or some

multiple thereof. This is a result of the grain boundaries acting as barriers to crack growth. However as polymers such as PMMA do not have a microstructure, the value of L seems to correspond to the size of a craze which is the mechanism of failure associated with the material. Larger values of L can be attributed to the occurrence of non-propagating cracks and also to the existence of plasticity.

Regarding the phenomenon of σ_o being greater than σ_u,, two possible explanations have been put forward by Taylor (Taylor 2007). Firstly the experimentally recorded σ_u may not actually be the true strength of the material. This could be due to the presence of defects such as porosity or inclusions in the material which would reduce the strength of the material. Alternatively, the value of σ_o may indeed be larger than σ_u, but may actually have no real meaning. The value of σ_o is determined by assuming linear elastic behaviour. However the stress in the region close to the defect may be modified by the existence of non-elastic behaviour, such as plasticity in metals, which acts a toughening mechanism.

3.6. Summary

This chapter has presented data validating the theory of critical distances. It has been shown that the TCD can be used successfully to predict the effect of stress concentrations on the static and fatigue behaviour of a range of materials. Despite the TCDs extensive use it has never been used to predict fatigue failure in any polymer. Therefore one of the main aims of this thesis was to validate the theory in this respect.

Chapter 4

Materials and Methods

4.1. Introduction

In this chapter the design of two experimental tests are presented. The first testing procedure consisted of uniaxial fatigue testing of 'dog-bone' shaped specimens of both PMMA based bone cement and pure PMMA in the form of Perspex. Various stress concentrations in the form of notches, circular holes and hemispheres were machined into these specimens and were compared to that of plain unnotched specimens. The plain specimens contained varying levels of porosity depending on how they were prepared. The second testing procedure consisted of a 2D reconstruction of a cemented artificial implant. Different stem geometries were tested under cyclic torsional loading and the interaction between various stress concentrations in the form of the stem and porosity were determined. This testing procedure reproduces some of the features of a real cement mantle. This chapter begins by describing the materials and the material preparation methods used in this study. It then proceeds to describe the design of the specimens, moulds, and testing rigs, and then concludes by describing the experimental protocols.

4.2. Material

4.2.1. PMMA based bone cement

Various bone cements are available commercially; these differ principally in the amounts of certain additives used, such as radiopacifiers and antibiotics, which have been shown to exert a minor effect on mechanical properties (Davies 1989; Ginebra 2002). A typical, generic bone cement material was produced by mixing powdered PMMA with liquid monomer (Simplex Rapid, Kemdent, U.K.), omitting these additives. This material has a molecular weight and mechanical properties which are similar to those of commercial bone cements.

The cement used consists of a Simplex rapid liquid monomer (corresponds to BS EN ISO 1567: 1995) and a Simplex rapid powder (corresponds to ISO 1567: 2000). The cement has a powder-to-liquid ratio of 2:1.

4.2.2. Pure PMMA

Pure PMMA in the form of commercially extruded perspex was also used in this study. Perspex is commonly considered as a 'perfect' form of bone cement as it is prepared under optimal conditions. Preparation under optimal conditions results in a defect free material which has a higher molecular weight in comparison to PMMA based bone cement. Perspex also differs to bone cement in that it does not contain pre-polymerised beads of PMMA.

4.3. Material Preparation

The techniques used to mix cement have evolved throughout the years. Initially hand-mixing was the only form of mixing available to the surgeon. As porosity became known as a major defect in the cement, new mixing techniques were introduced to reduce the level of porosity. The mixing technique used to prepare the cement can greatly affect its final properties. Two mixing techniques were used during this study, hand mixing and vacuum mixing. Each specimen was prepared in a fume cupboard at a temperature of 18°C ± 2°C. An increase or decrease in temperature has the effect of increasing or decreasing the polymerisation rate.

4.3.1. Hand-mixing

Hand-mixing was carried out in a ceramic mixing bowl at atmospheric pressure. The liquid monomer was added initially. The powder was then added gradually and was continually mixed using a spatula. The cement was mixed for a period of 60 seconds at one beat per second. The spatula was moved from the centre of the mixture outwards in order to limit the amount of air entrapment during the mixing process. After the 60 seconds the mixture was left to rest for approximately 30 seconds to allow any trapped air to surface. The mixture was then poured into the mould.

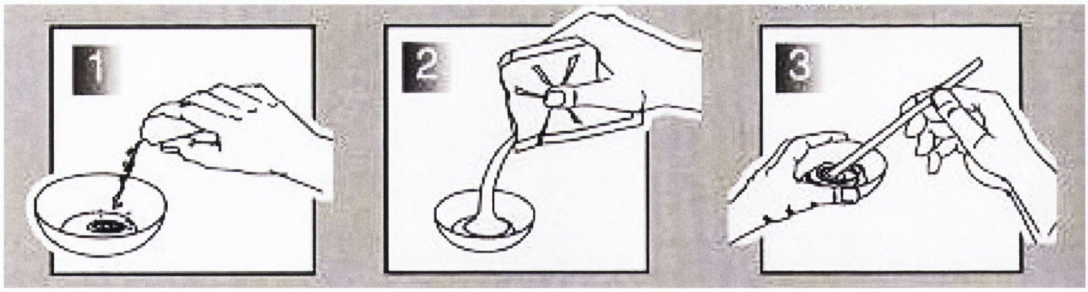

Figure 4.1: Hand-mixing schematic.

4.3.2. Vacuum-mixing

Vacuum mixing was carried out using an Ultra-mix vacuum mix system (DePuy Johnson & Johnson Ultramix). The monomer was initially added to the bowl which was quickly followed by the powder. The bowl was then sealed and a vacuum of -75kPa was applied. The container was left for 20 seconds to allow all the air to be fully removed from the chamber. The components were then mixed for 60 seconds. Once mixing was completed the mixture was allowed to rest for 30 seconds before the vacuum was released. The mixture was then poured into the mould.

Figure 4.2: Illustration of a vacuum-mixing chamber

4.4. Specimen/ Mould Design

Various factors come into play when choosing the correct specimen and mould. Such factors include:

Specimens

a) The uniaxial specimens need to be large enough so that there is room for the various stress concentrations to be incorporated.
b) The torsional specimens representing a 2D cross section through the cement mantle need to be of similar dimensions to that found *in vivo*.
c) The torsional specimens need to be easily removed from the experimental rig to allow monitoring of crack growth throughout the test.

Moulds

a) The mould needs to be simple to use and manufacture.

In this study, two specimens/moulds were used to determine the fatigue behaviour of acrylic bone cement.

4.4.1. Uniaxial fatigue

The uniaxial specimens used in this thesis were previously developed and used by Murphy, (Murphy 2001b). The specimens are rectangular in cross-section and dog-bone shaped (see figure 4.3 for dimensions). The bone shape design was used to ensure that the plain specimens would fail in the required region. In addition, the large tabs at either end are present to aid in the clamping and gripping of the specimens. The thickness of 3.5mm was used; as that is the average width of a cement mantle *in vivo*. Various defects were then introduced to this specimen to simulate a range of possible defects found in the cement mantle of a joint replacement.

The moulds used in the preparation of the uniaxial specimens were developed and used by Murphy (Murphy 2001b). The mould used consists of two outer aluminium plates, two inner polyethylene plates and one central polyethylene plate that contains the specimen profile. The three polyethylene plates make up the main part of the mould, the aluminium plates are there solely for rigidity.

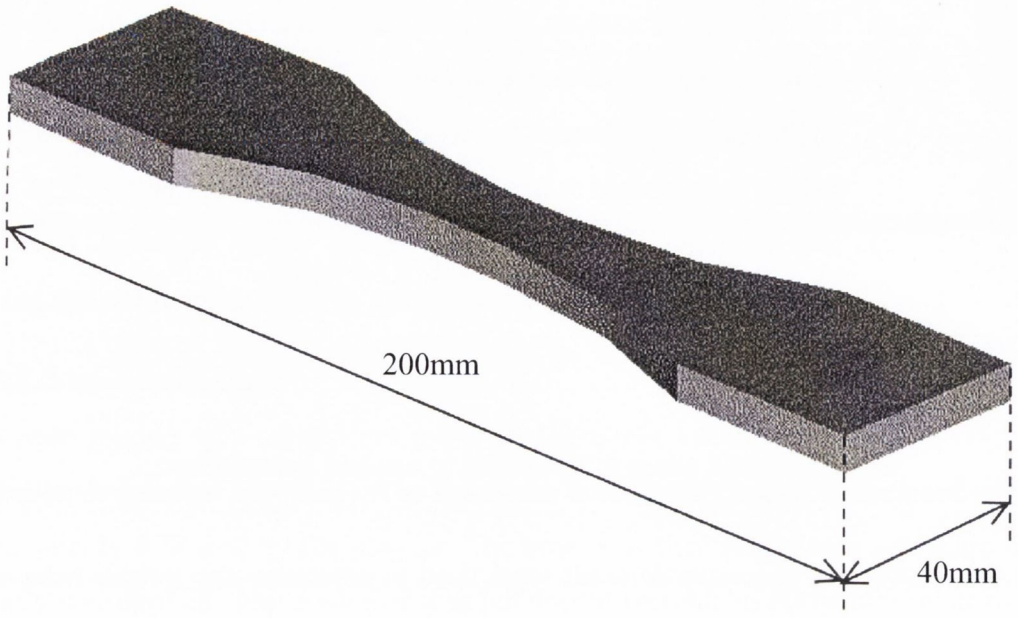

Figure 4.3: Schematic of specimen used, with a 16mm x 16mm gauge section and a thickness of 3.5mm.

4.4.2. Torsional fatigue

The torsional specimens used were purposely designed for this study. The aim was to create a 2D cross section of a cemented artificial hip implant. Each sample consisted of a stainless steel stem surrounded by hand-mixed cement which was in turn surrounded by an aluminium ring, representing the bone. Grooves were ground into the aluminium ring to ensure that debonding and subsequent slipping did not occur at this interface. The thickness of the sample was 3mm, which ensures plane strain conditions. It has been shown that plane strain conditions occur in PMMA for specimen thicknesses greater than 0.6mm (Kinloch 1983). The dimensions of the stem and bone elements were typical of *in vivo* values. Three different stem designs were manufactured to incorporate into these specimens (see figure 4.4).

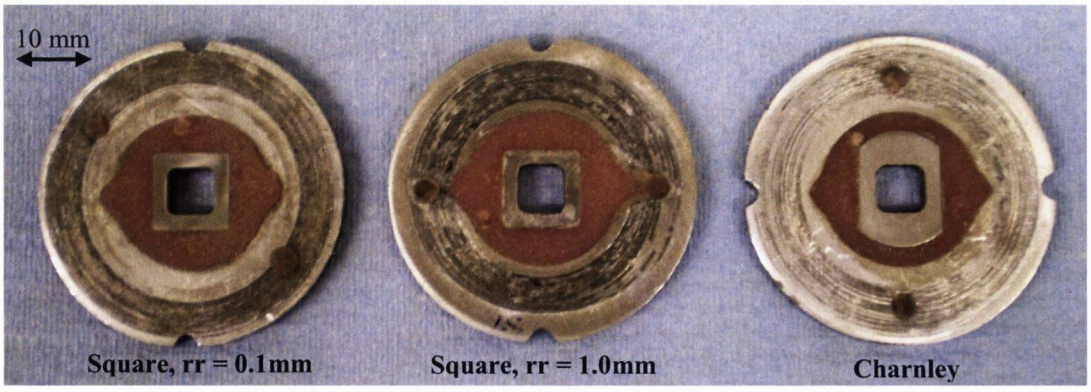

Figure 4.4: Image of each of the three stem geometries tested.

The mould used in the preparation of the torsional specimens was purposely developed for this study. The mould consists of two polyethylene plates. The lower plate was machined so that the aluminium ring and stem sit securely and centred in the mould. The upper plate is flat but contains a pressure relief hole for the overflow of cement (see figure 4.5).

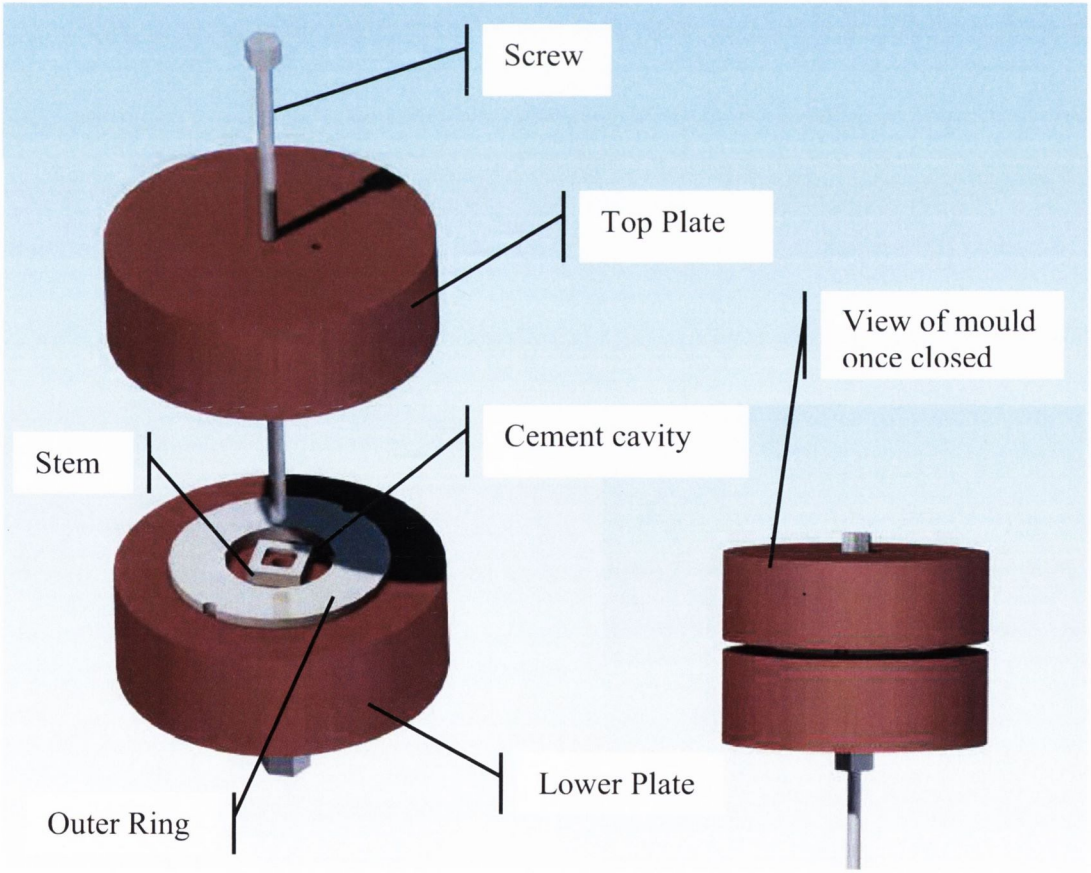

Figure 4.5: Schematic of specimen and mould developed for torsional fatigue testing.

4.4.3. Heated torsional fatigue

As polymerisation shrinkage away from the stem has been highlighted as a source of porosity, a method was developed to heat the outer ring of the torsional fatigue sample described above to body temperature. A 50mm diameter nozzle heater was used in conjunction with a Carel control system to regulate the temperature (see figure 4.6). This set-up allows a similar distribution of temperature to that found *in vivo*, i.e. the heat flows from the outer ring (the bone) towards the stem.

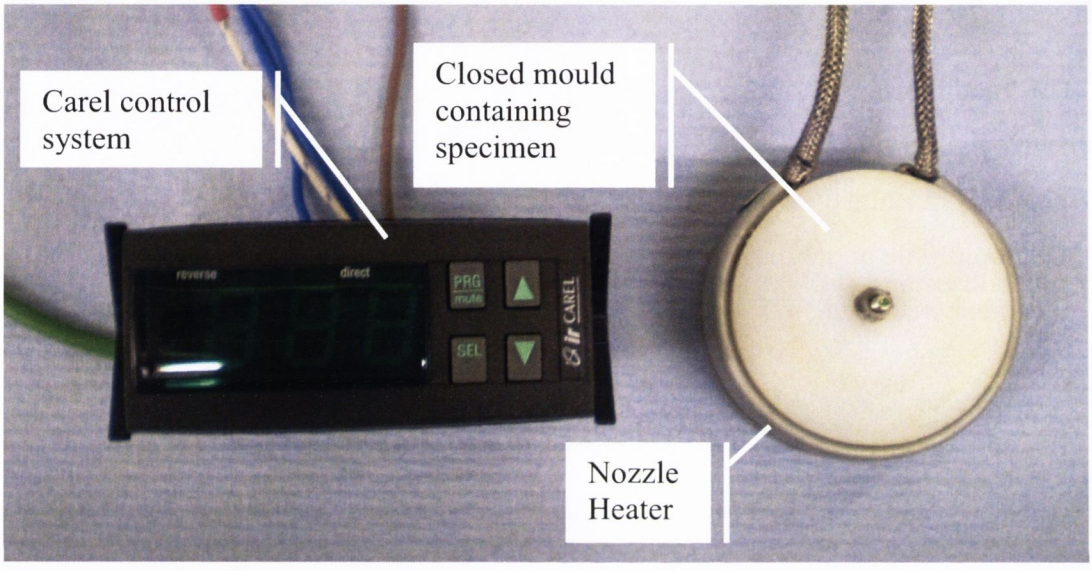

Figure 4.6: Schematic of heated set-up for the torsional fatigue sample.

4.5. Testing Rigs

Two different experimental rigs were used in this project; one for the uniaxial fatigue tests and a second for the torsional fatigue tests. The experimental rigs were designed to test acrylic bone cement in a physiological environment under controlled cyclic loading conditions.

4.5.1. Uniaxial fatigue

The uniaxial experimental rig used was previously developed by Murphy, (Murphy 2001b). The rig was used in conjunction with an Instron servo-hydraulic testing machine (model 8501). Various alterations were made to the rig used by Murphy. A

new heating system was introduced in the form of a) and b) below. Also new grips were manufactured from stainless steel as the previous grips began to rust after prolonged testing periods. The complete testing rig consisted of six main parts:

a) An insulated water bath
b) A water pump, heater and thermostat
c) A set of connecting rubber tubes
d) A set of stainless steel grips
e) A perspex container
f) A polyethylene tap

The new heating system allowed a constant circulation of heated water. The temperature was kept at a constant 37°C ± 0.5°C, an increase in consistency of 1°C in comparison to Murphy. A thin copper wire was used to secure the tubing entering the Perspex tank, as the tubing had a tendency to slip.

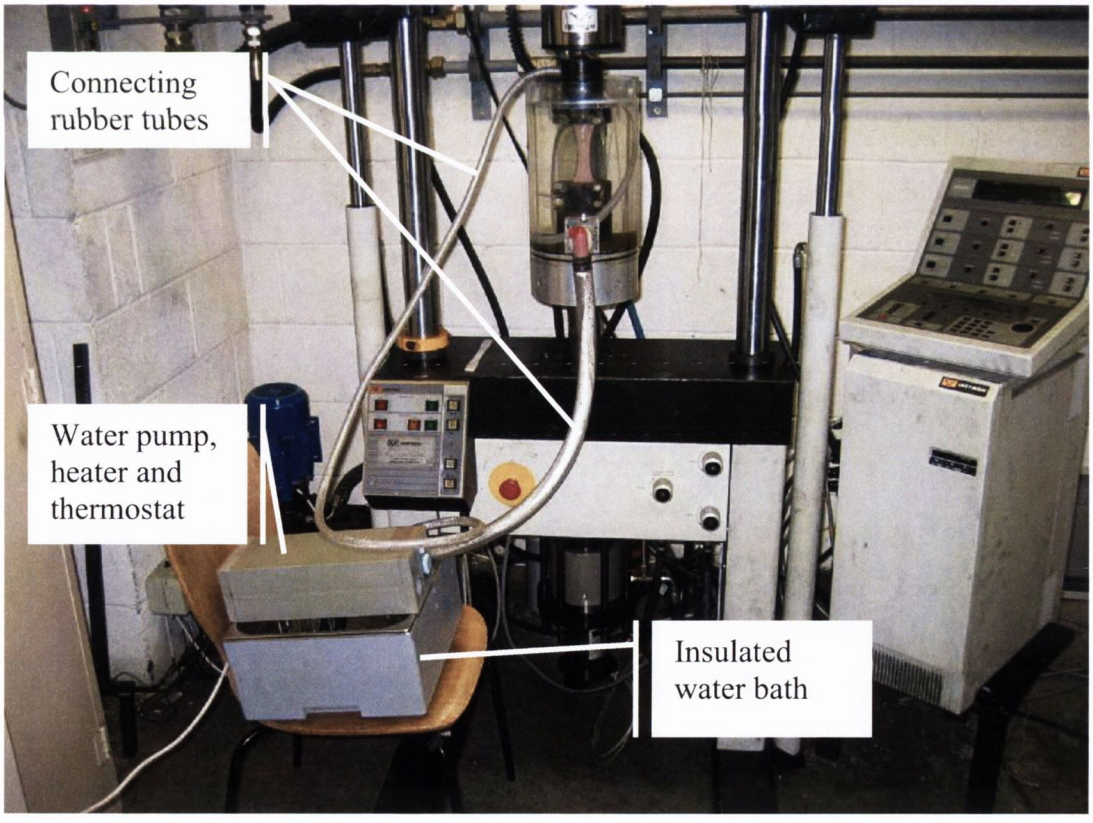

Figure 4.7: INSTRON 8501, experimental rig and water pump/heater.

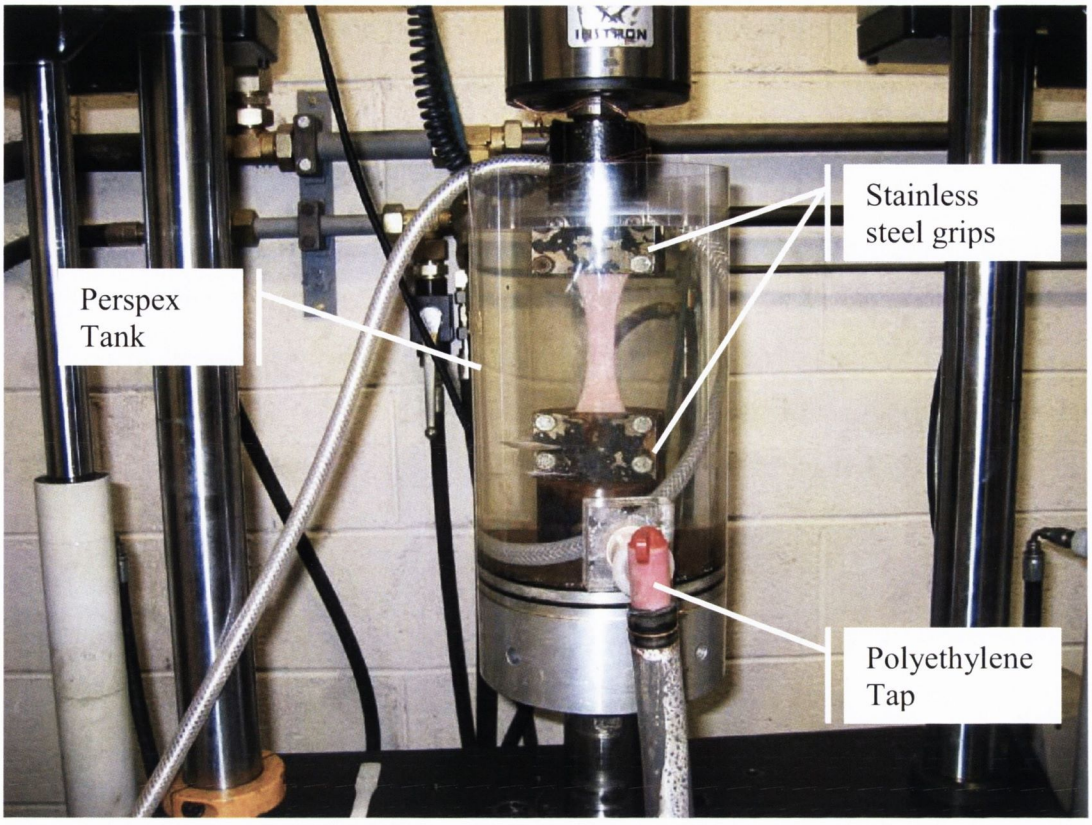

Figure 4.8: Close up of experimental rig (Perspex tank, two grips, tap and tubing).

4.5.2. Torsional fatigue

The experimental rig used to test the cement mantle cross section was purposely designed and built for this study. The rig was used in conjunction with an Instron servo-hydraulic testing machine (model 8874), which allows direct application of a cyclic torsional load to the stem. Other studies have used a loading moment arm to apply a torque (Hertzler 2002), which may result in out of plane bending moments and axial loads on the stem. This is not a concern with the rig used in this study. The complete testing rig consisted of four main parts:

a) A perspex water tank
b) Two heating pads
c) Aluminium base containing specimen support pins
d) Stainless steel driving rod

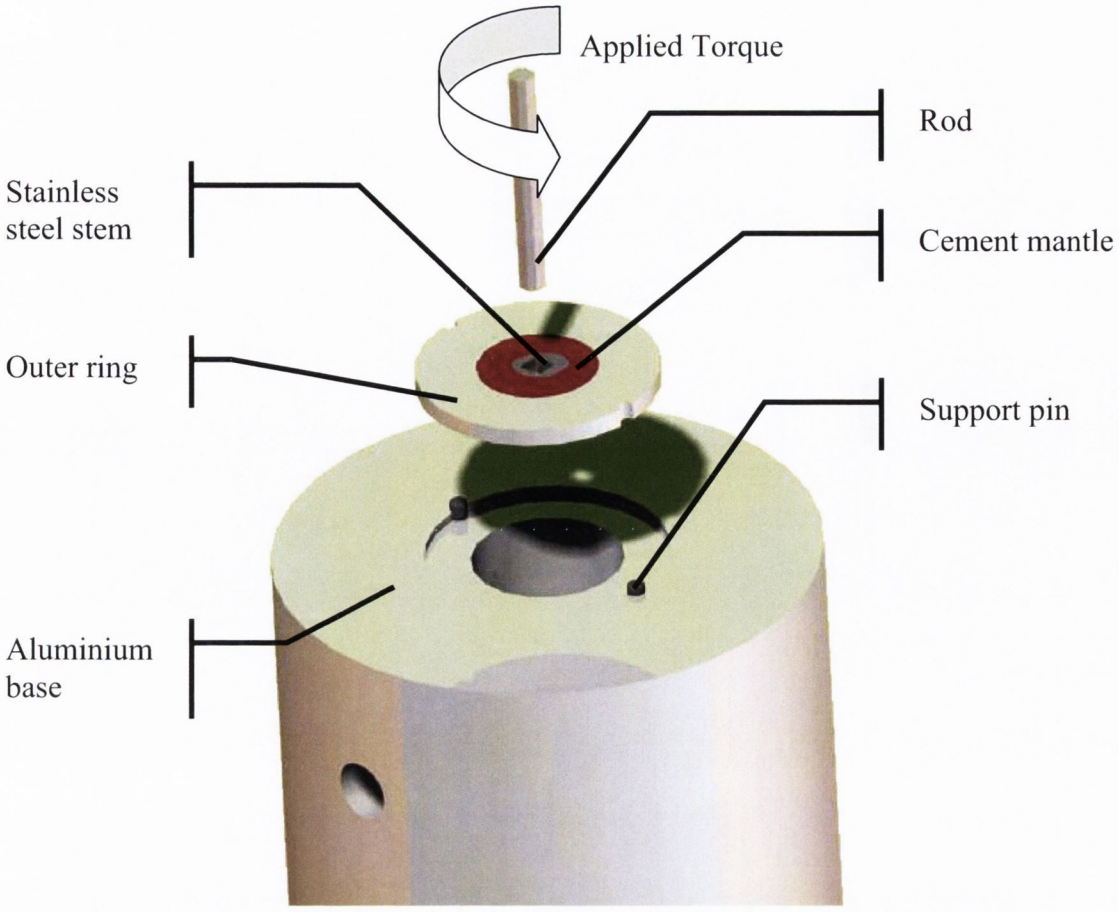

Figure 4.9: 3D model of torsional fatigue experimental rig

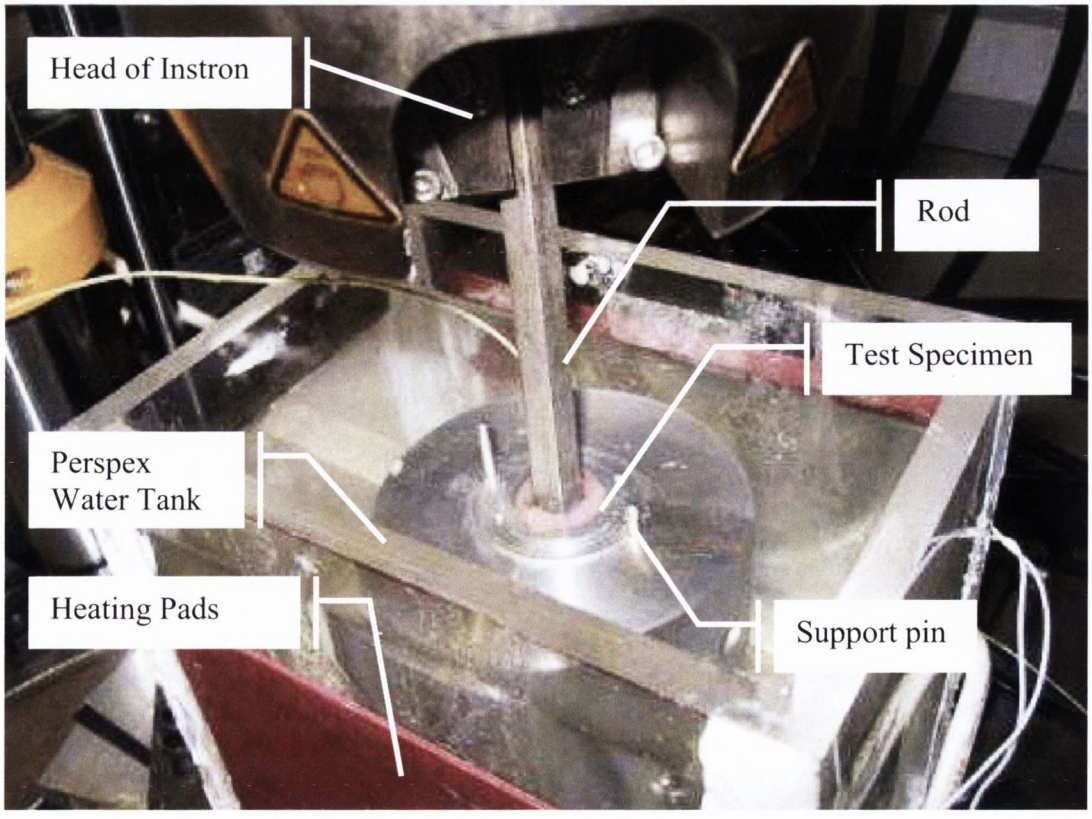

Figure 4.10: Close up of torsional fatigue experimental rig

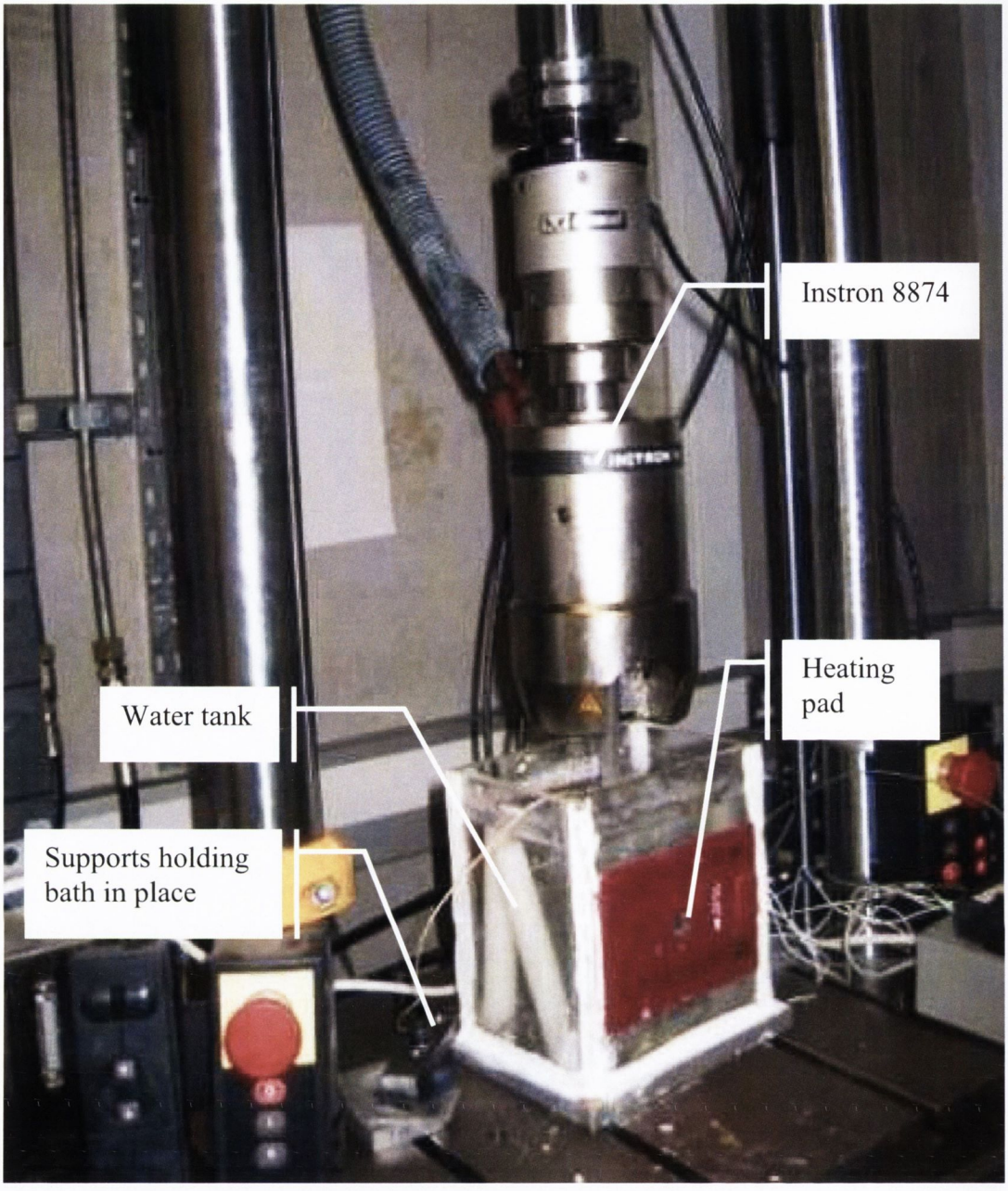

Figure 4.11: INSTRON 8874 and torsional fatigue experimental rig.

4.6. Finite element analysis

Finite Element Analysis (FEA) is a computer-based numerical technique for calculating the strength and behaviour of engineering structures. It can be used to calculate deflection, stress, vibration, buckling behaviour and many other phenomena. In FEA, the structure is broken into simple blocks or elements. These

elements can then be represented with a relatively simple set of equations. The equations describing the individual elements are then joined into an extremely large set of equations that describe the behaviour of the whole structure. Finite element analysis is a way to explore structures that are more complex than can be dealt with analytically using partial differential equations. FEA handles complex boundaries better than finite difference equations can, and gives answers to "real world" structural problems. It has continued to rapidly improve since it was first used some 40 years ago (www.ansys.com 2008).

Ansys is a Finite Element Analysis (FEA) program. Ansys (10.0) is used to model the various specimens tested in this study. From these models, stresses were taken along a path drawn normal to the underlying surface at the point of maximum stress concentration and plotted on a graph of stress against distance from the defect.

A linear elastic analysis was conducted using typical material properties for PMMA based bone cement (Young's modulus = 2.38GPa and a Poisson's ratio = 0.4) (Lewis 1997) and pure PMMA (Young's modulus = 2.5GPa and a Poisson's ratio = 0.33) (Taylor 2004a). Both 2D (4-noded quadratic elements) and 3D (10-noded tetrahedral elements) analysis was conducted as appropriate. More details on the individual models can be found in the relevant results chapters.

4.7. Porosity analysis

4.7.1. 2D (ImageJ)

Fracture surfaces were coated with black ink to highlight any irregularities. These fracture surfaces were then examined under a toolmaker's microscope (Mitoutoyo, Tokyo, Japan) to determine the fracture surface porosity. An image of each fracture surface was captured. The images were analyzed using ImageJ software. ImageJ is a public domain image analysis program that was developed at the National Institutes of Health. It can display, edit, analyze and process 8-bit, 16-bit and 32-bit images. The fracture surface area and 2D porosity levels were then established for each specimen.

4.7.2. 3D (Scanco μ-CT 40)

Samples roughly 16x3.5x3.5mm in size were taken from each sample and scanned using a Scanco μ-CT 40 scanner. The Scanco μ-CT 40 can achieve a resolution of 9 μm at 10mm object size. A μ-CT scanner works as follows, a micro-focused X-ray source illuminates the sample, which is positioned on a precision manipulator. The x-ray Shadow Images are acquired by a sensitive X-ray camera. During the Image Acquisition the sample is rotated one step at a time through 180 degrees. Images are recorded at each rotation. Using complex software these 2 dimensional images (or slices) based on x-ray density can be recalculated from the x-ray Shadow Images. One or more of these 2D images can be stored in the computer and then using another software package a stack of these images can be added together to form a 3D model of the sample. The software allows for numerical data to be calculated from the morphology of the samples structure. Therefore, the 3D volume porosity levels for each sample could then be determined.

4.8. Experimental protocols

This section details the main points of the experimental procedure from specimen moulding through to the analysis of failed specimens.

4.8.1. Moulding procedure

Before each mould was used, all the components were cleaned using alcohol. In addition, the pressure relief holes and all screws were recoated with grease. The following procedure was then followed,

Uniaxial specimens

- The lower aluminium and polyethylene plates were assembled and the eight screws were put in place. The central plate containing the specimen profile was then put on top.
- The cement was then mixed in the appropriate manner.
- The cement was then poured from one end of mould to the other.

- The cement was then finger packed into the mould to ensure all areas are filled.
- The top polyethylene and aluminium plates were then placed on top and the nuts were tightened until the mould was completely sealed.
- The cement was then left for an hour at room temperature. After this time the mould was disassembled and the specimen was removed.

Torsional specimens

- The lower polyethylene plate and the central screw were put in place. The outer aluminium ring and stem was then placed on top of the polyethylene plate.
- The cement was then mixed in the appropriate manner.
- The cement was then poured in the cavity between the outer ring and the stem.
- The cement was then finger packed into the mould to ensure all areas are filled.
- The top polyethylene plate was then placed on top and the nut was tightened until the mould is completely sealed.
- The cement was then left for an hour at room temperature. After this time the mould was disassembled and the specimen was removed.

Heated torsional specimens

- The nozzle heater was connected to the control system and the target temperature was set to 37°C with a temperature differential setting of -0.1° C, i.e. the control system would apply a voltage to the heater when the temperature dipped below 36.9°C, and deactivate when the temperature rose above 37°C.
- A thermocouple was connected from the control system and taped against the side of the heating element to monitor and control the temperature.
- The plastic plates of the mould were placed within the heating element in their closed position with the outer aluminium ring placed inside.

- The thermocouple was then placed between the lower disc and heating element. The system was then allowed to run for 10 minutes to ensure that the entire setup would be at body temperature prior to the pouring of the cement.
- Once the mould had reached the desired temperature, it was disassembled and the stem (room temperature) was placed into position.
- The procedure as described for the torsional specimens was then followed.

4.8.2. Pre-test procedure

Before each specimen could be tested, a few further steps were needed.

Uniaxial specimens

- The rough edges on the specimens were removed using 320-grit silicon carbide grinding paper.
- The area where the cement extruded through the pressure relief holes was smoothed flat using 320-grit silicon carbide grinding paper to ensure that the specimens fitted smoothly into the clamps.
- Before each sample was secured in the rig, they were dated, numbered and the stress range was written on each sample using a permanent marker.

Torsional specimens

- Both the upper and lower surfaces of the specimens were polished using 320-grit silicon carbide grinding paper.
- Any cement sticking to the aluminium outer ring was removed using a scalpel to ensure the specimen fitted precisely into the aluminium base and support pins.
- Before each sample was secured in the rig, they were dated, numbered and the torque range was written on each sample using a permanent marker.

4.8.3. Fatigue test conditions

The following fatigue test conditions were maintained throughout testing.

- Each specimen was kept in a water bath at a constant 37°C for the duration of each test.
- The tests were conducted at various stress levels depending on the specimen type. This was to ensure that each specimen reached 100,000 cycles to failure.
- Each sample was tested until failure and the maximum number of cycles before failure was recorded. However if a sample reached 250,000 cycles it was stopped and considered a run-out.
- For the torsional samples, the test was stopped every 20,000 cycles to allow monitoring of crack growth. This was repeated until failure occurred or a run-out was declared.
- The fatigue testing was performed using a ratio of minimum stress to maximum stress of 0.1.
- All tests were performed in load control.
- Loading cycle was sinusoidal.
- Test frequency was 3 Hz (uniaxial) and 1Hz (torsional).

4.8.4. Crack Analysis

Fracture surface

The fracture surface of the uniaxial and torsional specimens were examined by coating the specimens in gold and observing the fracture surface features with a scanning electron microscope (Hitachi Ltd., Model S-3500N, Japan).

Crack growth

Fatigue cracks were monitored in the torsional specimens using two different techniques. The torsional tests were stopped every 20,000 cycles and any cracks were examined and measured using an inverted microscope (Olympus IX51, PA, USA). This allowed accurate measurements of cracks on the surface of the specimen. In order to examine the crack growth within the specimen, the cement mantle from a failed specimen was removed from the outer ring and mounted in an epoxy resin. This was then ground down to approximately half way through the

specimen and polished to a roughness of 1μm. The cracks were then observed and images were taken using an optical microscope (Leica DMLM, Wetzlar, Germany).

Chapter 5

Fatigue failure in Bone Cement

Stress concentration effects

Published in: Hoey, D., Taylor, D., "Fatigue in porous PMMA: the effect of stress concentrations" International journal of fatigue, **30 (6):** 989-995, 2008.

5.1. Introduction

As discussed in chapter 2, stress concentrations play a major role in the fatigue behaviour of bone cement. Stress concentrations of all shapes, sizes and magnitudes arise in the cement mantle in the form of porosity, casting defects and design features. Despite the potential damaging effect of these stress concentrations, there have been very few systematic studies on the effect of notches or other stress concentration features on fatigue in polymers, despite the wealth of this type of data for metallic materials. The only example the author was able to find for PMMA was some data due to Gotham (Gotham 1973), on commercial PMMA, showing that notches of stress concentration factor (K_t) greater than 1.4 had a significant effect on fatigue strength.

Therefore this chapter had the following aims:

a) To conduct experiments to investigate the effect of introduced notches and other stress concentration features on the fatigue behaviour of PMMA based bone cement.

b) To investigate the interaction between the introduced defects and the naturally occurring porosity that is inherently found in the material.

c) To attempt to use the theory of critical distances (TCD) to predict these results.

5.2. Experimental details

Various stress concentration features were machined into the uniaxial tensile specimens described in chapter 4. Details of the geometry of each feature are shown in table 5.1, which also gives the stress concentration factor K_t, defined as the maximum stress divided by the nominal gross-section stress. These specimens were fatigue tested at different stress levels to failure. The aim was to establish the fatigue

strength at a life of 10^5 cycles in order to characterize the effect of notches in the high-cycle regime.

Defect Type	Root radius	Depth	Diameter	Location	K_t
Plain	-	-	-	-	1
Hole	-	-	2.2 mm	through thickness, drilled centrally	3.08
Notch	0.1 mm	2 mm	-	both edges, mid gauge length	11.04
Notch	0.75 mm	2 mm	-	both edges, mid gauge length	4.47
Notch	1.5 mm	2.2 mm	-	both edges, mid gauge length	3.52
Notch	4 mm	2 mm	-	both edges, mid gauge length	2.4
Notch	7 mm	2 mm	-	both edges, mid gauge length	2.03
Notch	50 mm	2 mm	-	both edges, mid gauge length	1.44
Hemisphere	-	-	1 mm	drilled centrally	2.17

Table 5.1: Description of each defect incorporated into the uniaxial test specimens. The K_t values were determined using the FE models created for each specimen.

Fatigue testing was conducted on an Instron servo-hydraulic testing machine (Model 8501). The cyclic stress employed was sinusoidal at a frequency of 3Hz. All tests were conducted in tension; the ratio of minimum stress to maximum stress (R) was kept at a constant value of 0.1. Since the material is sensitive to temperature, samples were tested in a water bath at body temperature (37°C).

A limited number of specimens produced using a commercially-available vacuum mixing system (DePuy Johnson & Johnson Ultramix) were also tested. This reduced the porosity to 1-5% but some pores still remained in the specimens. In order to test

material containing no pores, small specimens were machined from these specimens, choosing pore-free areas. This resulted in a pore-free gauge section of 8x8x3.5mm.

5.3. Results

Figure 5.1 shows stress-life data for three specimen types: plain hand-mixed specimens, those containing a 2.2mm diameter hole and those containing a sharp notch (depth 2mm, root radius 0.1mm). It is evident that increasing K_t reduced the fatigue strength, but it is also clear that the reduction factor is not as large as K_t. This is typical of the fatigue behaviour of other materials, such as metals. Data for the plain specimens showed considerably more scatter than those for specimens containing notches or holes. Failures in the plain specimens were initiated by pores: usually the initiation site contained two or more pores in a cluster. For the specimens containing features such as notches and holes, failure was invariably initiated at the feature, close to the predicted location of maximum stress.

Figure 5.2 shows data for the other 'sharp' notches tested while figure 5.3 shows data for the 'blunt' notches tested and also for specimens containing small hemispherical depressions. It is interesting to note that the hemispheres had no significant effect on the results, and in fact they were not the initiation sites in any of the specimens. Considering the very blunt notch (of root radius 50mm), this appeared to cause a small decrease in fatigue strength, but when the data was replotted using the net section stress this changed to a small increase.

Figure 5.4 shows data from the vacuum-mixed and pore-free plain specimens, again showing the plain-specimen data from figure 5.1 for comparison. Vacuum mixing, though it reduced the porosity considerably, caused only a small increase (12%) in the fatigue strength. The fatigue strength of the pore-free specimens was considerably higher.

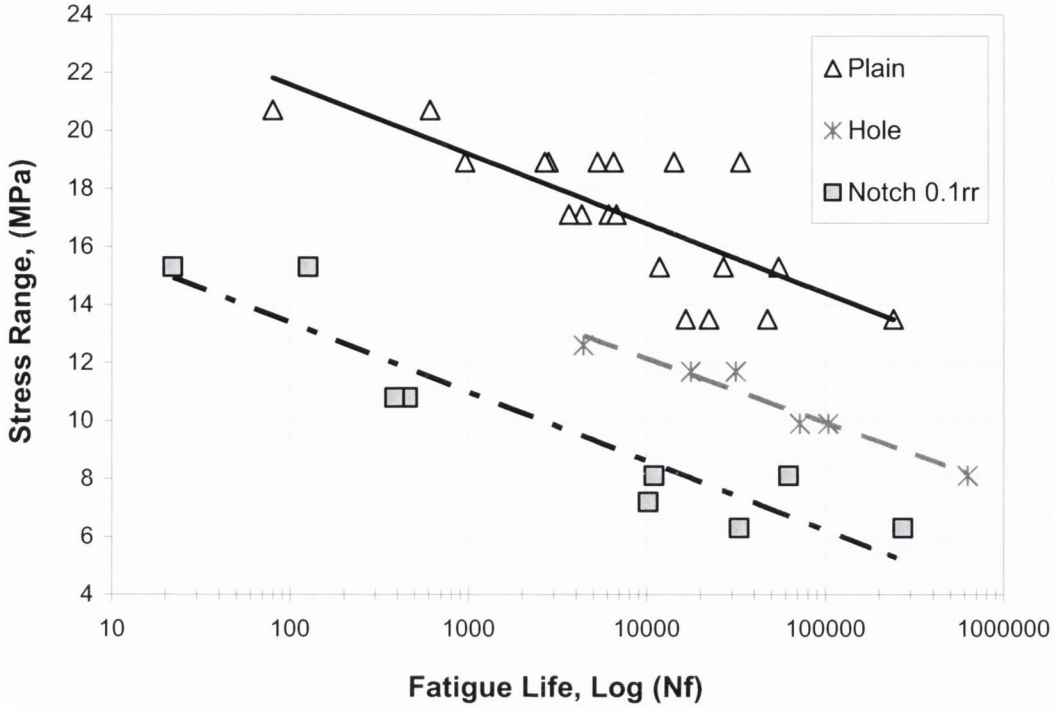

Figure 5.1: Stress-life data (nominal gross-section stress range at R=0.1 as a function of number of cycles to failure) for plain specimens and specimens containing holes (diameter 2.2mm) and sharp notches (depth 2mm, radius 0.1mm). rr = root radius.

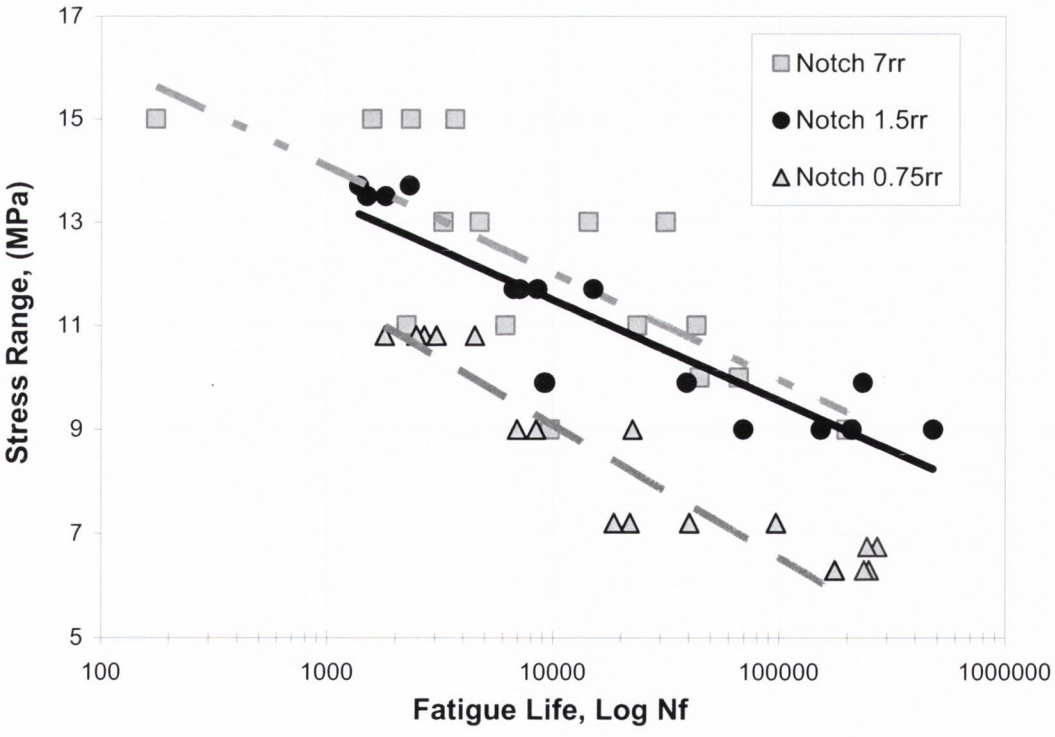

Figure 5.2: Stress-life data for specimens containing various 'sharp' notches. rr = root radius.

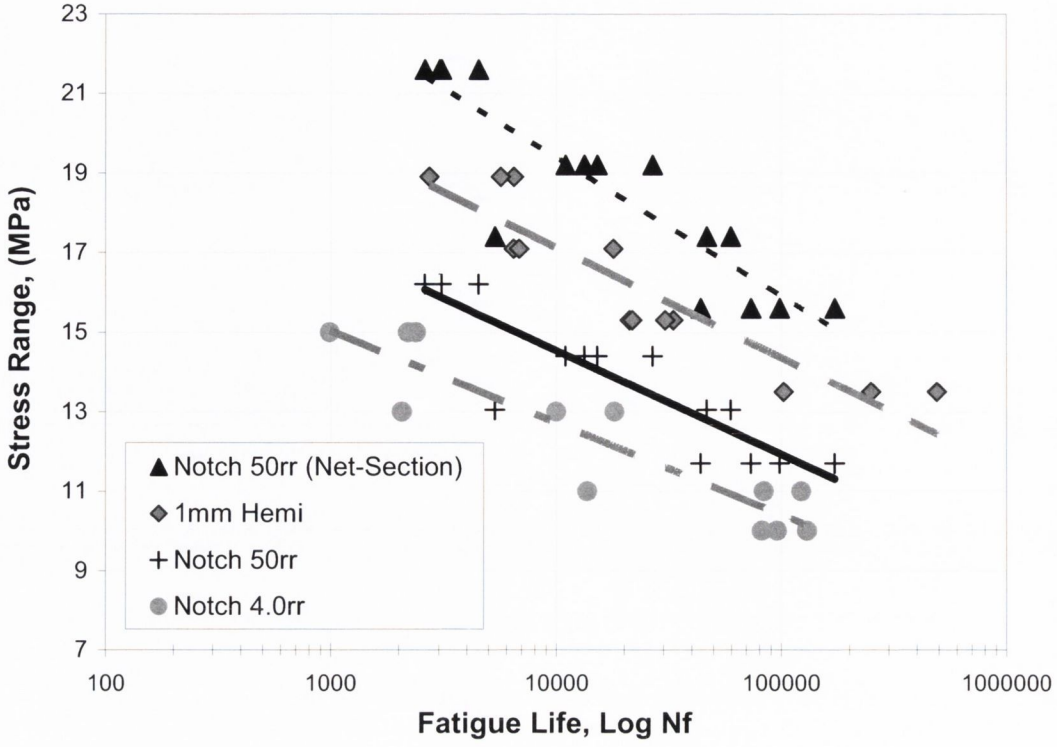

Figure 5.3: Stress-life data for specimens containing various 'blunt' notches, or small hemispheres. rr = root radius.

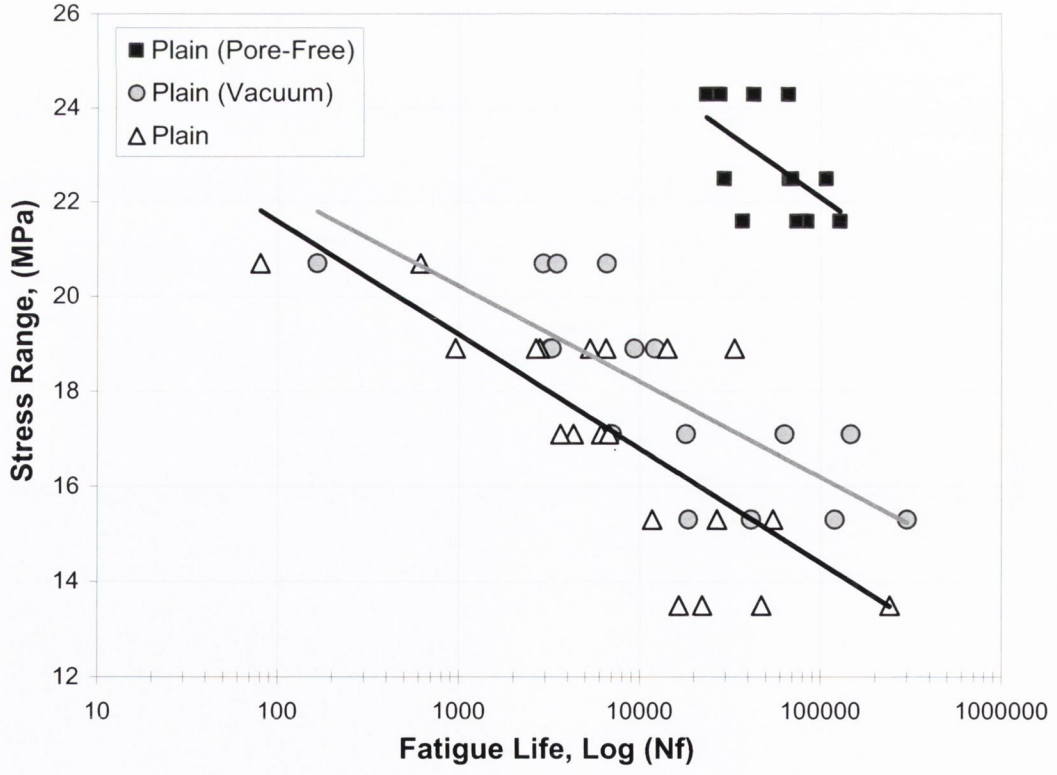

Figure 5.4: Stress-life data for plain specimens of vacuum-mixed material and pore-free specimens. The data for the hand-mixed plain specimens (from figure 5.1) is also shown.

In materials which do not show a clear fatigue limit, $\Delta\sigma_0$ is taken to be the fatigue strength at a given number of cycles to failure; in the present work 10^5 cycles was used. The fatigue limits for each specimen taken at 100,000 cycles can be seen in table 5.2.

Specimen	Fatigue Limit		Specimen	Fatigue Limit	
Plain Hand-mixed	14.4	MPa	Plain Vacuum-mixed	16.0	MPa
Plain Pore-free	22.4	MPa	Hole 2.2 mm Ø	9.9	MPa
Notch 0.1mm rr	6.21	MPa	Notch 0.75mm rr	6.66	MPa
Notch 1.5mm rr	9.54	MPa	Notch 4.0mm rr	10.41	MPa
Notch 7.0mm rr	9.95	MPa	Notch 50.0mm rr	11.93	MPa
Hemisphere 1.0mm Ø	14.35	MPa			

Table 5.2: Fatigue limits taken at 100,000 cycles for each specimen tested

5.4. Computational details

Each specimen type was modelled using finite element (FE) analysis (Ansys 10.0) to determine the linear elastic stresses in the vicinity of the features (see figure 5.5 and figure 5.6). Both 2D (4-noded Quad elements) and 3D (10-noded Tet elements) analysis was conducted, as appropriate. Each model consisted of on average 25,000 elements. The material was modelled as having a Young's modulus of 2.38GPa and Poisson's Ratio of 0.4 (Lewis 1997).

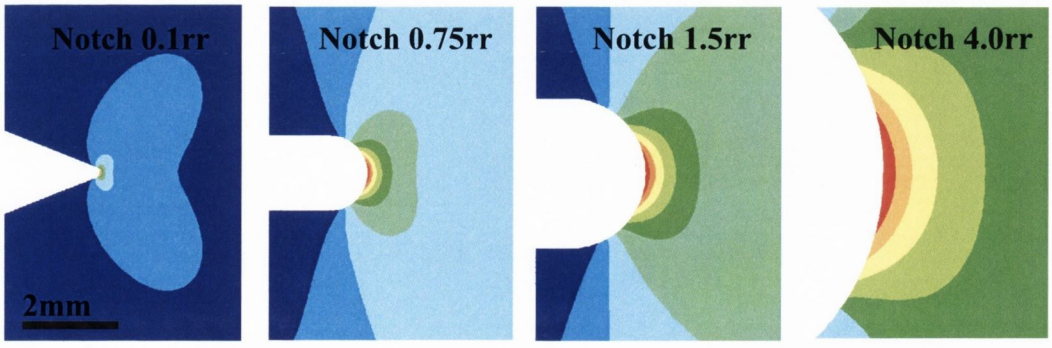

Figure 5.5: Finite element stress analysis of the 'sharp' stress concentrations tested illustrating the notch shape and stress distribution. (Note: contours are not representative of actual stress levels)

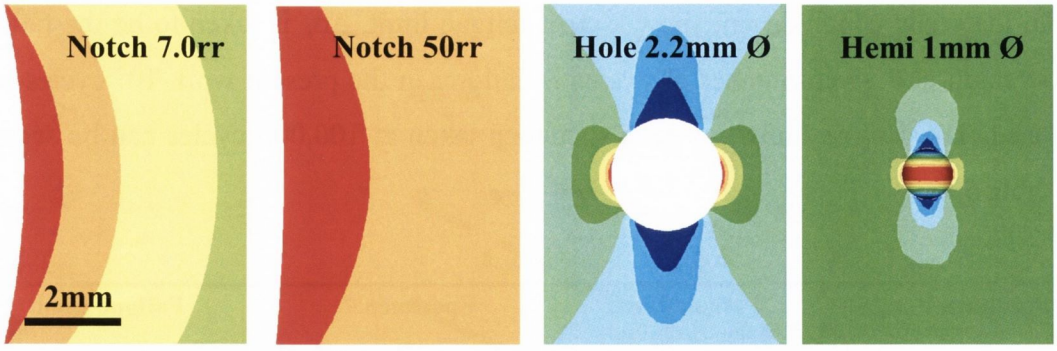

Figure 5.6: Finite element stress analysis of 'blunt' stress concentrations tested illustrating the notch shape and stress distribution. (Note: contours are not representative of actual stress levels)

5.5. Determining the critical parameters

An elastic stress analysis is conducted, using either analytical solutions or FEA (as above), allowing one to examine the stress as a function of distance (r) from the notch root. Stresses are considered along a line corresponding to the direction of expected crack growth, which for simple tension will be a line perpendicular to the applied stress (see figure 5.7). The relevant stress parameter in this case is the maximum principal stress, though other parameters are used for mixed-mode loading, which are not considered here. The theory assumes the existence of a critical length parameter for the material, denoted L, assumed to be a constant for a given material. Fatigue of the notched specimen is predicted to occur when the stress range at a distance r = L/2 is equal to the fatigue strength of the material as measured using plain specimens, $\Delta\sigma_o$. This is known as the point method of the TCD. Both L and $\Delta\sigma_o$ will depend on the R ratio and N_F. The underlying idea is to take account of stress gradient effects by examining the stress at some distance from the notch root.

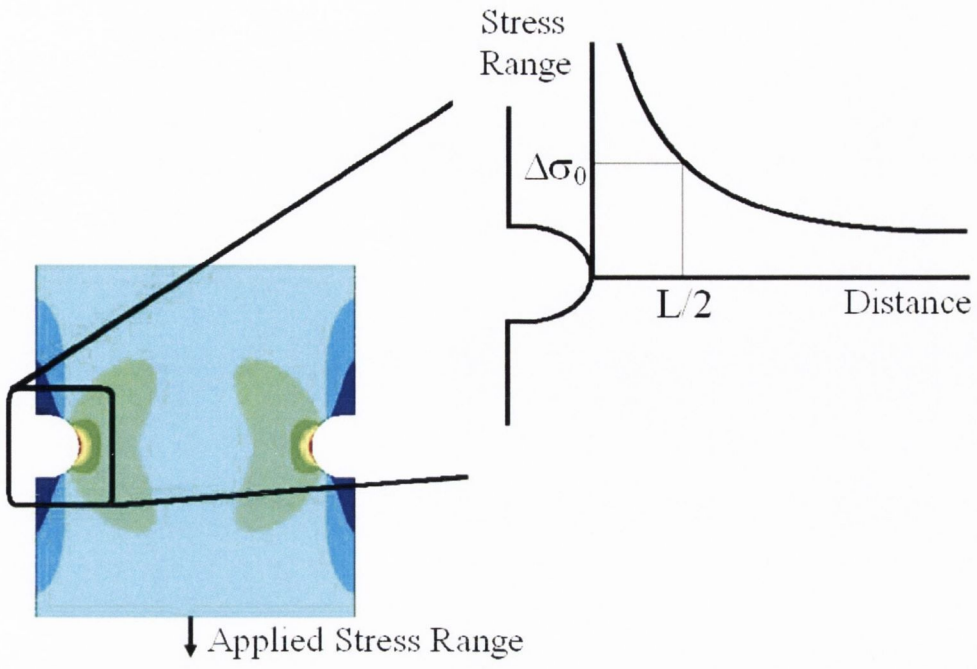

Figure 5.7: Schematic showing the principle of the TCD (Point Method)

The point method (PM) is applied to the present data by considering stress-distance curves drawn for applied loads corresponding to 10^5 cycles to failure, for the various specimens tested. Figure 5.8 shows the appropriate curves for the hole (diameter 2.2mm) and sharp notch (depth 2mm, root radius 0.1mm); also shown is the fatigue strength of plain hand mixed specimens at the same number of cycles to failure. If the PM is applicable, then all three lines should intersect at the same point, corresponding to L/2 and $\Delta\sigma_o$, but clearly they do not. It was hypothesised that this problem arose due to the porosity in the plain specimens; it was reasoned that this was reducing their fatigue strength below the true value for the material. If so, then the true fatigue strength might be found from the intersection of the other two curves on this figure. This intersection point occurs at a stress of 25MPa and at a distance of 0.1mm, so it was assumed that these were the values of $\Delta\sigma_o$ and L/2 respectively.

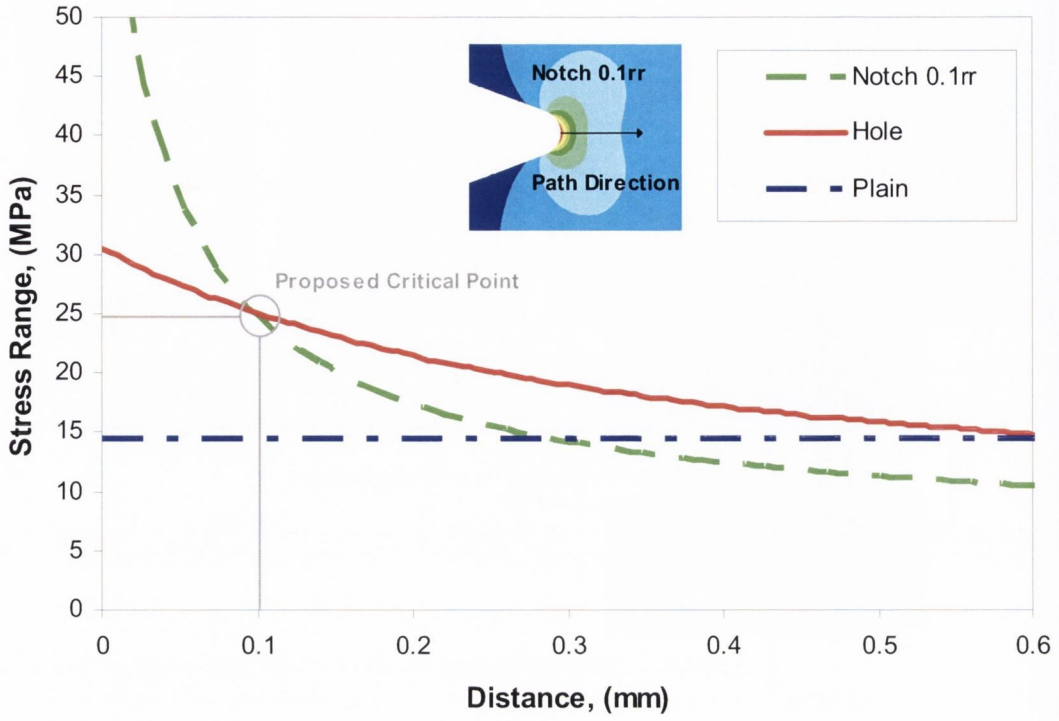

Figure 5.8: Stress as a function of distance from the defect root for specimens containing holes and sharp notches, at applied loads corresponding to 10^5 cycles to failure. Also shown is a line representing the fatigue strength of the plain specimens of hand-mixed material, for the same number of cycles to failure.

Critical Distance,	L/2	=	0.1 mm	} *Bone Cement*
Critical Stress Range,	$\Delta\sigma_0$	=	25 MPa	

5.6. Predictions

Predictions can now be made based on the assumption that stress-distance curves drawn for applied loads corresponding to 10^5 cycles to failure for all notched specimens tested should intersect at a common point, defined by $\Delta\sigma_o$ and L/2. Figure 5.9 shows an example of the prediction for the specimen containing a notch of root radius 0.75mm. The stress results from the FE analysis of this notch fulfil the above criterion when the applied stress is 7.2MPa, so this is the predicted fatigue strength for that specimen. The linear-elastic nature of the analysis makes it

particularly straightforward to do this calculation because all stresses in the specimen are directly proportional to the applied load.

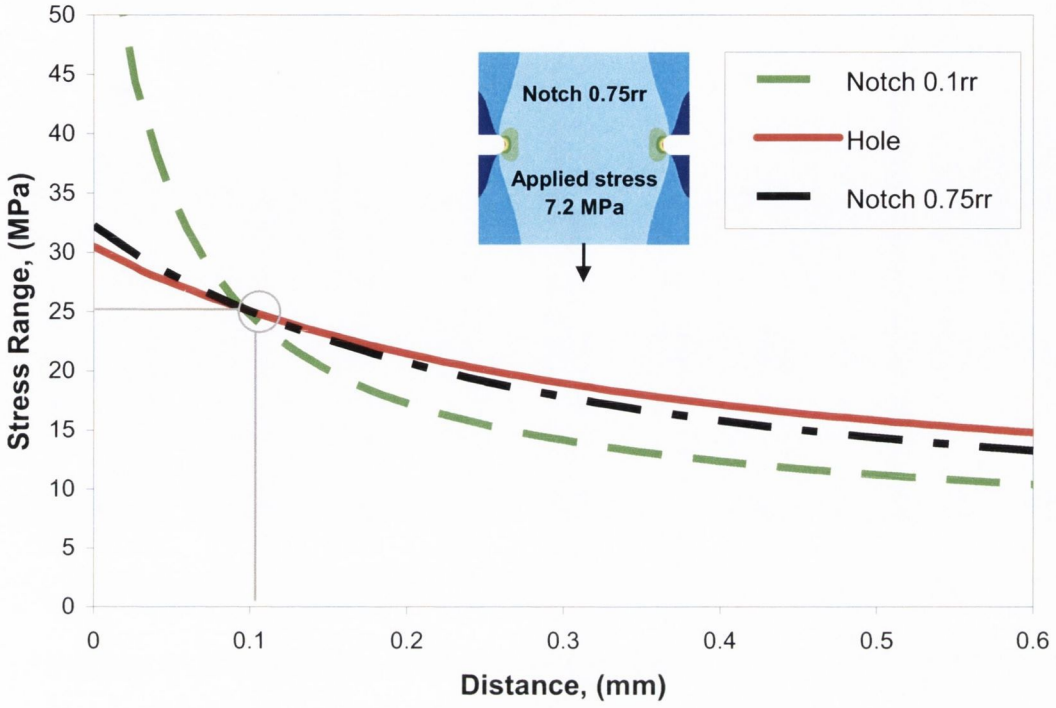

Figure 5.9: Illustration of the use of the TCD to predict the fatigue strength of the 0.75rr notch. An applied stress of 7.2 MPa resulted in a stress distance curve that intersected the critical point, i.e. 7.2 MPa is the predicted fatigue strength for the 0.75rr notch at 10^5 cycles.

Figure 5.10 shows the experimental and predicted fatigue strengths at 10^5 cycles for all specimen types. Since the 0.1mm-radius notch and the 2.2mm diameter hole were used to determine the critical constants, these predictions will necessarily be perfect. Successful predictions (with a maximum error of 16%) were made for all the other features, except the two 'blunt' notches (rr = 7 and 50 mm), which had a much lower fatigue strength than predicted. In the case of these two notches, a prediction simply based on reaching the plain-specimen fatigue strength over the net cross-section was found to be accurate, i.e. this notch had no role in reducing fatigue life except insofar as it reduced the load-bearing area. For the hemispheres both methods gave reasonable predictions, but the use of the plain fatigue strength was more accurate than the TCD.

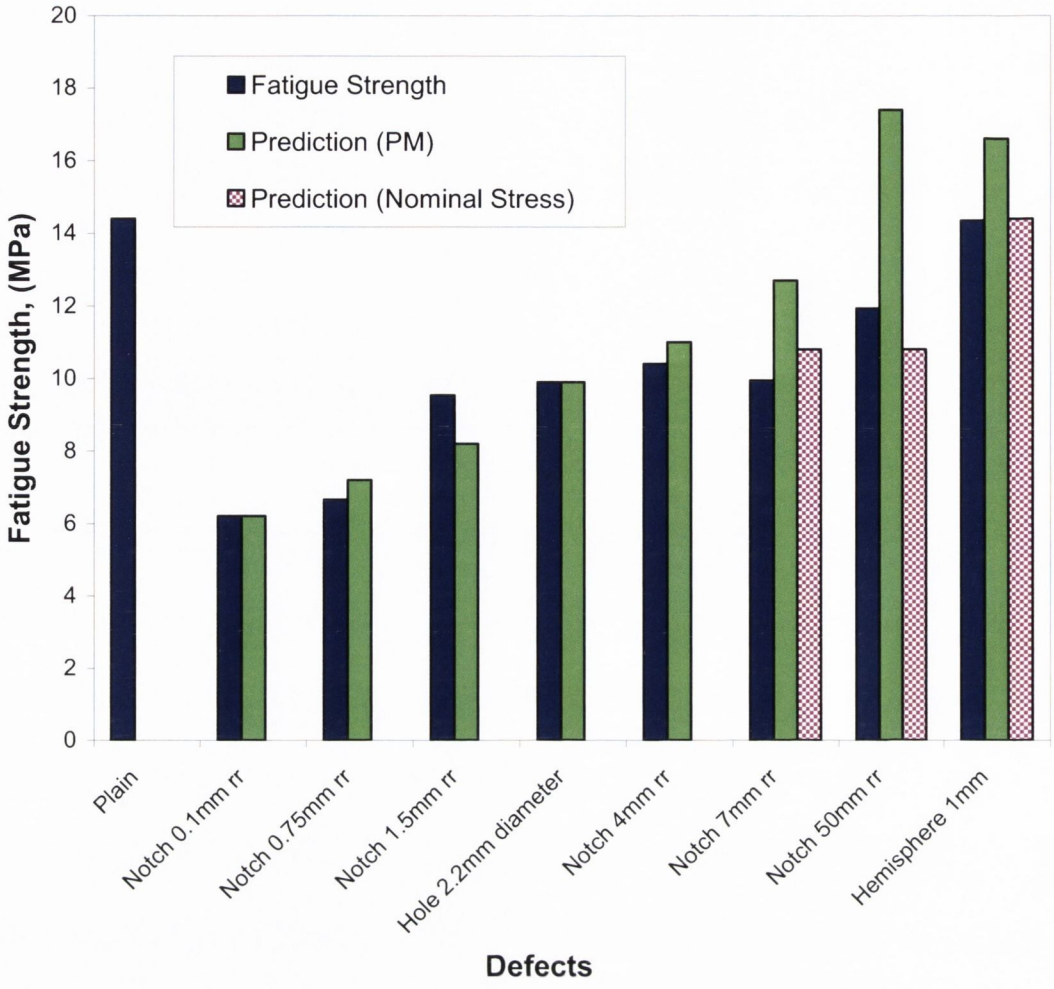

Figure 5.10: Measured fatigue strength for 9 different specimen types, with predictions using the TCD and also using the nominal stress on the reduced cross section. This shows that the three notches on the right are "Safe Notches", causing no reduction in fatigue strength.

5.7. Discussion

The series of tests described here is the most comprehensive study conducted to date on the effect of stress concentrations on the fatigue behaviour of bone cement, and as such it provides a useful resource with which to test the effectiveness of predictive theories and to estimate the effects of stress concentrations, especially large casting defects with dimensions of the order of millimetres. Further work is needed to clarify the effect of porosity and other sub-millimetre defects (see

chapters 6 and 7), though the present chapter provides some clues in this respect. The relatively low fatigue strength of the hand-mixed plain specimens can certainly be attributed to porosity, since the pore-free samples performed much better. Interestingly, the critical stress of 25MPa as deduced from the data on notched specimens is close to the measured fatigue strength of the pore-free specimens, which was 22MPa, just 12% lower. On closer inspection very small pores were found on the fracture surfaces of some of these specimens, which may explain this small difference. This implies that, in specimens with sufficiently sharp notches, the true fatigue strength of the material is realised because there are no pores in the critical region close to the notch root. Pore-free specimens are difficult to produce, so it is very useful to find that the true fatigue strength of the material can be obtained using notched specimens of imperfect, porous material.

The vacuum-mixed material did not have a significantly longer fatigue life when compared to the hand-mixed material. We found that, whilst the overall porosity was lower, the vacuum-mixed material still contained a few pores which were relatively large; this has also been noted by numerous other authors (Murphy 2000; Dunne 2003).

These findings also suggest why the vacuum-mixed material, though it sometimes shows superior performance to hand-mixed in laboratory tests, does not seem to improve performance in artificial joints. In these joints, unlike tensile test specimens, stress varies considerably from place to place, usually being highest at the interface between the cement and the metal implant, where the shape of the implant can give rise to local stress concentrations. Thus, as with the sharp notches, the chances are that no pore will be present in the critical, highly-stressed region. Therefore the full, pore-free strength will be realised even in material which has quite a high level of porosity. A similar conclusion was reached by Janssen et al (Janssen 2005b) who used a damage mechanics approach to compare the effect of porosity in computer simulations of test specimens and implants. This conclusion gains real significance when considering the effort and considerable cost involved in developing modern mixing techniques such as vacuum-mixing.

The 50mm-radius notch is an interesting case: the PM predicted a much higher fatigue strength than that of the plain specimen, which is clearly invalid. This seems to be because in this specimen the critical region of high stress near the notch is sufficiently large that some pores will be found there and thus influence the fatigue strength. However the volume of this region is obviously smaller than that of the whole specimen so, on average, the pores to be found here will be less damaging. This is reflected in the slightly higher fatigue strength of this notch, when expressed in terms of the net-section stress. In any case the differences were small, so a reasonably accurate prediction could still be obtained. The results imply that a significant effect will arise for specimens or components having much larger (or smaller) stressed volumes. In practice the volumes of cement used in artificial joints and other orthopaedic applications are similar to those of the specimens used here, so the results will be applicable.

The effect of having a larger or smaller stressed volume is evident when comparing the samples containing a 4mm rr notch to that of the 7mm rr notch. The TCD predicts that the 4mm rr notch should demonstrate the inferior fatigue strength of the two, which isn't surprising given its higher stress concentration factor. However, due to the larger stressed volume of the 7mm rr notch, which increases the likelihood of porosity influencing failure, it is this notch which demonstrates the inferior fatigue strength.

The 1mm-diameter hemispheres had no effect on fatigue strength and did not even act as initiation sites. This is not surprising since the material contained other pores of similar size, sometimes in clusters. Since clusters of pores were seen at crack initiation sites in the plain hand-mixed specimens, the combined effect of two or more pores in close proximity needs to be considered. The importance of clustering has been noted by other workers using damage mechanics simulations of test specimens and implants (Jeffers 2005).

In this study, the testing was confined to tensile loading, but cement mantles and other cement structures experience more complex types of loading, including compression and shear, with high local stresses caused by, for example, contact with metallic components of various shapes. The literature on metal fatigue contains

many examples of this so-called 'multiaxial loading', and it has already been shown that the TCD can be used in these circumstances, at least for metals (Susmel 2003a; Susmel 2006).

5.8. Conclusion

1) Sharp notches and holes had a significant effect on the high-cycle fatigue strength of porous PMMA as used in bone cement. Blunt notches and small hemispheres had no detrimental effect, and a vacuum mixing technique, whilst it reduced porosity, conferred no significant improvement on fatigue strength.

2) The effect of relatively sharp stress-concentration features (with K_t factors of 2.4 or more) could be predicted using the Theory of Critical Distances in the form of the Point Method.

3) Porosity, in the form of sub-millimetre spherical pores, reduced the fatigue strength of plain specimens, but did not affect the behaviour of specimens containing relatively sharp notches. The critical stress for these notches was found to be similar to the true fatigue strength of pore-free material. The non-effect of blunt notches, small hemispheres and vacuum mixing could be explained by reference to the pre-existing porosity.

4) The non-effect of porosity when the material contains a sharp notch provides an explanation for the lack of clinical improvement *in vivo* even when porosity is reduced using modern mixed techniques.

Chapter 6

Porosity in Bone Cement

Pore Size Vs Pore Distribution

Published in: Hoey, D., Taylor, D., "Quantitative analysis of the effect of porosity on the fatigue strength of bone cement" Acta Biomaterialia, doi:10.1016/j.actbio.2008.08.024, 2008

6.1. Introduction

It was concluded from chapter 5 that introduced stress concentrations in the form of notches play a major role in the fatigue failure of bone cement. This role could be predicted for specimens containing stress concentrations with K_t values greater than approximately 2.4. However for specimens containing stress concentrations with K_t values less the 2.4, the introduced defect was found to have no effect on fatigue failure. This non-effect was attributed to porosity.

Therefore this chapter had the following aims:

a) To investigate whether the TCD can be used to predict the effect of porosity on the fatigue strength of bone cement.

b) In the light of previous observations, to consider in particular the effect of clusters of pores in reducing fatigue strength.

c) To use this approach to develop general rules governing the role of pore size and distribution which could be used to determine optimal pore distributions.

6.2. Experimental Details

In order to analyse the effect of porosity, samples from chapter 5 were examined. Plain hand-mixed, vacuum-mixed and pore-free specimens were fatigue tested at varying stress levels to failure. Figure 6.1 reproduces these results, showing the number of cycles to failure as a function of the nominal stress range.

To determine the distribution of pore size in the material, each sample was sectioned at 3 locations. The surface of each section was coated with black ink to highlight any pores. The surfaces were then examined under a toolmaker's microscope (Mitoutoyo, Tokyo, Japan) and an image of each surface was captured.

The images were analyzed using ImageJ software (NIH, Maryland, USA), allowing the pore diameter to be measured. This data was imported into Matlab (7.0), which used a distribution fitting tool to determine the distribution of the pore sizes in hand-mixed and vacuum-mixed cement. In order to visualise the distribution of porosity, both hand-mixed and vacuum-mixed specimens were scanned using a Scanco μ-CT 40 system (source voltage – 70kV, current – 115mA, global threshold – 43, resolution - medium).

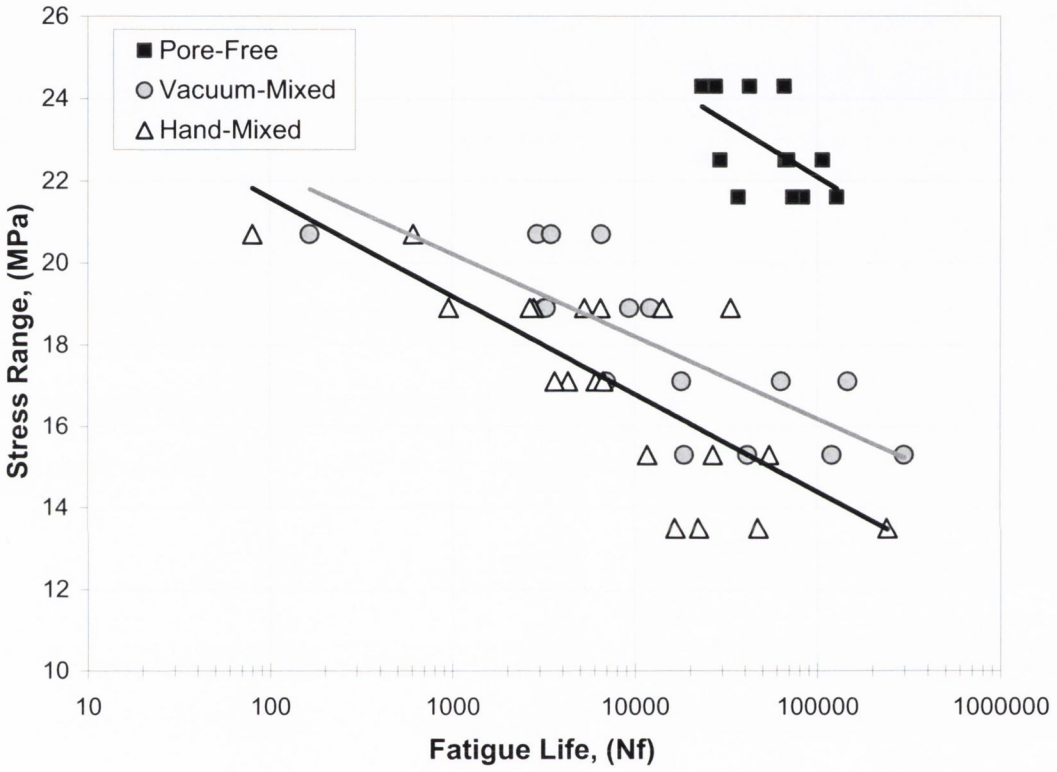

Figure 6.1: Stress-life data for plain specimens of hand-mixed, vacuum-mixed and pore-free bone cement specimens.

6.3. Computational details

Pores were modelled using finite element analysis (Ansys 10.0). A 3D linear elastic analysis was conducted to determine the stresses in the vicinity of the pores. Each model consisted of on average 40,000 10-node tetrahedral elements. The material was modelled as having a Young's modulus of 2.38GPa and Poisson's Ratio of 0.4

(Lewis 1997). In order to generate models of pore clusters that initiated failure *in vitro*, the cluster was examined using a toolmakers microscope to obtain accurate coordinates and dimensions of the pores within the cluster. Accurate models could then be developed manually using Ansys 10.0 (see figure 6.2).

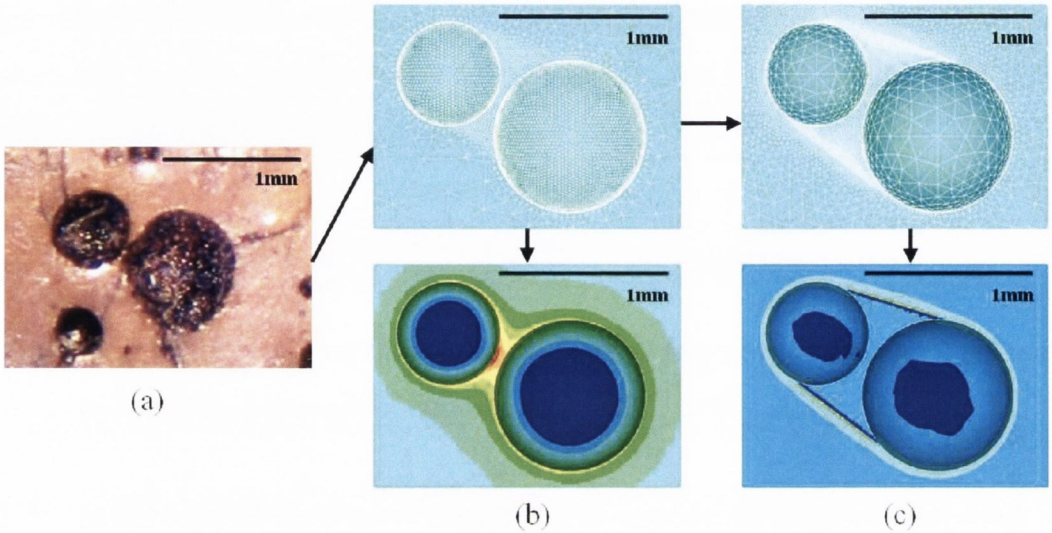

Figure 6.2: (a) Fracture surface of a specimen which failed from a cluster of pores (surface was coated with black ink to highlight the porosity). (b) FEA model of the fracture surface indicating the stress concentration of the two pores. (c) FEA model of a cluster, post initial cracking.

6.4. Results

6.4.1. Pore Size Distribution

It was found that pores in hand-mixed cement followed a lognormal distribution, while the pores in the vacuum-mixed cement followed a weibull distribution (see table 6.1 and figure 6.3). Figure 6.4(a) illustrates the distribution of porosity in a typical sample of hand-mixed cement. As can be seen, there is a considerable distribution of porosity throughout the sample mainly consisting of small pores (micro-porosity). Figure 6.4(b) shows the porosity in a typical vacuum-mixed sample. The image has been inverted to clearly illustrate the porosity. As can be seen the even distribution of micro-porosity found in the hand-mixed cement has

been eliminated by vacuum mixing, however there remains a pore which is much larger than any found in the hand-mixed sample.

	Hand Mixed	Vacuum Mixed
Number of specimens	20	16
Number of pores measured	1209	60
Distribution	Lognormal	Weibull
Distribution Parameters	$\mu = -1.5374$, $\sigma = 0.5625$	a=1.40, b=1.31
y = Density, (mm^{-1}) x = Pore Ø, (mm)	$y = f(x;\mu,\sigma)$	$y = f(x;a,b)$
	$y = \frac{1}{x\sigma\sqrt{2\pi}} e^{\frac{-(\ln x-\mu)^2}{2\sigma^2}}$	$y = ba^{-b}x^{b-1}e^{-\left(\frac{x}{a}\right)^b}$
Mean Pore Ø, (mm)	0.2518	1.2929
S.D. Pore Ø, (mm)	0.1536	0.9973

Table 6.1: Distribution of pore sizes in hand-mixed and vacuum mixed bone cement laboratory specimens.

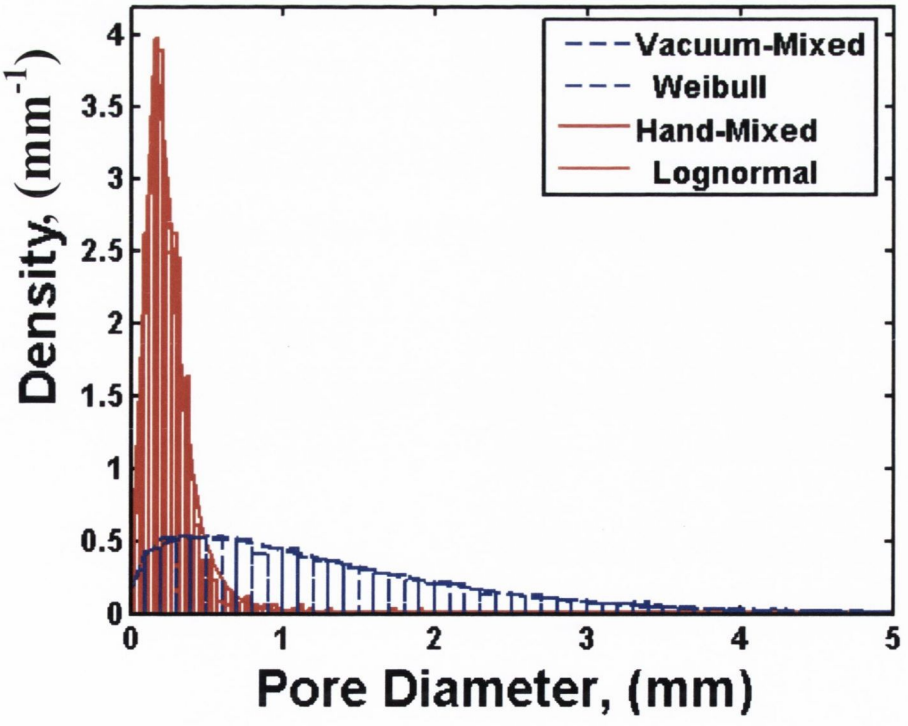

Figure 6.3: Density plot of pore diameters for hand mixed and vacuum mixed bone cement.

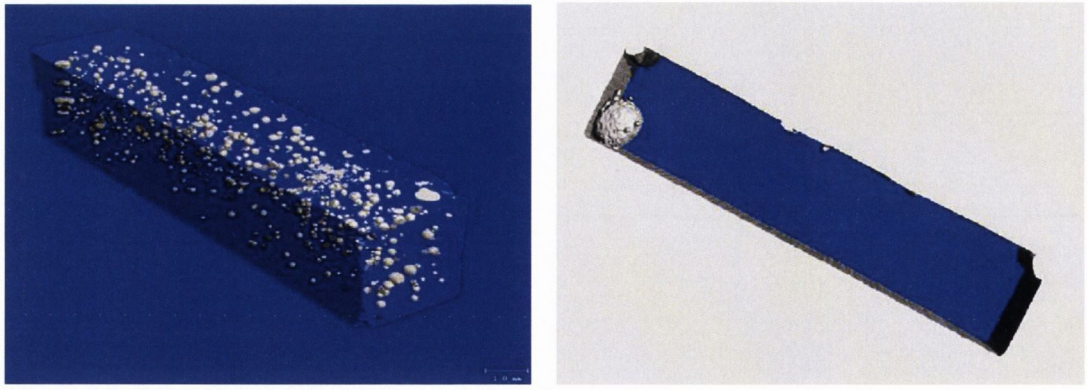

(a) (b)

Figure 6.4: (a) μ-CT image of a hand-mixed plain specimen. The dimensions of the specimen are 16x3.5x3.5mm. (b) Inverted μ-CT image of a vacuum-mixed sample

6.4.2. Pore size

As the TCD has been used successfully in chapter 5 to predict the effect of singular stress concentrations in this material, the theory was again used, to predict the effect of pore size on the fatigue strength of bone cement. As can be seen from figure 6.5, as pore size increases the fatigue strength of bone cement is dramatically reduced, with pores greater than 1mm becoming particularly damaging.

In the literature, porosity is considered as a major defect in bone cement, with numerous studies showing cracks emanating from pores. One would assume the major cause of crack formation is due to the stress concentration set up by a pore. Assuming that pore size is a dominant factor in the failure of bone cement, figure 6.5 should be capable of predicting the fatigue strengths of the three specimen types (hand-mixed, vacuum-mixed and pore free), once the pore size is known. Using the average pore diameters determined above, predictions were made based on pore size.

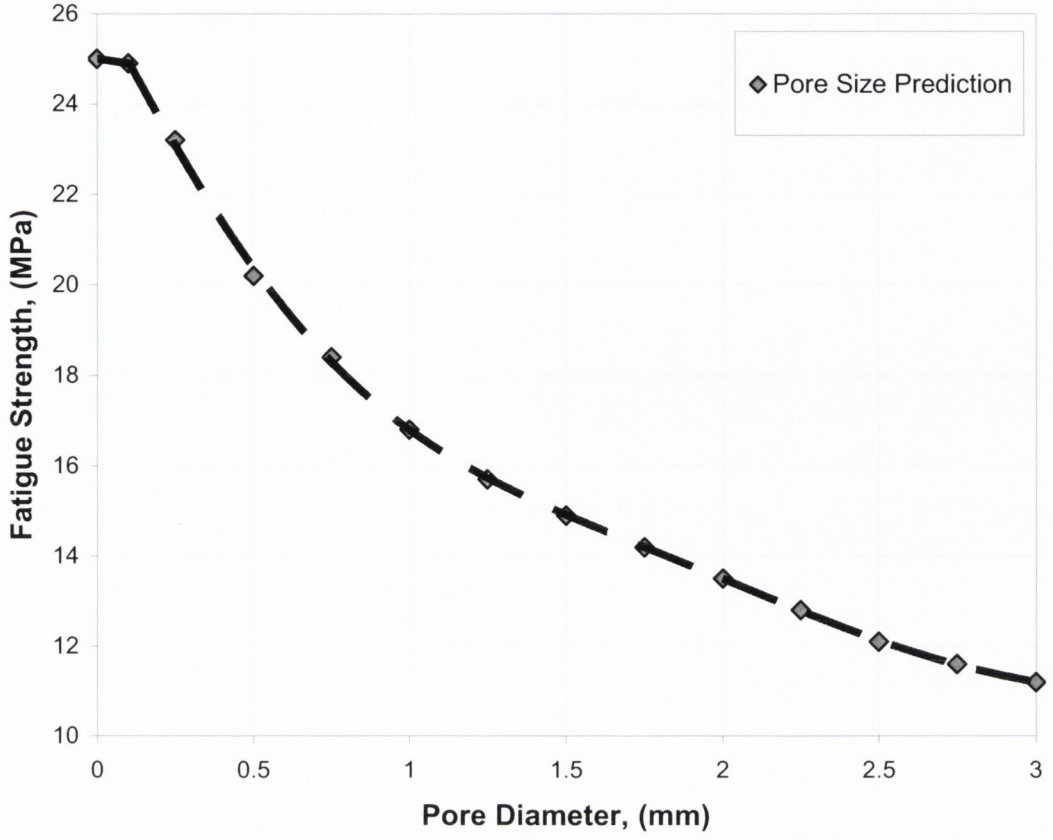

Figure 6.5: Predicted fatigue strengths at 10^5 cycles for singular pores of different diameters in a specimen with a cross-section of 16x3.5mm.

Specimen Type	Pore Free	Vacuum Mixed	Hand Mixed
Average Pore Ø	0.0 mm	1.29 mm	0.25 mm
Experimental Fatigue Strength	22.5 MPa	16.2 MPa	14.4 MPa
Predicted Fatigue Strength	25 MPa	15.58 MPa	23.2 MPa
Error	11.1 %	3.83 %	61.11 %

Table 6.2: Predictions for pore-free, vacuum-mixed and hand-mixed cement based on average pore size.

As can be seen from table 6.2 the pore size prediction works well for the pore-free and vacuum-mixed material. Regarding the pore-free data, it is interesting to note that an accurate prediction was possible even though the material constants were derived from data on porous hand-mixed specimens. In vacuum-mixed cement, porosity appears in the form of large singular pores as is evident from the μ-CT scans shown above. The occurrence of large singular pores is also well documented in the literature (Murphy 2000; Dunne 2003). It is therefore not surprising that the pore size failure criterion achieves acceptable results. However, using pore size to predict failure in hand-mixed cement resulted in a significant overprediction of the fatigue strength. It is therefore clear that pore size alone is not adequate to predict the effect of porosity in hand-mixed cement.

6.4.3. Pore Distribution

From the hand-mixed specimens examined, the point of failure commonly coincided with a collection of pores, indicating that the cluster of pores was responsible for failure. This clustering was also witnessed by many other authors (James 1992a; Murphy 2000; Kurtz 2005) suggesting that clustering may be an important mechanism in practice. It is proposed in this study that due to the high local stresses between pores in close proximity, cracking occurs between the pores at a very early stage. This cracking would essentially link the pores together forming a pore of more complex shape and inevitably higher stress concentration factor. It is then assumed that complete failure of the material will initiate from this pore of more complex shape. To verify this hypothesis, the TCD was used to predict the fatigue strength of six specimens where it was clear that failure initiated from a cluster of pores.

Initially, using the TCD it was predicted whether cracking would occur between the pores. This was done by applying the experimentally applied load to the model and examining the stresses between the pores (see figure 6.2(b)). If the stresses were above the critical stress at the critical distance, it was assumed that cracking would occur, linking the pores. This was found to be true for all specimens. Figure 6.2(c) shows the FE model of the resulting cluster. Predictions were then made by applying the TCD to this model.

Figure 6.6 shows the predicted fatigue strengths of the six specimens analysed, for N_f=100,000 cycles to failure. To provide a comparison, the experimental stress ranges applied to these specimens were adjusted to find the stress range which would have caused failure in this same number of cycles. This adjustment was carried out using the gradient of the stress/life curve, i.e. the slope of the best-fit line for hand-mixed cement in figure 6.1. The experimental and predicted values agreed very well, with a maximum error of 13%. This demonstrates that the TCD can accurately predict the effect of a known cluster of pores.

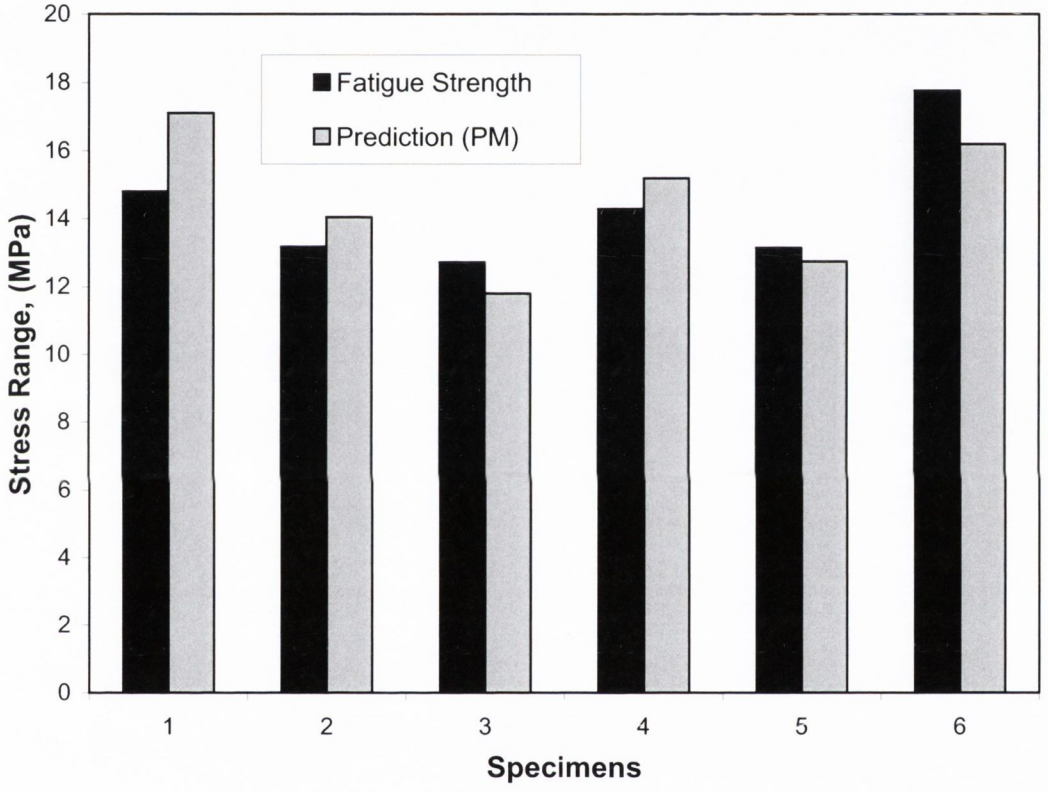

Figure 6.6: Experimental fatigue strength at 10^5 cycles for six specimens where failure initiated from a cluster of pores and a fatigue strength prediction made using the theory of critical distances.

Given that the TCD can be used to predict the effect of clustering, further systematic analyses was conducted. Figure 6.7 predicts the effect of clustering for three different sized pores. The three prediction lines show how fatigue strength changes with pore separation for a cluster of two pores of equal size. Taking the 1mm diameter pore cluster prediction for an example, when the pores are in very close

proximity, (0-0.2mm), cracking between the pores will happen at a very early stage linking the pores together. Once the pores have coalesced the resulting cluster will have a predicted fatigue strength in the region of 13MPa. However, when the pores are a larger distance apart (0.2-0.8mm), larger stresses will be needed to initiate failure between the pores. Once these pores have coalesced the stresses are already so high that the cluster will immediately fail, this is clear from the increase in fatigue strength as the pores move further apart. As the pores move significantly apart, the fatigue strength prediction coincides with the prediction of a single pore (as shown in figure 6.5), indicating that the pores are sufficiently far apart to eliminate the likelihood of clustering occurring.

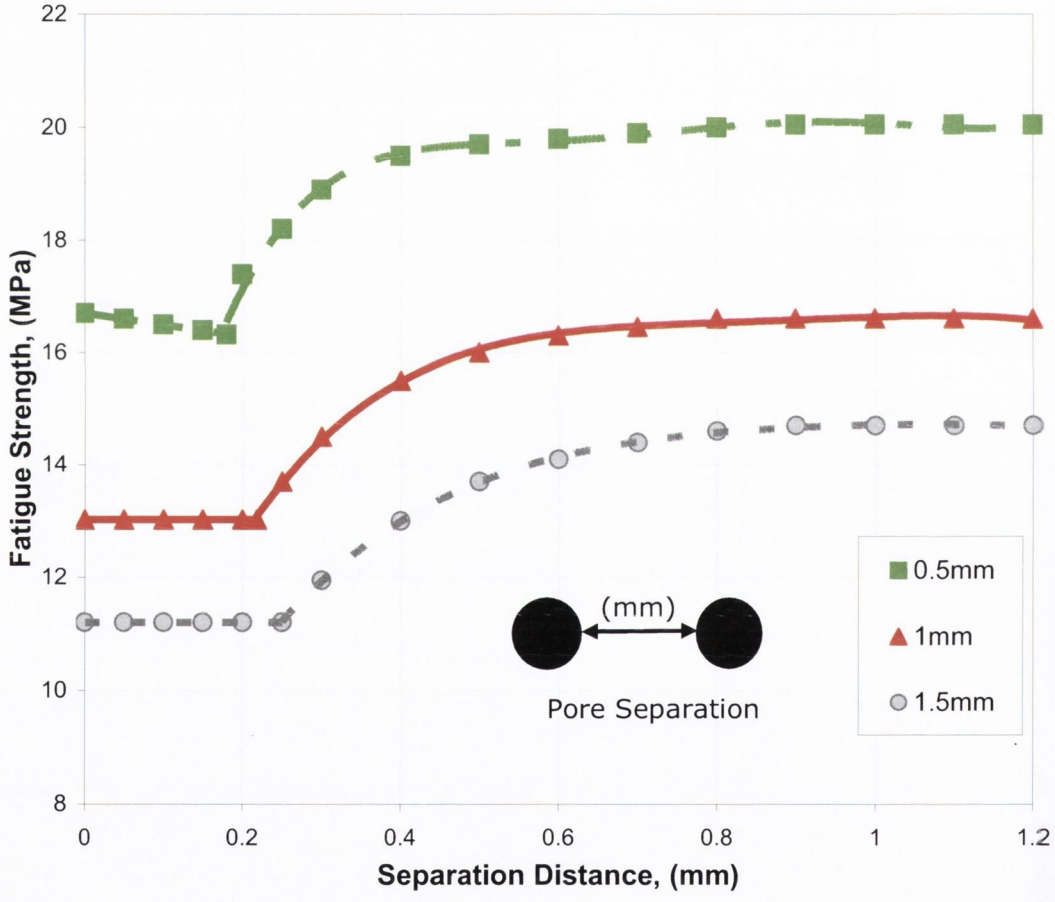

Figure 6.7: Fatigue strength predictions of the clustering effects of porosity, showing the effect of pore separation on fatigue strength at 10^5 cycles for three different pore diameters i.e. for pores of diameter 0.5mm, 1.0mm and 1.5mm.

6.5. Discussion

The role of porosity in the fatigue strength of bone cement has been a controversial topic in recent times, with various studies stating that pores are essentially defects and should be eliminated, while others suggesting that pores are needed for drug dispersion, bone ingrowth and also as a method of blunting propagating cracks. Therefore a quantitative understanding of the effects of porosity on bone cement is indispensable to determining a compromise.

On comparing the fatigue strengths at 10^5 cycles of pore-free cement to hand-mixed and vacuum-mixed cement it is clear that porosity is a harmful defect which results in a significant decrease in life. The damaging effect of porosity is twofold. Firstly, the presence of porosity causes a decrease in the load bearing area, which in turn will result in an increase in the nominal stress. Secondly, the presence of porosity will result in stress concentration. However, the mode of stress concentration is different depending on the method used to prepare the cement.

This analysis has established that pore size is the dominant contributor to failure in vacuum-mixed cement; explaining the difference between the fatigue strength of pore-free and vacuum-mixed material (see table 6.2). Evans *et al* (Evans 2006) suggested that larger pores are more dangerous because a crack emanating from a large pore would spend more time in the stress concentration and so will grow quicker. This size effect is well captured by the TCD analysis. Regarding the hand-mixed cement, pore size alone was not capable of predicting failure. From examination of the fracture surfaces, it was clear that pore distribution was an important factor, with pores in close proximity interacting to increase the likelihood of failure. It is interesting to compare the systematic analyses of the effect of pore size and pore distribution (figures 6.5 and 6.7), as it was found that a single pore of 2mm diameter or more would cause a significant decrease in the fatigue strength, however two pores of only 1mm diameter in close proximity would be equally damaging, demonstrating the importance of not only pore size but pore distribution. More importantly looking at the hip construct itself, numerous studies have found pores preferentially forming at the stem-cement interface. This preference seems to

be due to polymerisation shrinkage of the cement. As this interface has been highlighted as a weak zone in the hip construct the occurrence of pore clustering in this area should be a major concern.

It is unclear whether porosity is the main contributor to failure in the cement *in vivo* (Ling 1998; Janssen 2005b). However it is unquestionable that porosity is detrimental to the fatigue strength of laboratory specimens with pore size and pore distribution being particularly important (Murphy 2000; Dunne 2003). Nevertheless, porosity has also been associated with beneficial effects. The release of antibiotics from the cement requires the penetration of dissolution fluids, which requires a certain level of porosity (Baker 1988; van de Belt 2000). The presence of porosity can encourage bone ingrowth, resulting in a better fixation of the prostheses (Bruens 2003; Karageorgiou 2005) and finally it has been suggested that pores could act to blunt propagating cracks (Topoleski 1993). Therefore it is clear that a compromise may be a viable solution. Given the findings of this chapter a possible step forward in the development of surgical bone cements may involve a compromise consisting of an even distribution of relatively small pores, eliminating the detrimental effects of large pores and of the phenomenon of clustering that was quantified in this chapter. Crucial factors here are the size distribution and number-density of pores, which will combine to determine the probability of a large pore or a cluster occurring; this issue is addressed in chapter 7.

Some limitations of the present chapter should be mentioned. The cement used in this study does not contain additives such as radiopaque agents which have been known to act as an alternative source of fatigue cracking in some surgical bone cements. However as this study aimed to understand the role of porosity in bone cement it was preferable not to have other stress concentration features in the material. Predictions were made for a finite number of cycles to failure (10^5 cycles), i.e. the length of time for a crack to initiate and grow entirely through the specimen. This represents a relatively short time *in vivo*, of the order of one month; however data for larger numbers of cycles to failure were not available owing to the very long testing times involved. The methodology and general conclusions however will be applicable to longer times of the order of 1-10 years *in vivo*. The predictions were made using only the initial conditions of crack growth and do not consider

how the crack would grow throughout the specimen. Nevertheless, a crack in this material will be relatively small for the majority of its life and so the stress field surrounding the defect mostly controls the crack's behaviour. It is worth noting that the stress field *in vivo* is rather more complex than that found in a tensile specimen due to design features such as the stem. Therefore, the relationship between porosity and clinical failure may be different to that found in this chapter; this issue is addressed in chapter 9.

6.6. Conclusions

1) The fatigue life of both hand-mixed and vacuum-mixed cement is significantly reduced by porosity. Failure initiated from large pores (common in vacuum-mixed cement) or from clusters of pores in close proximity (common in hand-mixed cement).

2) Singular pores can concentrate stress resulting in crack initiation and failure of the material; the size of the pore has a strong effect in reducing fatigue strength. The TCD can predict the effect of singular pores and is also very effective in predicting this size effect.

3) Pores in close proximity can result in localised stress concentration and cracking between the pores forming a new pore of more complex shape. The TCD can be used to predict this clustering effect and further systematic analyses of clustering revealed the extent to which this phenomenon is detrimental to the fatigue strength of bone cement.

4) It is clear that porosity can be damaging to the fatigue strength of bone cement but it also has been associated with several beneficial effects. Therefore in order to maintain these benefits a possible solution may be a compromise of small evenly distributed pores throughout the cement mantle.

Chapter 7

Porosity in Bone Cement

Probability of failure

7.1. Introduction

The role of porosity in the fatigue strength of bone cement was quantified in chapter 6, where it was shown that pore size and pores in close proximity play a major role in the fatigue failure of the material. However, crucial factors in failure are the size distribution and number-density of pores, which will combine to determine the probability of a large pore or cluster occurring. Therefore in order to predict the fatigue strength of a porous material, these factors need to be taken into account, resulting in a predicted range of fatigue strengths.

Therefore this chapter had the following aims:

a) Conduct experimental testing to determine a relationship between porosity level and fatigue life for both hand-mixed and vacuum mixed cement.

b) Create a virtual specimen of bone cement using the size distribution of pores determined in chapter 6.

c) Incorporate the effect of porosity previously quantified in chapter 6 into the virtual specimens and use this to predict the behaviour of porosity determined from the experimental testing.

d) Use this model to determine the probability of a large pore or a cluster of pores occurring in both hand-mixed and vacuum-mixed cement

7.2. Experimental details

Bone cement samples were prepared by both hand-mixing and mixing the cement under a vacuum in an attempt to reduce porosity. The mixture was then transferred to a mould, and allowed to set for one hour. This produced tensile samples as described in chapter 4.

All fatigue testing was conducted on an Instron servo-hydraulic testing machine (Model 8501). The cyclic stress employed was sinusoidal at a frequency of 3Hz; the ratio of minimum stress to maximum stress (R) was kept at a constant value of 0.1. Each sample was tested in pure tension under load control, in a water bath at 37°C.

7.3. Experimental results

Ten samples of hand-mixed and vacuum-mixed bone cement were fatigue tested at the same stress range (15.3MPa) and the number of cycles to failure was recorded. For each sample tested, the fracture surface percentage porosity (2D) and bulk percentage porosity (3D) were determined (see section 4.7). The results are represented here on plots of percentage porosity against number of cycles to failure.

Figures 7.1 and 7.2 represent the effect of porosity on the fatigue strength of hand-mixed and vacuum-mixed bone cement respectively. Regarding the hand-mixed data, a negative correlation between porosity level and fatigue life is evident. However there is considerable scatter in the results, making the results difficult to interpret. This scatter is highlighted in the R values where R is the correlation coefficient (0.268 – 3D, 0.56 – 2D). Regarding the vacuum-mixed data, a more definite negative correlation is evident and is reflected in the R values, however significant scatter is still present (0.66 – 3D, 0.693 – 2D).

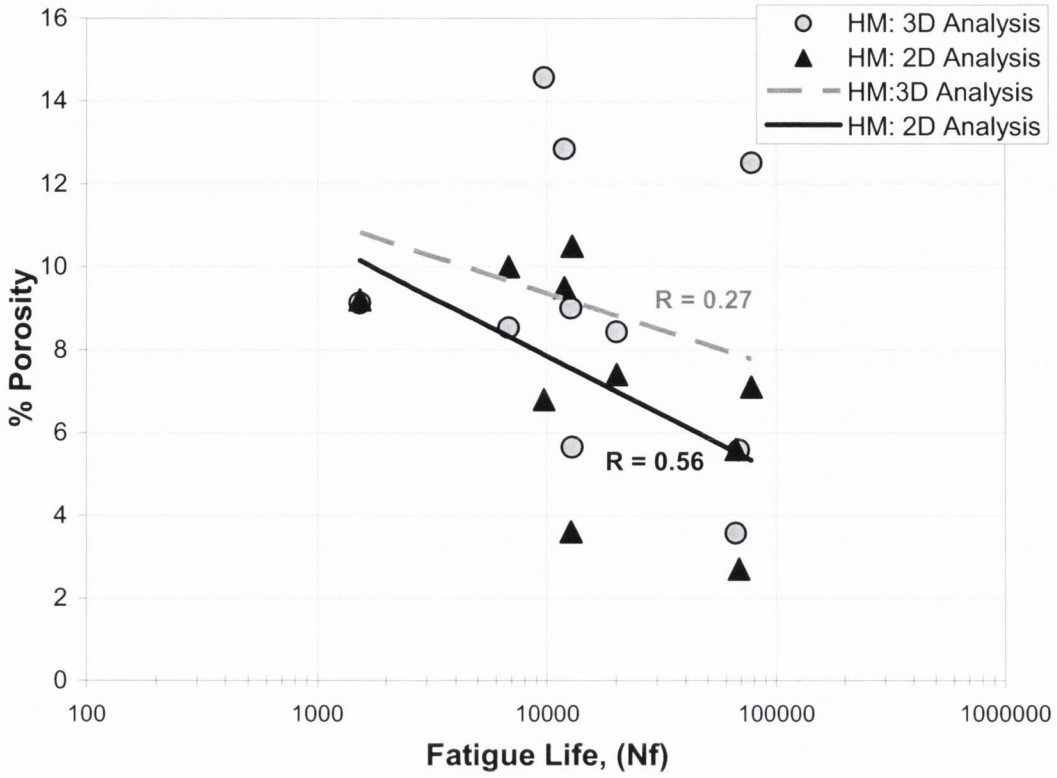

Figure 7.1: Percentage porosity as a function of number of cycles to failure, for plain hand-mixed specimens.

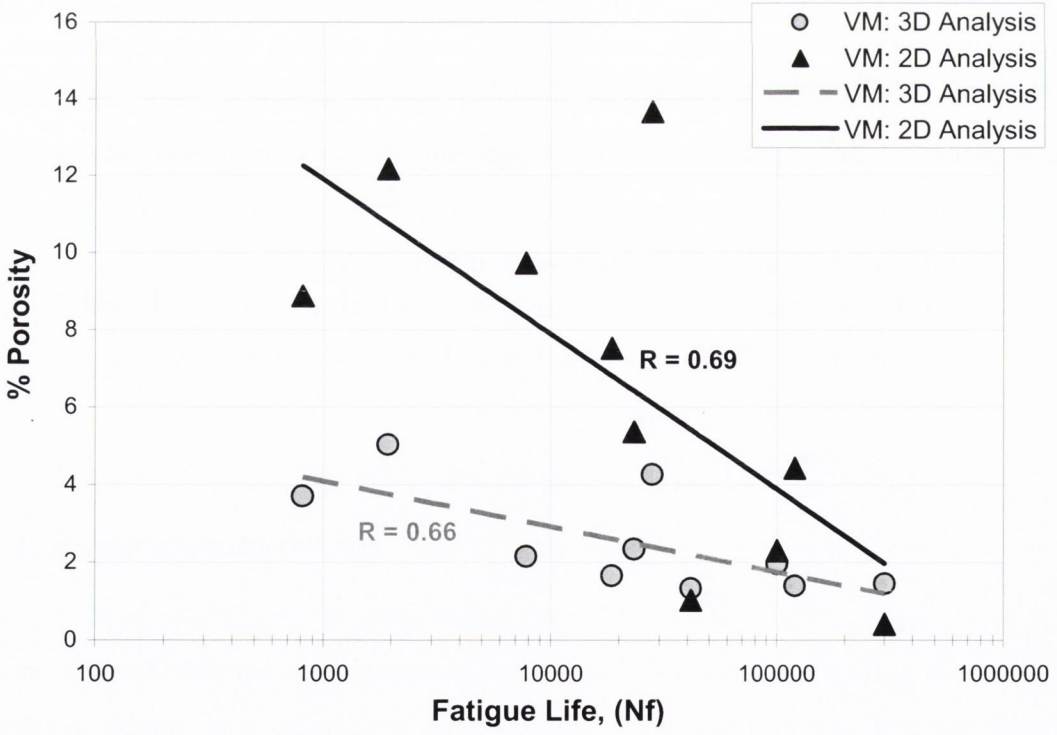

Figure 7.2: Percentage porosity as a function of number of cycles to failure, for plain vacuum-mixed specimens.

7.4. Computational Details

Crucial factors in the failure of porous bone cement are the size distribution and number-density of pores. The pore size distribution was determined for both hand-mixed and vacuum-mixed cement in chapter 6 and is reproduced below (see table 7.1). For hand-mixed bone cement, the pore size distribution was lognormal while for vacuum-mixed bone cement, the distribution followed a Weibull distribution. Virtual bone cement test specimens could then be created using MatLab (7.0), taking into account these factors. Both 2D and 3D virtual specimens were created for both hand-mixed and vacuum-mixed cement.

	Hand Mixed	**Vacuum Mixed**
Distribution	Lognormal	Weibull
Distribution Parameters	$\mu = -1.5374$, $\sigma = 0.5625$	a=1.40, b=1.31
y = Density, (mm^{-1}) x = Pore Ø, (mm)	$y = f(x;\mu,\sigma)$	$y = f(x;a,b)$
	$y = \frac{1}{x\sigma\sqrt{2\pi}} e^{\frac{-(\ln x-\mu)^2}{2\sigma^2}}$	$y = ba^{-b}x^{b-1}e^{-\left(\frac{x}{a}\right)^b}$

Table 7.1: Distribution of pore sizes in hand-mixed and vacuum-mixed cement.

7.4.1. 2D virtual specimen

The 2D virtual specimens consisted of the same dimensions to that of the fracture surface of the experimental specimen, i.e. 16x3.5mm. An illustration of a 2D hand-mixed and vacuum-mixed virtual specimen is given in figure 7.3. The X-Y plane corresponds to the fracture plane of an experimental specimen. The location of pores was assumed random and the number of pores could be varied to achieve different levels of porosity.

Porosity can increase the likelihood of failure in two ways: reducing the load bearing area and concentrating stress. The effect of porosity in reducing the load bearing area was incorporated into the virtual model using the gradient of the plain SN data collected in chapter 5. The effect of porosity in concentrating stress can be

split into a further two ways: the effect of pore size and the effect of pore clustering. As the experimental specimens were loaded at a stress range of 15.3MPa, the effect of pore size on the fatigue strength quantified previously (see figure 6.5) was converted to the effect of pore size on fatigue life at an applied load of 15.3MPa (see figure 7.4). This was achieved using the same gradient as above. This graph can be imported into the model giving a prediction for pore size.

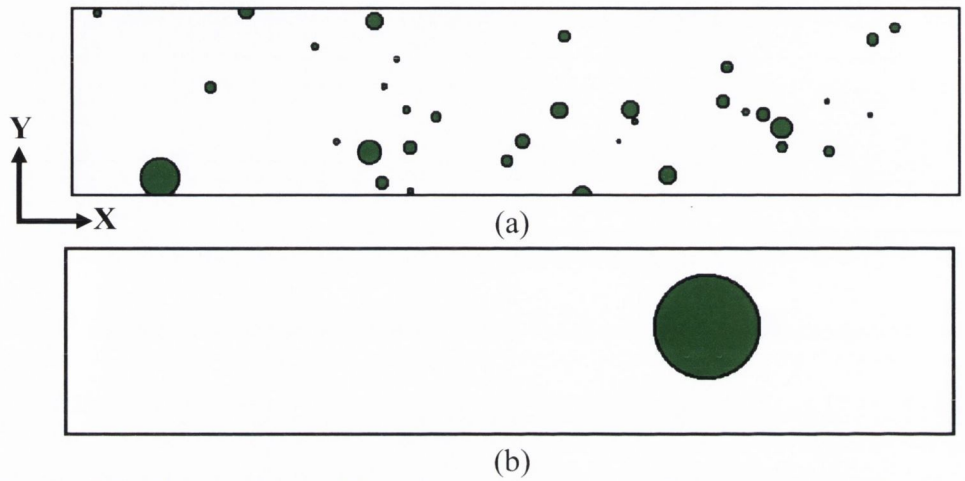

Figure 7.3: Illustration of 2D virtual specimens. (a) 3% porosity hand-mixed and (b) 5.1% porosity vacuum-mixed (dimensions: 16x3.5mm).

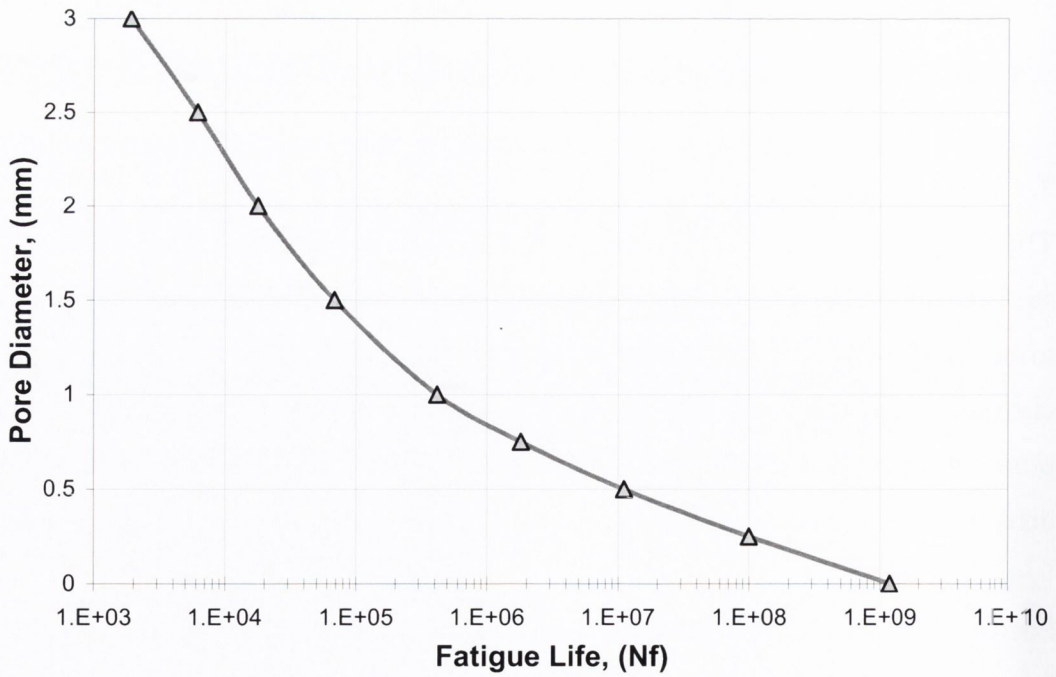

Figure 7.4: Effect of pore size on fatigue life of a bone cement sample loaded at a stress range of 15.3 MPa

Incorporating the effect of pore interaction is more complicated. The effect of pore clustering was quantified in the previous chapter for pores of the same geometry. As this is most certainly not the case in reality and given that quantifying all possible likelihoods of a cluster is unrealistic, a simpler approach to quantify pore clustering was determined. This simpler approach implicated the following rules. A cluster was declared if the surfaces of two pores were within 0.2mm of one another. This parameter was chosen because a cluster was shown to be most damaging when this criterion was met (see figure 6.7). Given that a cluster was declared, the effect of this cluster was assumed to be that of a singular pore equal in size to the cluster of pores, (the rules are illustrated in figure 7.5). This approach allowed the graph demonstrating the effect of pore size to predict all possible scenarios. This simplified approach was verified by predicting the fatigue strength of the six clusters previously predicted using the alternative method (see figure 6.6). The simplified approach was found to be less accurate but was still capable of predicting the effect of all clusters within 20%.

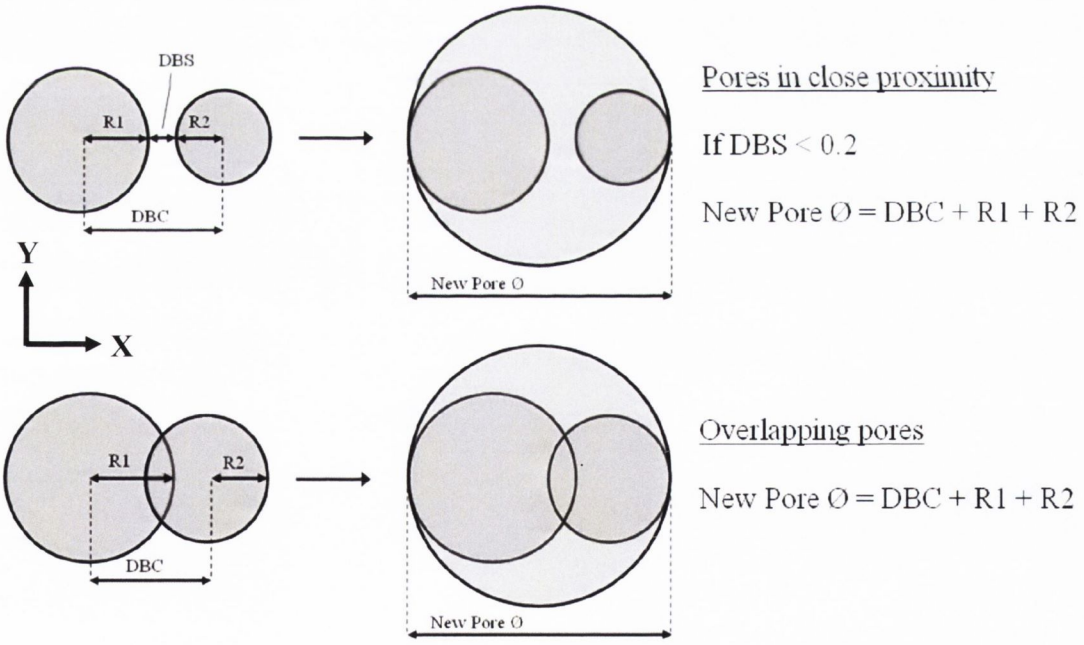

Figure 7.5: Schematic of rules developed to incorporate pore clustering into the virtual specimens. R = radius; DBC = distance between centres; DBS = distance between surfaces; All measurements in mm.

7.4.2. 3D virtual specimen

The 3D virtual specimens consisted of the same dimensions to that of the experimental specimens used to determine the 3D porosity level, i.e. 16x3.5x3.5mm. An illustration of a 3D hand-mixed and vacuum-mixed virtual specimen are given in figure 7.6. The X-Y plane corresponds to the fracture plane of an experimental specimen with the load being applied in the Z direction. The location of pores was assumed random and the number of pores could be varied to achieve different levels of porosity.

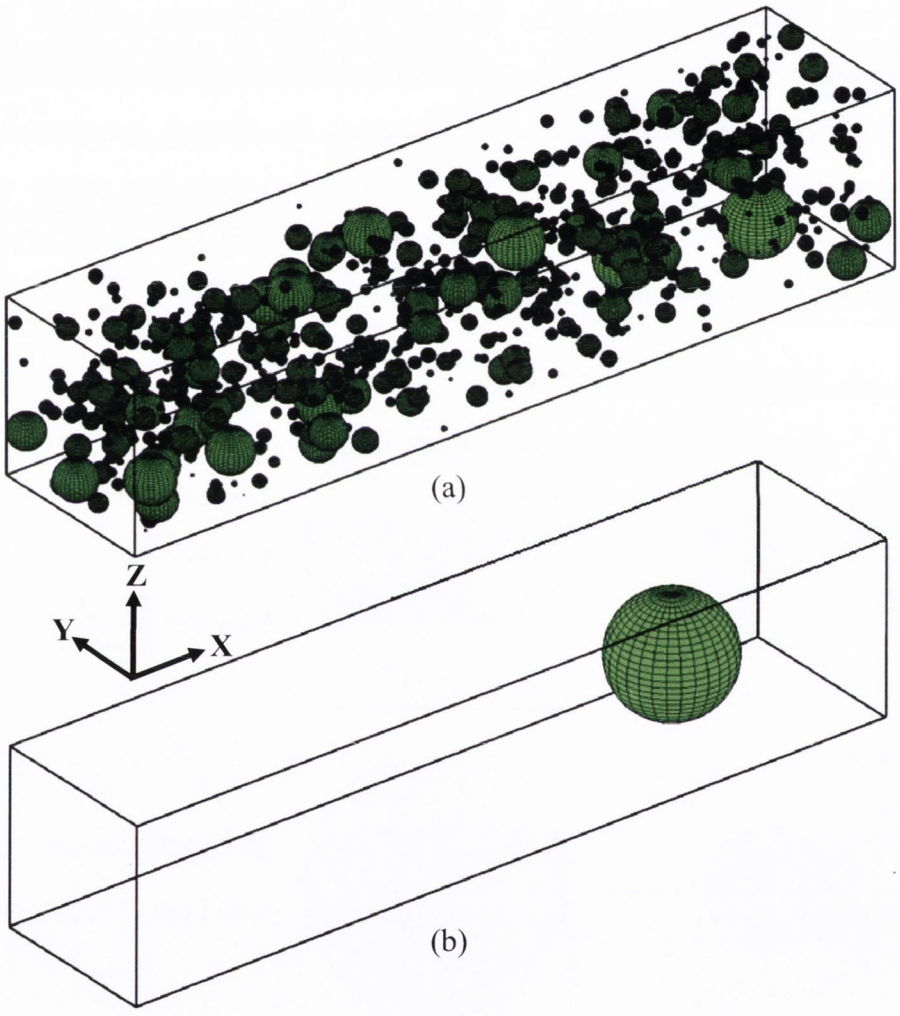

Figure 7.6: Illustration of 3D virtual specimens. (a) 8.9% porosity hand-mixed and (b) 1.5% porosity vacuum-mixed (dimensions: 16x3.5x3.5mm).

The same approach to predict the fatigue life of a 2D virtual specimen can be applied to the 3D model. However the definition of a cluster is more complicated in

a 3D scenario. The added complexity arises from the proximity of pores in the Z-direction, i.e. is a pore directly above or below a corresponding pore. A spherical pore experiencing a uniaxial load will generate tensile stresses surrounding its 'equator' but will generate compressive stresses at its 'poles', therefore no crack will grow from the top or bottom of the pore (see figure 7.7). This needs to be taken into account when defining a cluster in a 3D scenario. The distance between the centres of two pores in the Z direction will be referred to as the Z-value.

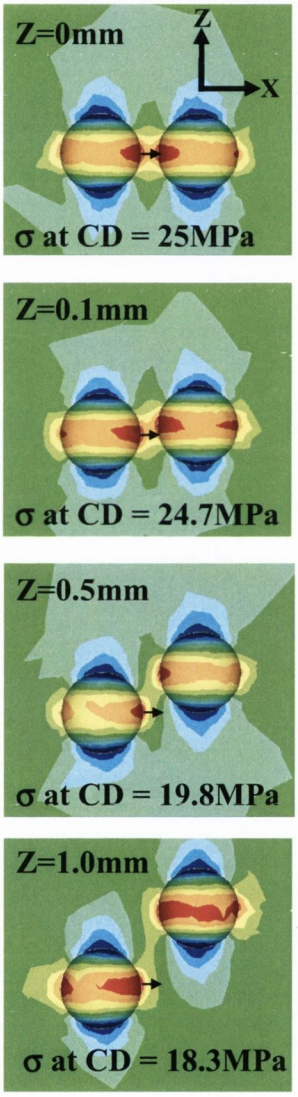

An example of the effect of the Z-value on cluster formation is demonstrated in figure 7.7. The top image in figure 7.7 illustrates the stress distribution surrounding two 1mm diameter pores, 0.2mm apart, located on the same plane, i.e. Z=0. From an applied load of 12.9MPa the stress at the critical distance from the edge of the pore on the left is 25MPa, therefore the TCD predicts that these pores will cluster. The subsequent images represent the same pores, with the same applied load, but the pore on the right is slightly above the pore on the left, i.e. the Z value is equal to 0.1, 0.5 and 1.0mm. As the Z value becomes larger the stress concentration between the pores becomes less, decreasing the likelihood of the two pores forming a cluster. It is clear from figure 7.7 that once the Z value is approximately half the diameter of the two pores in question the stress at the critical distance is significantly lower than 25MPa, indicating that the pores will not cluster.

Figure 7.7: Stress distribution surrounding two 1mm diameter pores in close proximity with different Z-values. The black arrow indicates the path direction chosen when applying the TCD to predict failure between the pores

Although it is clear that the Z-value will change depending on the size of the pores in question, in order to incorporate cluster formation in the Z-direction into the model, a Z-value is required for both pore size distributions, i.e. for hand-mixed and

vacuum-mixed cement. It is evident from figure 7.7 that a Z-value of approximately half the diameter of the pores in question is a fair estimate of the correct Z-value. Therefore for this model, a Z-value corresponding to the radius of the average pore size for a given pore size distribution was chosen, i.e. Z=0.1259mm for hand-mixed cement and Z=0.6464mm for vacuum-mixed cement (average pore size taken from table 6.1). Therefore a cluster is defined in a 3D specimen if the centres of two pores are within the specific Z-value in the Z direction and the surfaces of the pores are within 0.2mm of each other on the X-Y plane. Once a cluster is defined, the size of the resulting cluster follows the same rules demonstrated in figure 7.5.

A flowchart illustrating the steps involved in making a prediction is presented in figure 7.8.

7.5. Computational results

7.5.1. Hand-mixed bone cement

Ten thousand virtual hand-mixed specimens were created and the TCD based failure criterion derived in section 7.4 was used to predict their fatigue lives. The virtual results for the 2D and 3D analysis are represented in figures 7.9 and 7.10 respectively. The hand-mixed experimental results are plotted again for the purpose of comparison.

7.5.2. Vacuum-mixed bone cement

Ten thousand vacuum mixed specimens were also created and the results for the 2D and 3D analysis are represented in figures 7.11 and 7.12 respectively. Also shown in these figures are the experimental results for the vacuum-mixed cement shown previously.

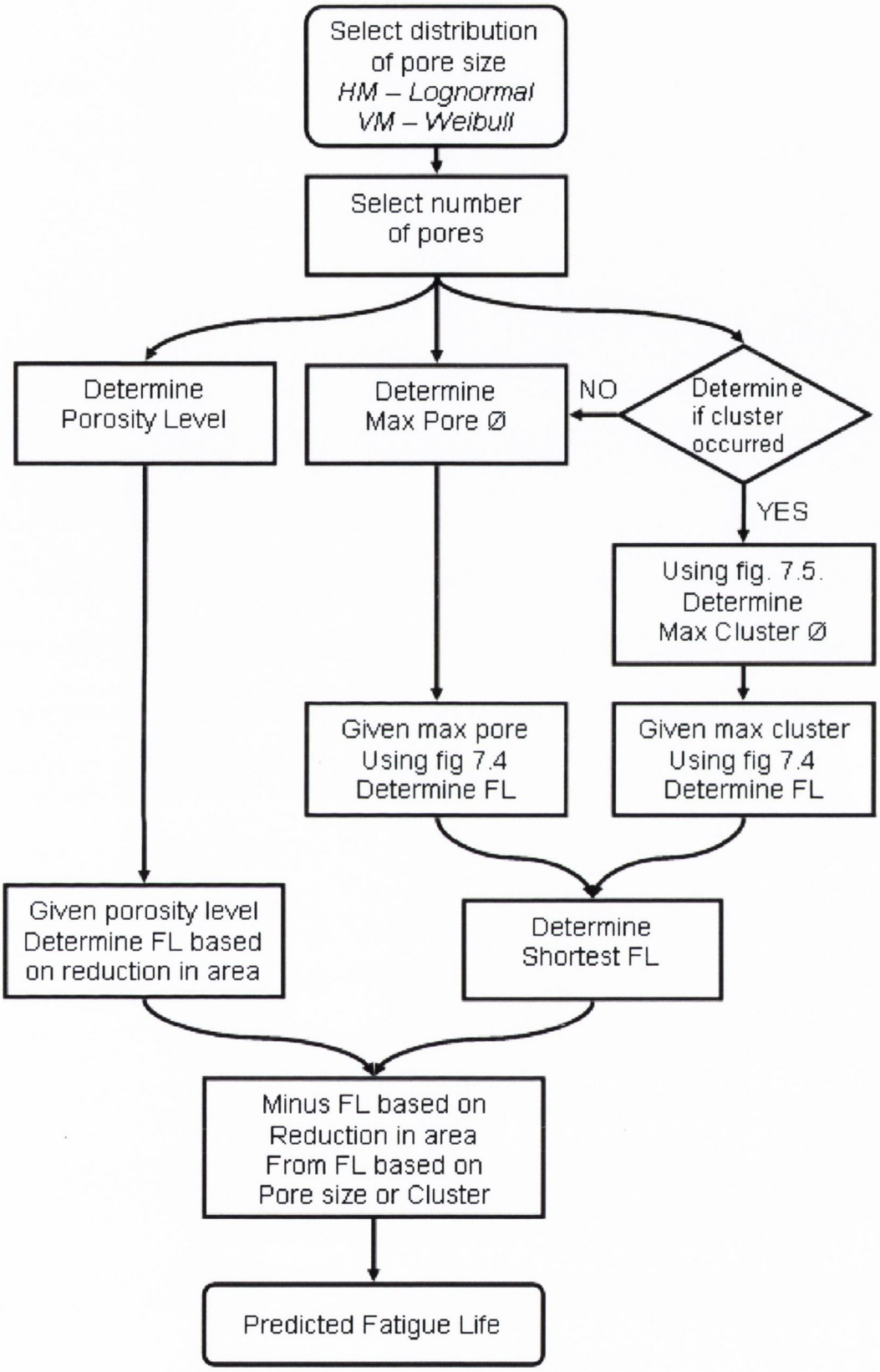

Figure 7.8: Flowchart illustrating the steps involved in making a fatigue life prediction of a virtual bone cement specimen

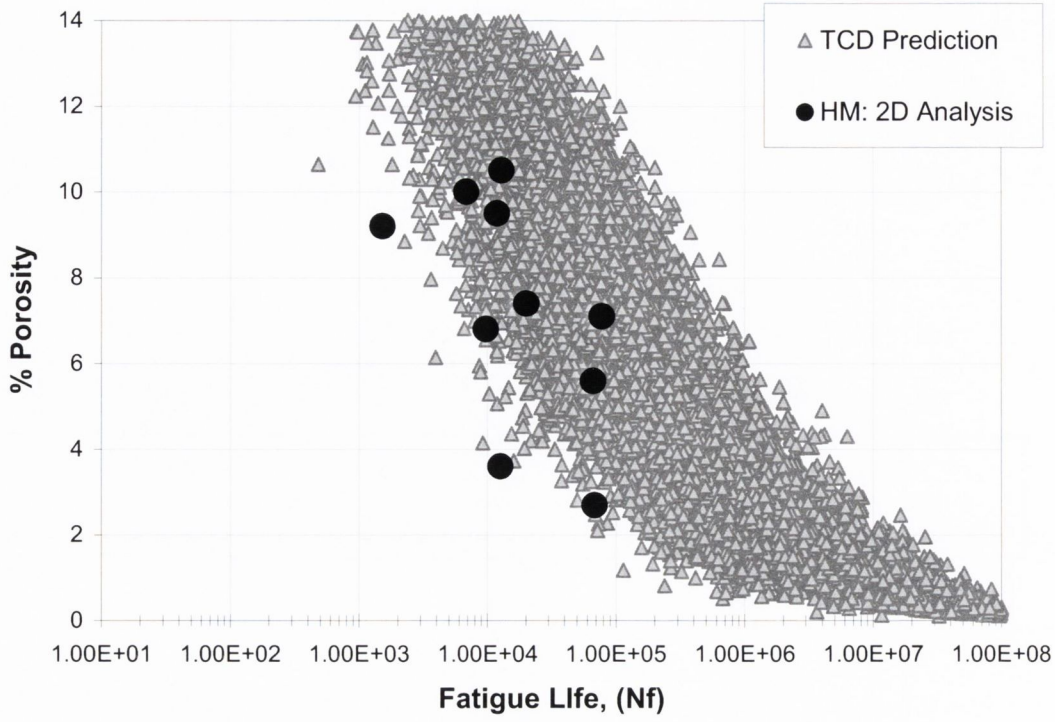

Figure 7.9: Percentage porosity as a function of N_f, for plain hand-mixed 2D virtual specimens. The experimental 2D HM data is also shown for comparison.

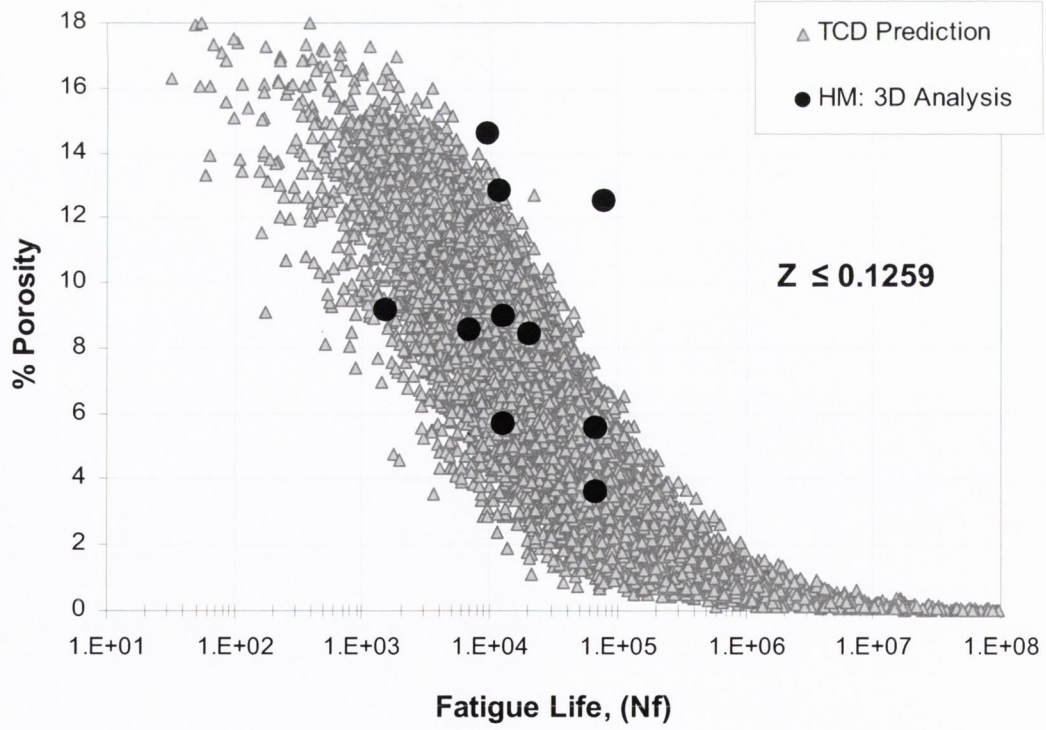

Figure 7.10: Percentage porosity as a function N_f, for plain hand-mixed 3D virtual specimens. The experimental 3D HM data is also shown for comparison.

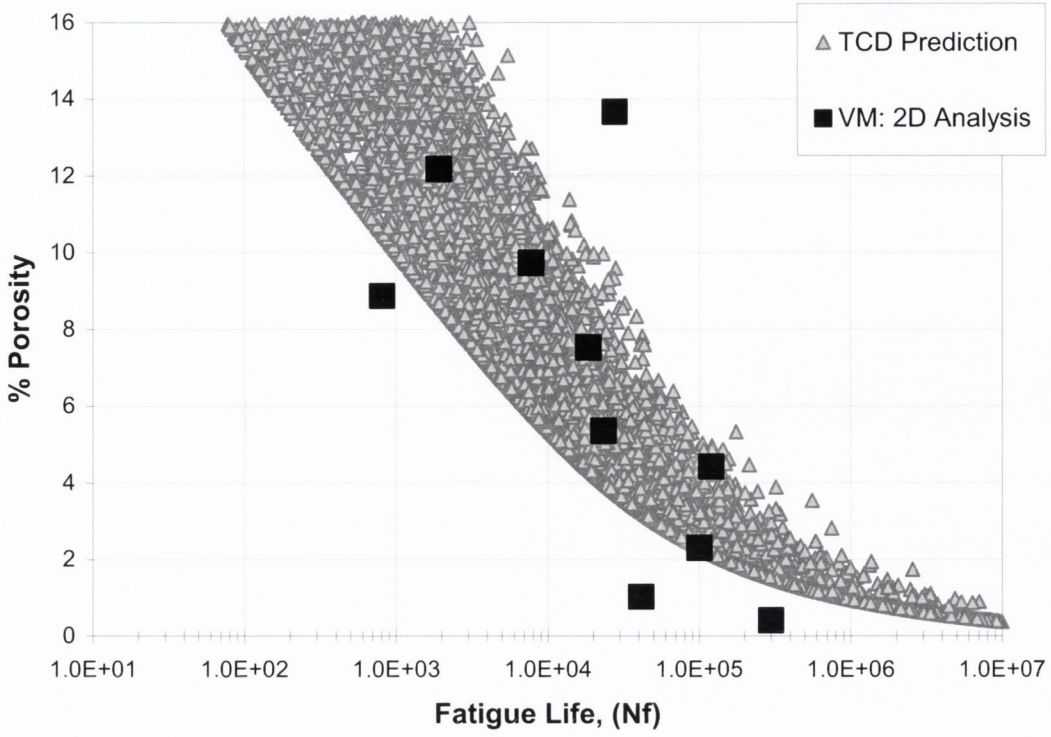

Figure 7.11: Percentage porosity as a function of N_f, for plain vacuum-mixed 2D virtual specimens. The experimental 2D VM data is also shown for comparison.

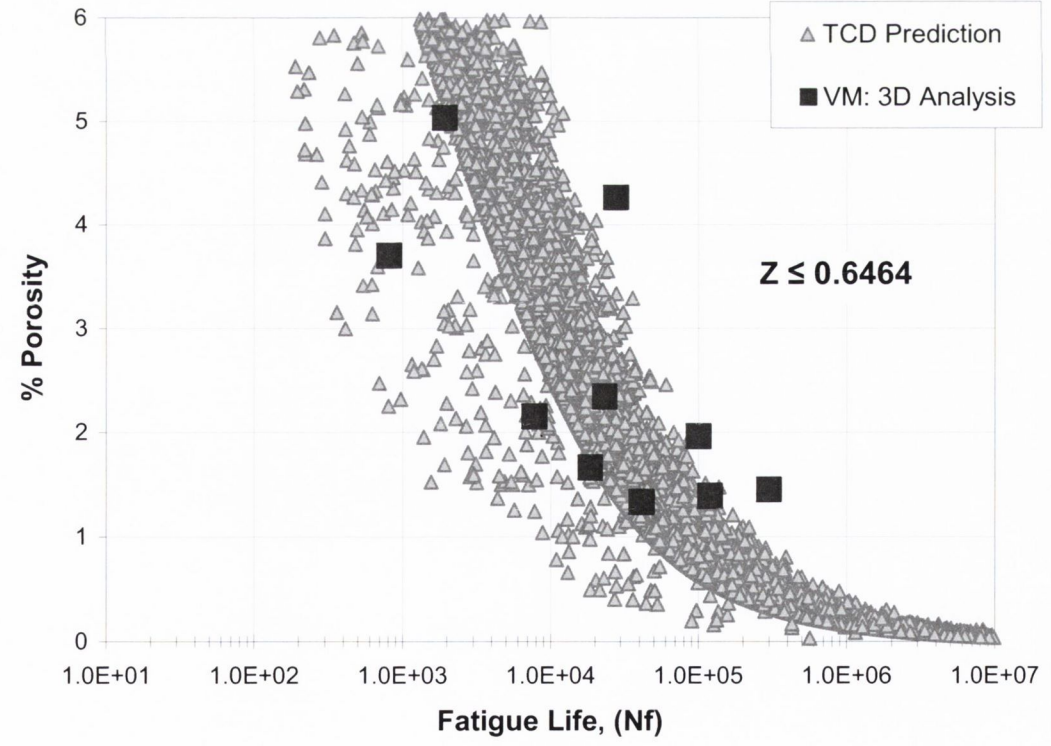

Figure 7.12: Percentage porosity as a function of N_f, for plain vacuum-mixed 3D virtual specimens. The experimental 3D VM data is also shown for comparison.

7.5.3. Probability of a cluster

Given the definition of a cluster in section 7.4, the virtual specimens can be used to determine the probability of a cluster occurring. Figure 7.13 represents the probability of a cluster occurring in hand-mixed 3D virtual cement specimens for different percentage porosities and also for different Z-values. As would be expected, decreasing the Z-value decreases the probability of a cluster occurring. However the probability of a cluster occurring is 1 for all Z-values above 5% porosity which is significant considering all but one experimental specimen had porosity levels greater than 5, indicating that clustering is a very likely phenomenon in practice.

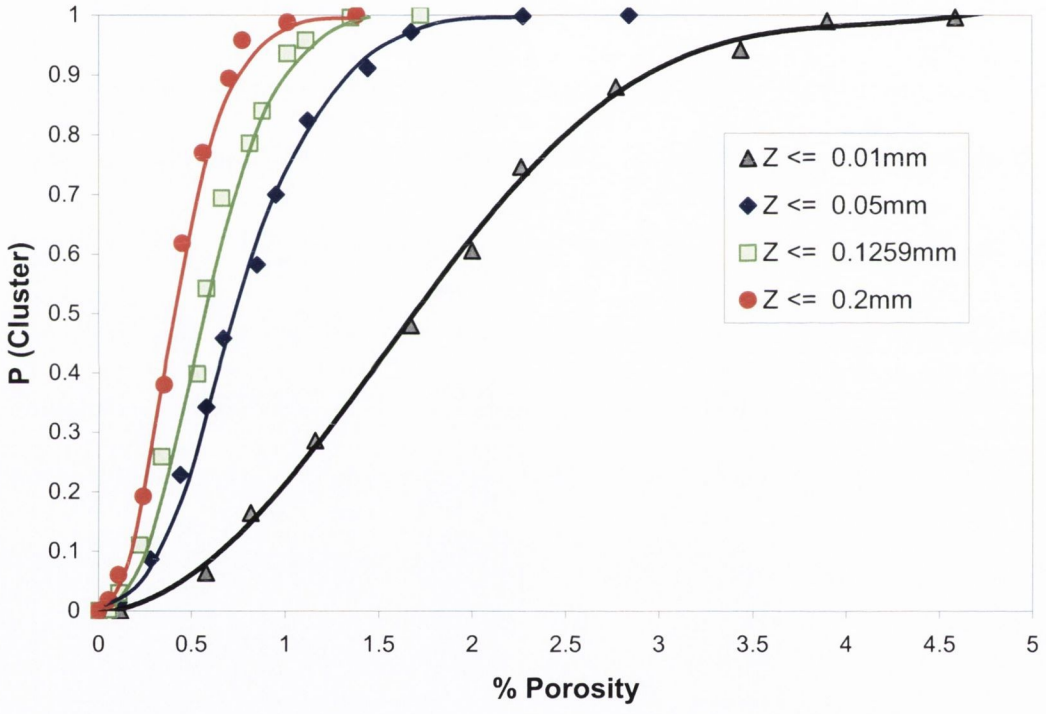

Figure 7.13: Probability of a cluster occurring in hand-mixed virtual specimens at different percentage porosities and different Z-values.

A similar analysis was conducted for vacuum-mixed cement but it was quickly determined that the phenomenon of clustering was extremely improbable. For example, the probability of a cluster occurring in a vacuum-mixed 3D virtual specimen containing 5% porosity and setting the Z-value to 0.6464mm was 0.06. Given that 5% porosity is the highest level recorded experimentally; this result verifies the unlikelihood of a cluster occurring in vacuum-mixed cement.

7.5.4. Probability of a large pore

The virtual specimens were also used to determine the probability of a large pore occurring. For this analysis a pore diameter of 1mm was chosen. Although this is not necessarily a very large pore, it was chosen so the results would be within a realistic range of porosities. Figure 7.14 represents the probability of finding a pore with a diameter greater than 1mm in both hand-mixed and vacuum-mixed cement. It is interesting to see that the probability is very similar for both forms of cement despite the pore size distributions being very different. This can be attributed to the number of pores found in hand-mixed cement. Despite the average pore diameter in hand-mixed being only 0.25mm, the number of pores is great therefore there is a greater probability of finding at least one large pore. For example, comparing the 3D virtual specimens created in this chapter, to achieve 6% porosity an average of 550 pores were required for the hand-mixed cement while on average only 3 pores were needed for the vacuum-mixed cement.

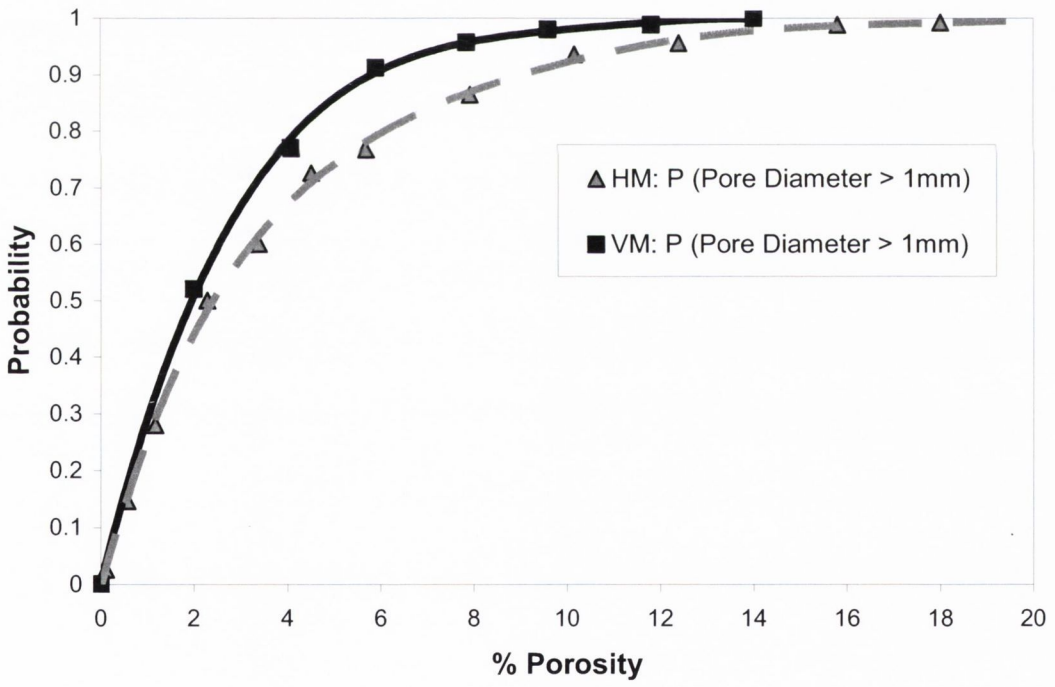

Figure 7.14: Probability of finding a pore with diameter greater than 1mm in hand-mixed and vacuum-mixed cement.

This then raises the question, is pore size or pore clustering the dominant contributor to failure in hand-mixed cement? To answer this question the

probability of finding a cluster with a diameter greater than 1mm was compared to that of finding a singular pore with a diameter greater than 1mm. As can be seen from figure 7.15, finding a cluster with a diameter greater then 1mm is more probable than finding a singular pore, especially at higher porosity levels indicating that clustering is indeed the dominant contributor to failure in hand-mixed bone cement.

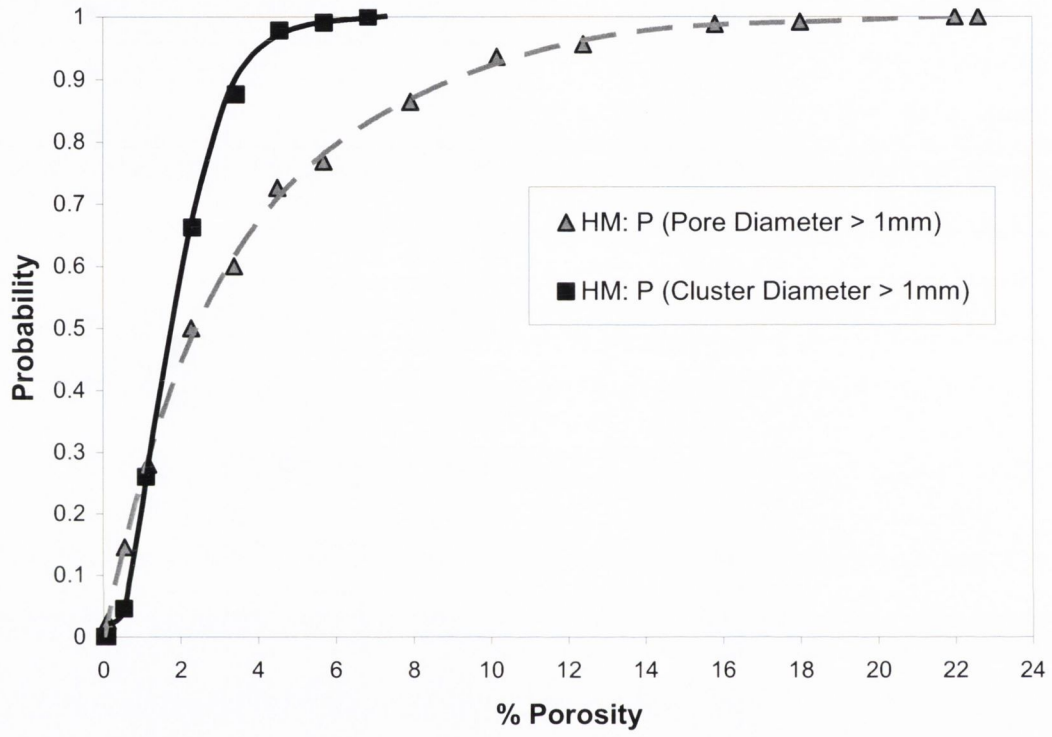

Figure 7.15: Probability of finding a singular pore or a cluster with a diameter greater than 1mm in hand-mixed cement at different porosity levels. The cluster was defined as having a Z-value of 0.1259mm.

7.6. Discussion

This chapter has demonstrated a negative correlation between porosity level and fatigue life in both hand-mixed and vacuum-mixed bone cement. Considerable scatter was present in the experimental results making them difficult to interpret. This negative correlation and scatter was predicted using a TCD based failure

criterion. This failure criterion allows the reader to gain a significant insight into the statistical distribution of the fatigue strength of porous bone cement and indeed any porous brittle material.

The effect in changing the Z-value is illustrated in figure 7.13. It is clear that increasing the Z-value increases the likelihood of a cluster occurring. It is difficult to determine what the correct Z-value is as this value will change depending on the size of the pores in question. Ultimately a Z-value of 0.1259mm was chosen for hand-mixed and a Z-value of 0.6464mm was chosen for vacuum-mixed cement. These values were based on the radius of the average pore size for the given distribution and despite the limitations of choosing a set value they resulted in a good fit to experimental data.

Regarding the hand-mixed analysis, the virtual 2D data agrees closely with the experimental findings (see figure 7.9). However, it is clear that the virtual data slightly underestimates the effect of porosity. This is a result of the Z-value discussed above. In reality the Z-value will be greater than zero, as is evident from the non-flat surface of a fractured specimen. This would increase the likelihood of a cluster occurring and for that reason increase the damaging effect of porosity. The 2D virtual specimens assume a Z-value of zero, and so slightly underestimate the experimental results. The 3D virtual analysis agrees very well with experimental findings assuming a Z value of 0.1259mm. All the data fell inside the scatter predicted by the virtual TCD predictions with the exception of one point. From examination of the fracture surface of this specimen, it was clear that the specimen failed from a small cluster of pores despite the sample as a whole being quite porous. Therefore the 2D porosity level (7.1%) is considerably lower than the 3D (12.51%). In fact the 2D level would fall inside the scatter of the virtual results. This also has another effect, if the porosity level on the plane of failure is low, the porosity's effect in reducing the load bearing area will also be low, and therefore the specimen will survive longer. The virtual specimens however calculate the increase in stress due to reduction in load bearing area according to the overall porosity level of the specimen and so will underestimate the fatigue life of specimens such as the one outlier.

Figure 7.16 illustrates the scatter in hand-mixed cement using a probability of failure graph for different levels of porosity. For each porosity level the fatigue life varies by over an order of magnitude. For example, a specimen contained 5% porosity may have a fatigue life varying from 10,000 cycles to anything up to 100,000 cycles.

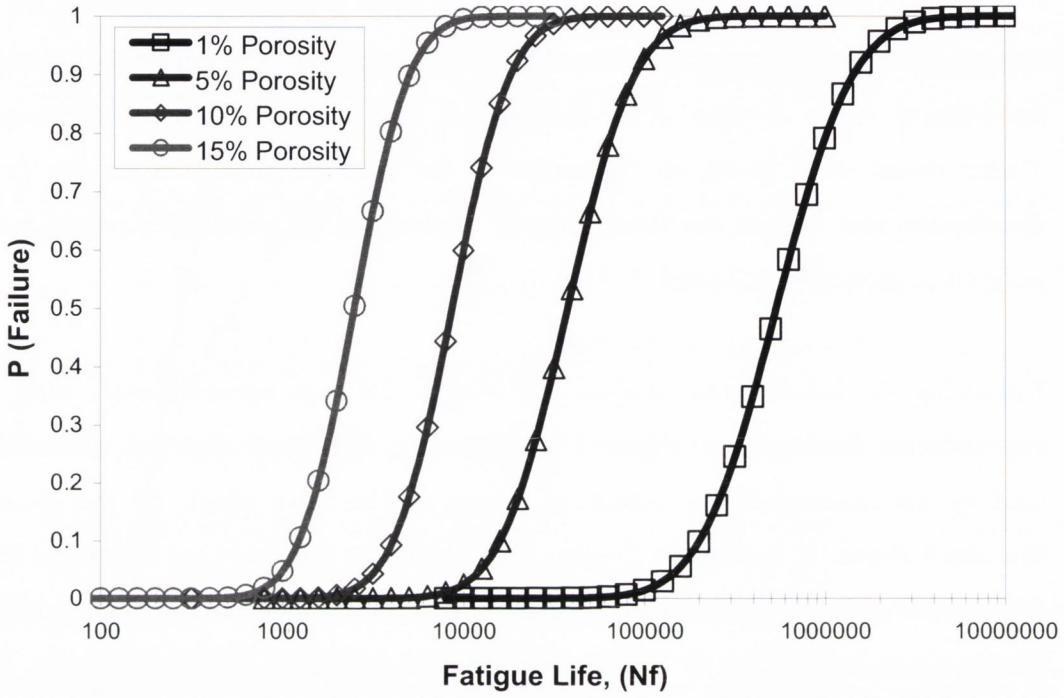

Figure 7.16: Probability of failure for hand-mixed bone cement loaded at 15.3MPa at different percentage porosities.

Regarding the vacuum-mixed analysis, the virtual results agree with the trends set by the experimental data but are conservative in their prediction of the scatter seen in the experimental results. This may be due to the pore distribution used in creating the virtual specimens. As vacuum-mixed cement is mostly free of pores, there were a limited number of pores available to determine their size distribution. A different pore distribution may increase the likelihood of a cluster, consequently increasing the scatter. Also the pores generated in the virtual specimens were assumed to be spherical, this was not always the case in vacuum-mixed specimens as the pores tend to be quite large and can become warped by contact with the specimen walls. In addition a clear boundary emerged along the left side of the virtual data. This boundary corresponds to the effect of a singular pore. As VM material consists of

very few pores, numerous specimens would only contain one pore. Therefore the virtual data would fall along this boundary. However if more than one pore is present, and assuming they don't cluster, the porosity level will increase but the fatigue life will remain constant. This is very much the case in the 2D data. In the 3D data however there are a few occasions were a cluster did occur and so some data points fall to the left of this boundary.

Figure 7.17 illustrates the scatter in vacuum-mixed cement using a probability of failure graph for different levels of porosity. As can be seen there is considerably less variance in the fatigue life in comparison to that of the hand-mixed cement, indicating that there is less scatter in vacuum-mixed cement which agrees with the finding from experimental testing.

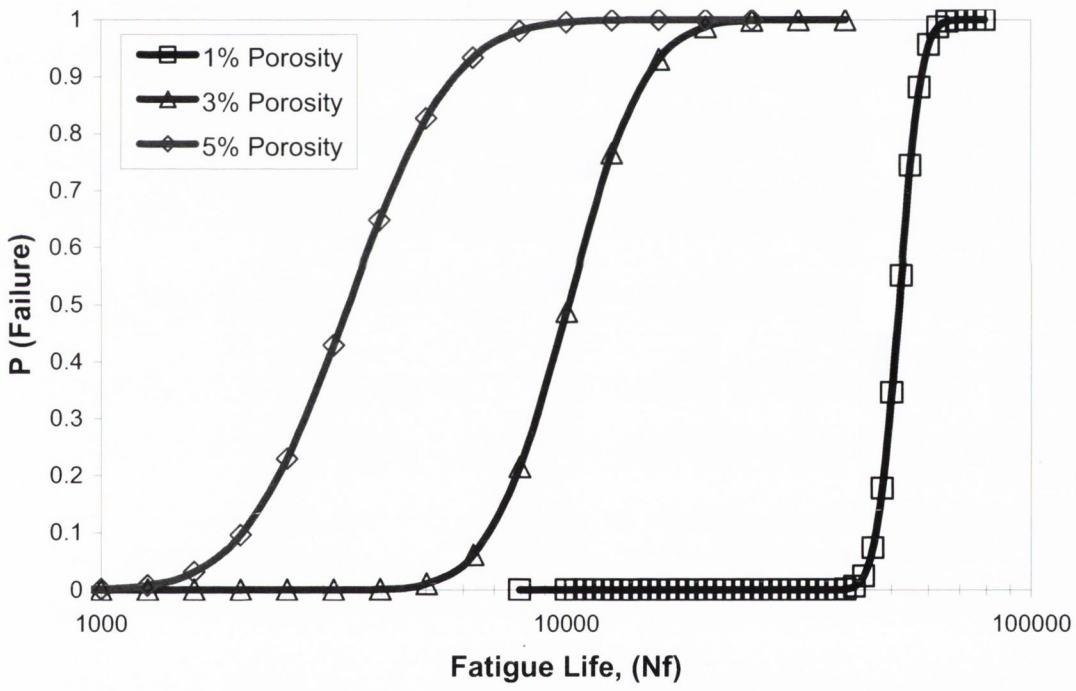

Figure 7.17: Probability of failure for vacuum-mixed bone cement at different percentage porosities.

It is interesting to compare the probability of failure for both hand-mixed and vacuum-mixed bone cement at the same porosity levels. As is evident from figure 7.18, for both porosity levels of 1% and 5%, hand-mixed cement is less likely to fail in comparison to vacuum-mixed when both contain the same level of porosity. This is somewhat surprising as vacuum-mixed cement is expected to demonstrate the

superior fatigue strength. This can be attributed to the pore size distributions. In hand-mixed cement, despite the sample as a whole being very porous, there are very few large pores. However in vacuum-mixed cement, the same level of porosity would consist of very few but yet very large pores, hence failure will initiate more quickly than in hand-mixed. This indicates that given the same porosity the pore distribution found in hand-mixed cement is safer to that found in vacuum-mixed.

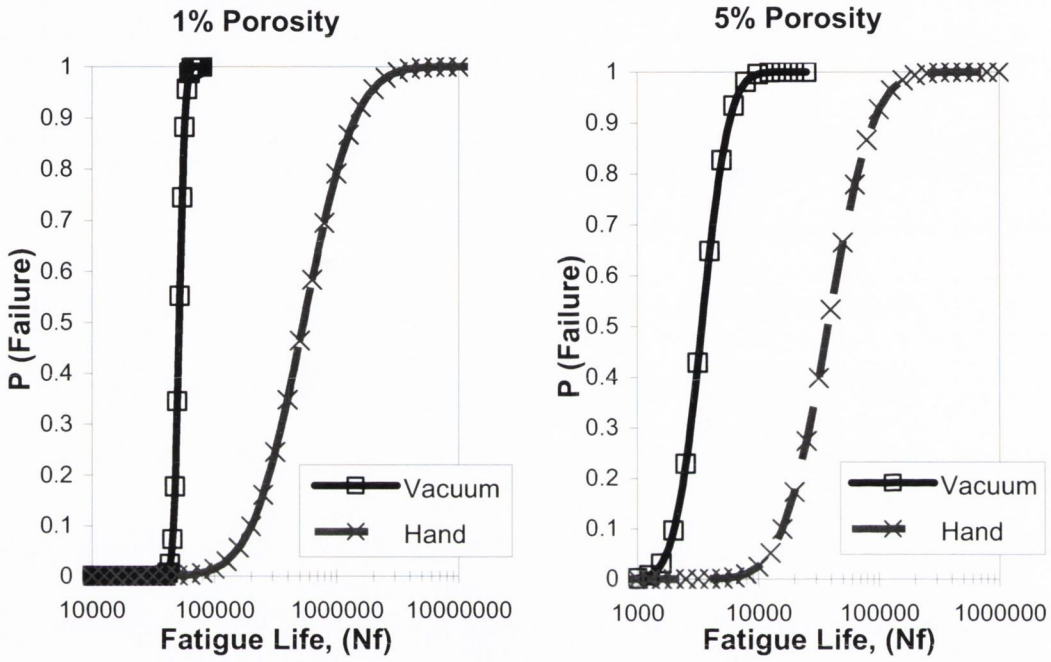

Figure 7.18: Probability of failure for both hand-mixed and vacuum-mixed cement containing the same level of porosity.

It was proposed in chapter 6 that pore clustering and pore size were the major contributors to failure in hand-mixed and vacuum-mixed respectively. Using the virtual models in this chapter this hypothesis was verified. The probability of a cluster occurring was found to be extremely improbable in vacuum-mixed cement. This conclusion verifies, by default, that pore size is the main cause of failure in vacuum-mixed cement. The probability of a cluster occurring in hand-mixed cement was found to be extremely high for all Z-values indicating that clustering is a very likely phenomenon in practice. However the probability of finding a large pore was also found to be very likely. Despite this unexpected likelihood of a large pore occurring, figure 7.15 verifies that a large cluster is more likely to cause failure,

verifying that pore distribution is the main contributor to failure in hand-mixed cement.

As discussed in the previous chapter, porosity does have beneficial effects such as improved drug dispersion, bone ingrowth and the possible blunting of propagating cracks. It was therefore proposed that a step forward in the development of bone cement may involve a compromise, where the ideal cement would contain an even distribution of small pores, eliminating the detrimental effects of large pores and the phenomenon of clustering that was quantified in chapter 6. The question is "can this be achieved using the available preparation techniques?" To answer this, let the maximum acceptable pore diameter be 1mm. According to figure 6.5 this would result in a fatigue strength of 16.8MPa. According to figure 7.14, for a porosity of approximately 2.25%, there is a 50% chance of a pore of diameter greater than 1mm occurring in both hand-mixed and vacuum-mixed cement. However as an even distribution of pores is required, vacuum-mixing can be discarded. Figure 7.13 states, assuming a Z-value of 0.1259mm, that the probability of a cluster occurring in hand-mixed cement is a certainty for a porosity of 2.25%. However figure 7.15 states that there is a 50% chance of this cluster being greater than 1mm if the porosity is slightly less, approximately 1.8%. To summarise, if the cement is hand-mixed and the porosity is kept below 1.8% there is still only a 50% chance of achieving a distribution of pores that would result in the required fatigue strength of 16.8MPa. Given that a 50% probability of achieving the required parameters is certainly not acceptable, and achieving a consistently low porosity level from hand-mixing the cement is very difficult, it can be concluded that the preparation techniques used in this study cannot be used to achieve the required compromise. Therefore if a safe, even distribution of porosity is required, further work is needed to develop a mixing technique capable of achieving this. Possible solutions are explored in chapter 10.

Some limitations of the present chapter should be mentioned. A cluster was defined as the interaction of two pores. However, in reality a cluster may consist of more than two pores which would increase the damaging effect of the cluster. However from examination of the experimental fracture surfaces, the vast majority of clusters consisted of only two pores. In order to define a cluster in a 3D specimen a specific

Z-value was introduced. However in reality this value would change depending on the size of the pores in question. Despite this simplification a good fit to experimental data was achieved. The location of pores throughout the virtual specimen was assumed random. Although this is most likely the case in the experimental specimens tested in this chapter, it may not be the case *in vivo*, where there have been reports of pores preferentially forming at the stem/cement interface. This would increase the likelihood of a cluster occurring over that which was predicted in this chapter.

7.7. Conclusions

1) A negative correlation between porosity level and fatigue life was determined for both hand-mixed and vacuum-mixed bone cement. Considerable scatter was present in the experimental results making them difficult to interpret.

2) This negative correlation and scatter was predicted using a TCD based failure criterion. This failure criterion allows the reader to gain a significant insight into the statistical distribution of the fatigue strength of porous bone cement.

3) It was verified using the virtual specimens that porosity contributes to failure through pore size in vacuum-mixed cement and pore clustering in hand-mixed.

4) Hand-mixed cement was found to demonstrate superior fatigue strength than vacuum-mixed cement containing the same levels of porosity.

5) The cement preparation techniques used in this study are not capable of producing a safe, even distribution of porosity.

Chapter 8

PMMA based Bone Cement

Vs

Pure PMMA

Hoey, D., Taylor, D., "Comparison of the fatigue behaviour of two different forms of PMMA" Fatigue and Fracture of Engineering Materials and Structures, In Review.

8.1. Introduction

It was concluded from chapter 5 that the theory of critical distances can be used to predict the effect of stress concentrations on the fatigue strength of PMMA based bone cement. Despite the success of the TCD, an interesting anomaly arose, where the critical stress which usually corresponds to the plain strength of the material was actually greater than the plain strength by a factor of 1.7. This was attributed to defects in the plain samples such as porosity. As pure polymethylmethacrylate (PMMA) in the form of Perspex is prepared under optimal conditions it is commonly considered as a 'perfect' form of bone cement. Therefore a direct comparison between perspex and bone cement may yield answers to questions which arose in chapter 5.

Given the load bearing application of both forms of PMMA, it is important that both are capable of withstanding the presence of stress concentrations which may arise during their use. The effect of stress concentrations on the fatigue strength of perspex has been demonstrated by Gotham (Gotham 1973). This study verified the damaging effect of a range of stress concentrations but also found that PMMA was not as susceptible to failure from defects as might have been expected given its brittle nature. A direct comparison of this study to the data collected in chapter 5 cannot be made due to the different testing frequencies, R ratio and geometry of stress concentrations tested. To the authors' knowledge, this is the only systematic study conducted to date on the effects of stress concentrations on the fatigue strength of polymers.

Therefore this chapter had the following aims:

a) To conduct experiments to investigate the role of stress concentrations in the fatigue strength of pure PMMA in the form of perspex which would allow a direct comparison to the data previously collected in Chapter 5.

b) To investigate the capability of the TCD to predict fatigue failure in polymers and to test this theory against the data collected on the two forms of PMMA.

8.2. Experimental details

Perspex specimens were machined from a 3mm thick sheet, producing tensile specimens with a gauge section of 16x16x3mm. Bone cement was prepared by hand-mixing the cement and transferring the mixture to a mould. This produced tensile specimens with the same gauge section as the perspex but with a slightly greater thickness (16x16x3.5mm). As the cement is prepared *in situ*, it tends to contain defects in the form of porosity. In order to make a direct comparison to perspex, pore-free samples were prepared as described in chapter 5. Various stress concentrations were machined into the perspex and bone cement, details of which are given in table 8.1.

Defect Type	Root radius	Depth	Diameter	Location	K_t
Plain	-	-	-	-	1
Hole	-	-	2.2 mm	through thickness, drilled centrally	3.08
Notch	0.1 mm	2 mm	-	both edges, mid gauge length	11.04
Notch	1.5 mm	2.2 mm	-	both edges, mid gauge length	3.52

Table 8.1: Description of each defect incorporated into the test specimens. The K_t values were determined using the FE models created for each specimen.

Fatigue testing was conducted on an Instron servo-hydraulic testing machine (Model 8501). The cyclic stress employed was sinusoidal at a frequency of 3 Hz. The ratio of minimum to maximum stress (R ratio) was kept at 0.1. As the fatigue

behaviour of PMMA is sensitive to temperature, all testing was conducted in a water bath at 37°C (body temperature).

8.3. Results

8.3.1. Experimental results

The experimental results for bone cement and perspex are shown in figures 8.1 and 8.2 respectively. The experimental results for bone cement are taken from Chapter 5 but are presented here again for the purpose of comparison to perspex. The data are represented on stress range against fatigue life graphs (SN plots), from which the fatigue strength at 10^5 cycles to failure was estimated. As expected, for such brittle materials, the presence of stress concentrations results in a significant decrease in the fatigue strength, however the decrease in strength is not as sizeable as a K_t analysis would predict. All failures initiated from the introduced defects.

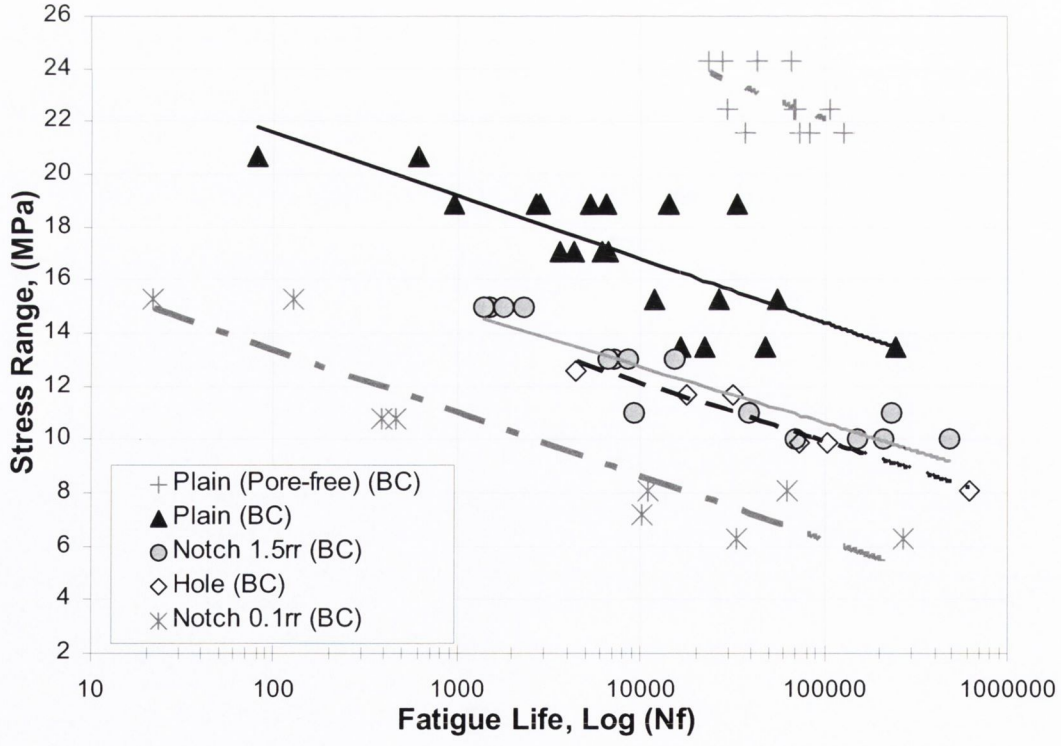

Figure 8.1: Stress-life data for plain pore-free and HM bone cement specimens and specimens containing stress concentrations in the form of circular holes and notches. rr = root radius.

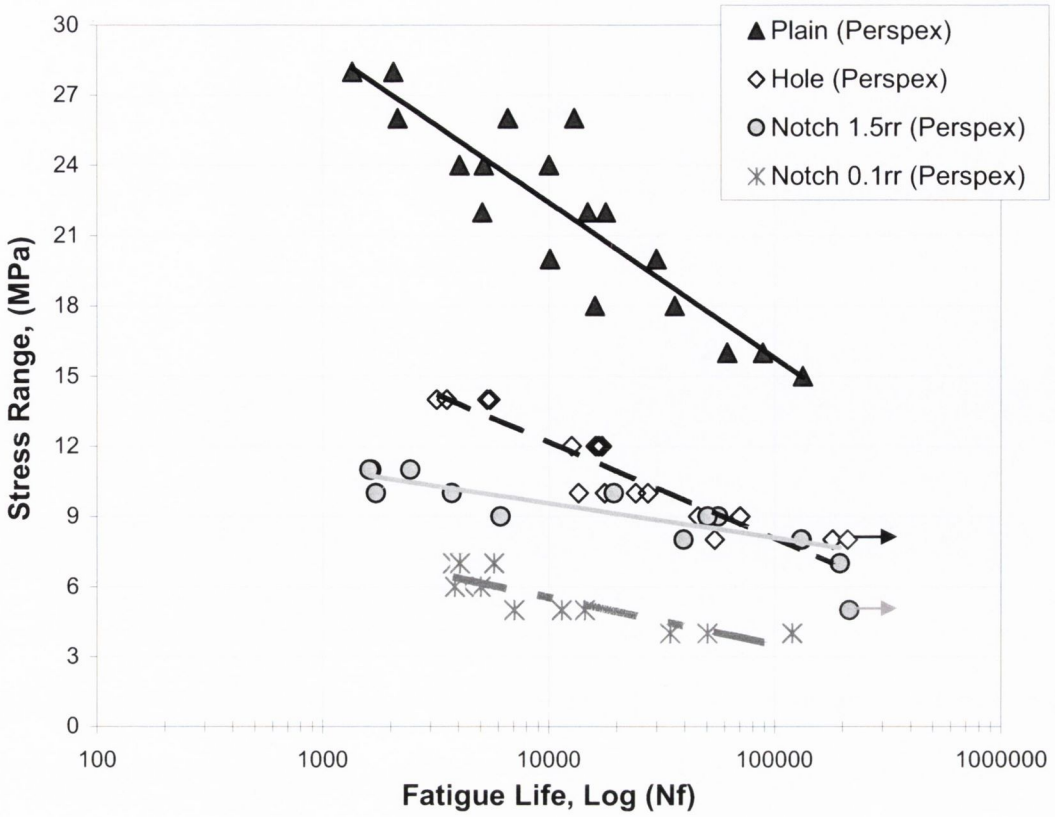

Figure 8.2: Stress-life data for plain perspex specimens and specimens containing stress concentrations in the form of circular holes and notches. Arrows indicate specimens which ran out. rr = root radius.

Fatigue strengths for all specimens were taken at 10^5 cycles and are presented in table 8.2 and are compared in figure 8.3. Regarding the plain samples, perspex performed slightly better in fatigue than the hand-mixed bone cement but was significantly weaker when compared to the pore-free cement. This is an interesting finding as perspex is considered as a 'perfect' form of PMMA. On comparing the samples containing stress concentrations, bone cement once again demonstrated superior strength, with the difference between the two materials being particularly large for the sharpest notch. This was somewhat surprising, as the bone cement containing stress concentrations was hand-mixed and so contained the same porosity as that of the plain samples.

Bone Cement			**Perspex**		
Specimen	Fatigue Limit		Specimen	Fatigue Limit	
Plain Hand-mixed	14.4	MPa	Plain	16.17	MPa
Hole 2.2 mm Ø	9.9	MPa	Hole 2.2 mm Ø	8.19	MPa
Notch 0.1 mm rr	6.21	MPa	Notch 0.1 mm rr	3.8	MPa
Notch 1.5 mm rr	9.54	MPa	Notch 1.5 mm rr	8.08	MPa
Plain Pore-free	22.4	MPa			

Table 8.2: Fatigue limits taken at 100,000 cycles for each specimen tested

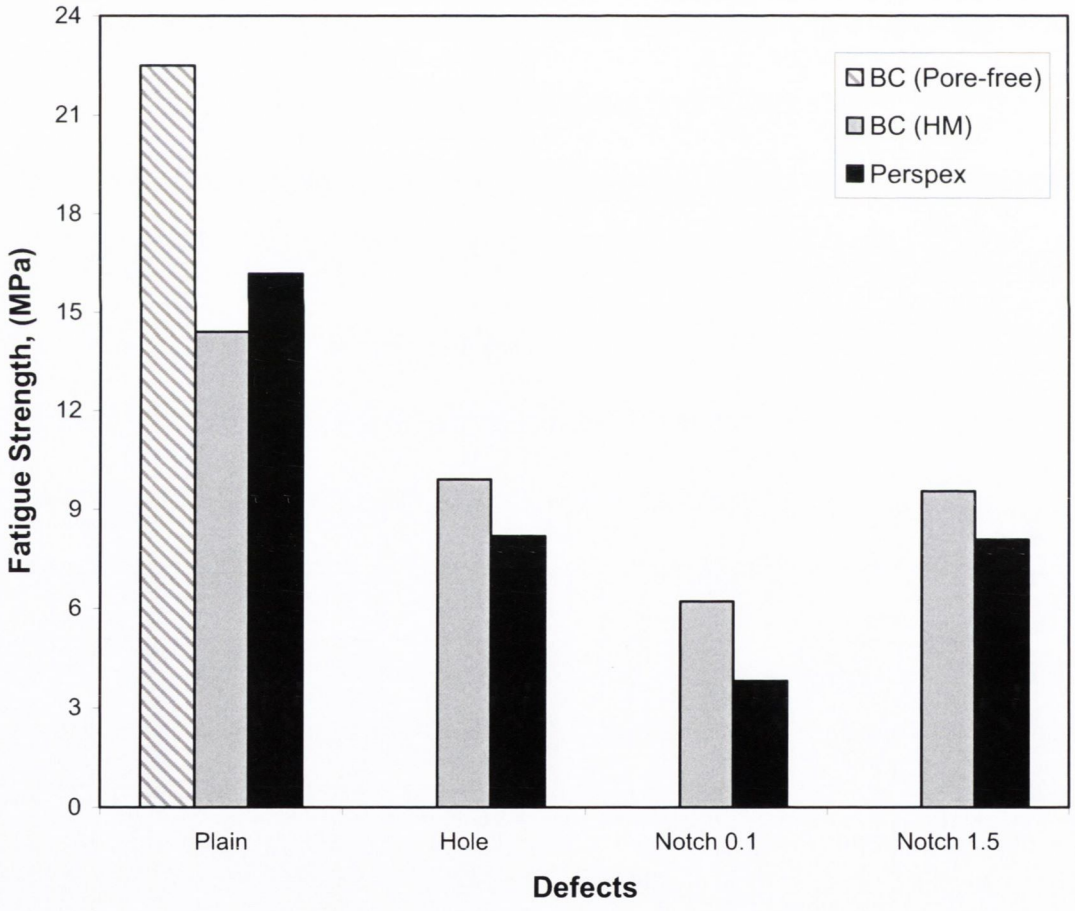

Figure 8.3: Fatigue strengths taken at 10^5 cycles for all perspex and bone cement specimens tested.

8.3.2. Fracture surface analysis

Scanning electron micrographs of the fracture surface of a plain hand-mixed bone cement sample and the plain perspex sample are presented in figures 8.4 and 8.5 respectively. Failure in the bone cement sample initiated from a cluster of pores. The pre-polymerised beads are clearly evident at higher magnification and can be seen protruding along the inside surface of the pore shown in figure 8.4(b). The perspex fracture surface is relatively flat with failure initiating from a corner. Moving away from the corner, typical fatigue beach marks become evident, indicating the direction of crack growth.

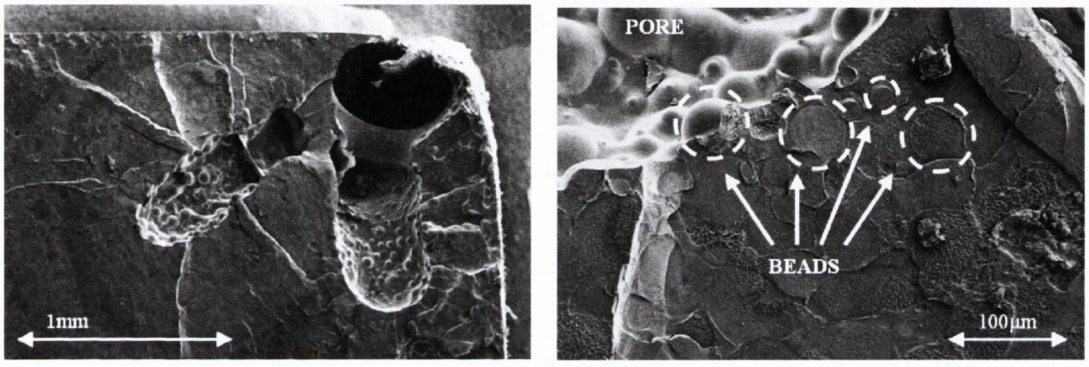

(a) (b)

Figure 8.4: Scanning electron micrograph showing the fracture surfaces of plain hand-mixed bone cement specimen. (a) Failure initiated from a cluster of pores. (b) Close up of pore illustrating the pre-polymerised beads.

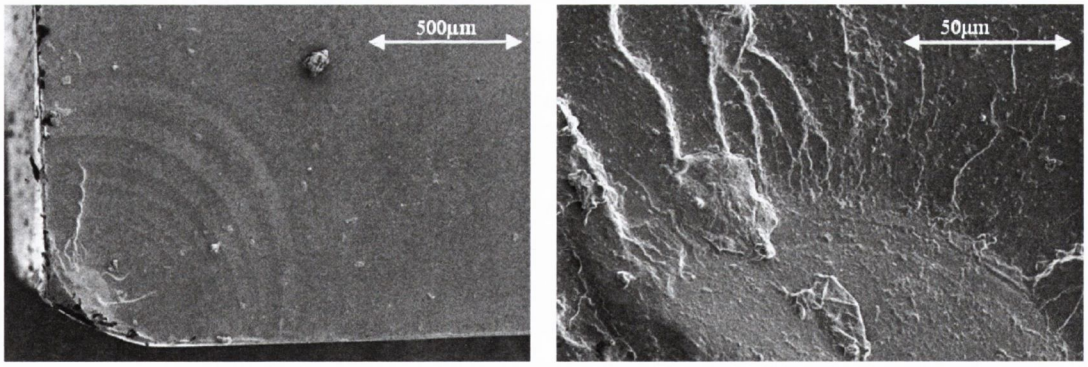

(a) (b)

Figure 8.5: Scanning electron micrograph showing the fracture surfaces of plain perspex specimen. Failure initiated from a corner and fatigue markings can be seen in (a) indicating the direction of crack growth. (b) Close up of a crack initiation site.

8.4. Computational details

A 2D linear elastic finite element analysis (Ansys 10.0, 4-noded Quad elements) was conducted on all samples to determine the elastic stresses in the vicinity of the introduced features (see figure 8.6). Each model consisted of on average 25,000 elements. Perspex and bone cement were modelled as having a Young's modulus of 2.5GPa and 2.38GPa and a Poisson's ratio of 0.33 and 0.4 respectively.

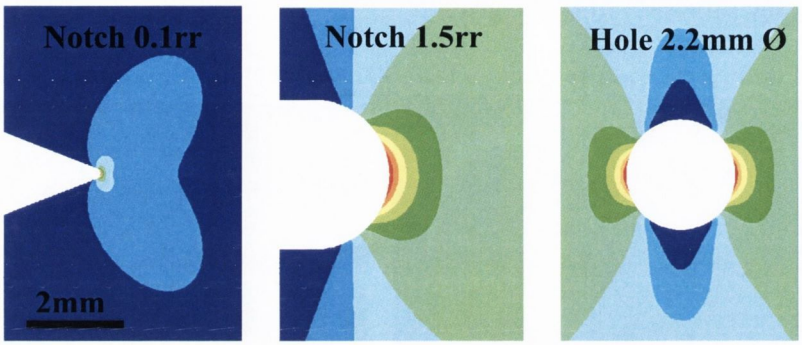

Figure 8.6: Finite element stress analysis of all stress concentrations tested illustrating the notch shape and stress distribution. (Note: contours are not representative of actual stress levels.

8.5. Determining the critical parameters

8.4.1. PMMA based bone cement

The critical parameters for PMMA based bone cement have been determined previously (see section 5.5).

Critical Distance, L/2	=	0.1 mm	} *Bone Cement*
Critical Stress Range, $\Delta\sigma_0$	=	25 MPa	

8.4.2. Pure PMMA

The critical parameters for pure PMMA in the form of perspex are determined as they were for bone cement in section 5.5. The stress-distance curves are plotted for each stress concentration tested, loaded at its respective fatigue strength. According to the TCD, all these curves should intersect at the same point, corresponding to the critical distance and critical stress range for that material. Figure 8.7 shows the appropriate curves for the sharp notch (depth 2mm, root radius 0.1mm), circular hole (diameter 2.2mm) and plain specimen of the perspex material. The respective fatigue strengths were taken at 10^5 cycles to failure.

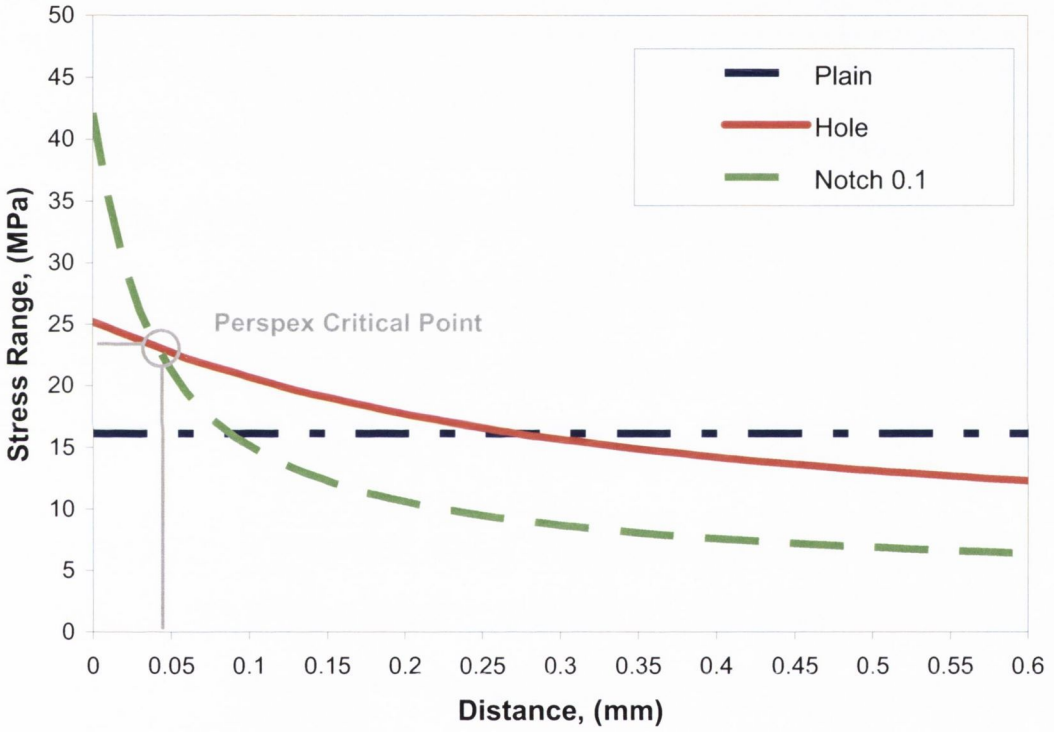

Figure 8.7: Stress as a function of distance from the defect root for perspex specimens containing holes and a sharp notch, at applied loads corresponding to 10^5 cycles. Also shown is a line representing the fatigue strength of the plain perspex specimen.

As can be seen, there is no common point of intersection. This was also found by Taylor *et al* when applying the TCD to static failure in PMMA (Taylor 2004a) and by the present author when applying the TCD to fatigue failure in PMMA based bone cement (Chapter 5). This study found that accurate predictions could still be

obtained if the critical point was taken as the intersection of the sharp notch and circular hole; possible explanations for this phenomenon are given later in the discussion section. Using this criterion the critical parameters for perspex were found to be:

Critical Distance, L/2	=	0.035 mm	} *Perspex*
Critical Stress Range, $\Delta\sigma_0$	=	23.1 MPa	

8.6. Predictions

Using the critical parameters determined above the Point Method (PM) can be used to predict the fatigue strength of any notched specimen. This is achieved by modelling the defect in question and finding the applied stress range needed in order to obtain the critical stress at the critical point. This method was applied to the perspex and bone cement specimens containing a 1.5mm root radius notch and accurately predicted their fatigue strengths within 14% (see figure 8.8).

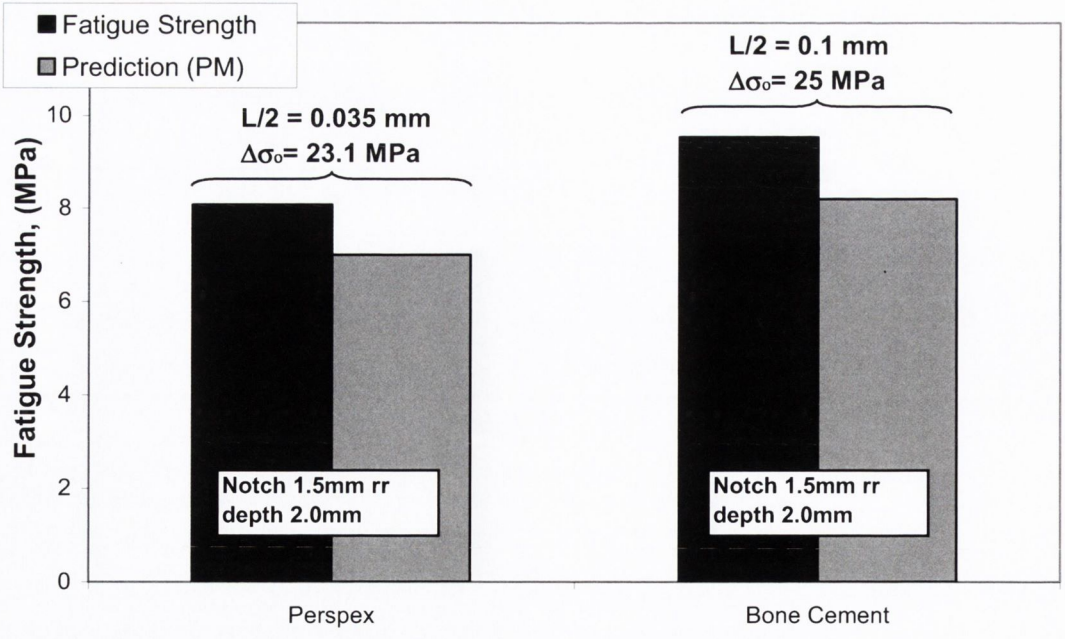

Figure 8.8: Experimental data and predictions using the PM for the fatigue strength of perspex and bone cement containing stress concentrations at 10^5 cycles to failure.

8.7. Discussion

The comparison of the plain samples presents an interesting case. On comparison of the perspex to the hand-mixed bone cement, it was found that perspex demonstrated the superior fatigue strength. However, as hand mixed bone cement contains large percentages of porosity; a direct comparison of the two materials can only be achieved with pore-free cement. Comparing the pore-free specimens to perspex it can now be seen that bone cement is indeed considerably stronger than perspex. This finding is somewhat unexpected as perspex is generally recognized as a 'perfect' form of bone cement, being manufactured under optimal conditions and having a higher molecular weight. Also, Taylor *et al* when comparing the fracture strength of perspex and bone cement found perspex to be the superior material (Taylor 2004a). From examination of the failed specimens a possible explanation for this difference could be due to the different microstructures.

Perspex is prepared under high temperatures and pressures, which results in a homogeneous, amorphous polymer. Perspex, as such, does not have a microstructure. Fatigue failure occurs through the formation of a craze which develops into a propagating crack carrying a craze at its tip. Bone cement, on the other hand, has a composite like microstructure consisting of pre-polymerised PMMA beads inside an interbead PMMA matrix (see figures 8.4 and 8.9). Crack initiation in bone cement tends to occur in the interbead matrix. Various explanations for this inclination were given by Topoleski *et al* (Topoleski 1993), in which they proposed that due to the interbead matrix being prepared under poorly controlled conditions, there may be less molecular chain entanglement in the matrix in comparison to the beads. Also shrinkage in the cement may result in residual tensile strain in the interbead matrix. This tendency is increased in surgical bone cements by the presence of radiopacifiers and antibiotics which are only found in the matrix. During the period of initial, slow, interbead crack growth, the energy at the crack tip may not be sufficient to propagate through a bead. Therefore the crack may arrest at a bead until sufficient energy has accumulated to resume crack propagation or alternatively the crack may propagate around the bead. A crack propagating through the interbead matrix would lose energy in crack deflection, the

longer crack path would increase fatigue life. The beads may also suppress craze formation in the material and affect the distribution of plastic deformation. The conclusion that beads act as barriers to crack growth has been the subject of speculation by other authors. Murphy and Prendergast (Murphy 2001a), Sinnett-Jones *et al* (Sinnett-Jones 2005) and Bhambri and Gilbertson (Bhambri 1995) all demonstrated cracks arresting at large beads along with cracks preferentially propagating through the interbead matrix. The SEM analysis in this chapter illustrated severed beads (figure 8.4), indicating that the beads act as temporary obstacles and not complete barriers to crack growth. Either way it is clear that beads are adding to the structural integrity of the material. Therefore it is important that the beads are not dispensed with in future cements as has been suggested by some authors (Lewis 2007).

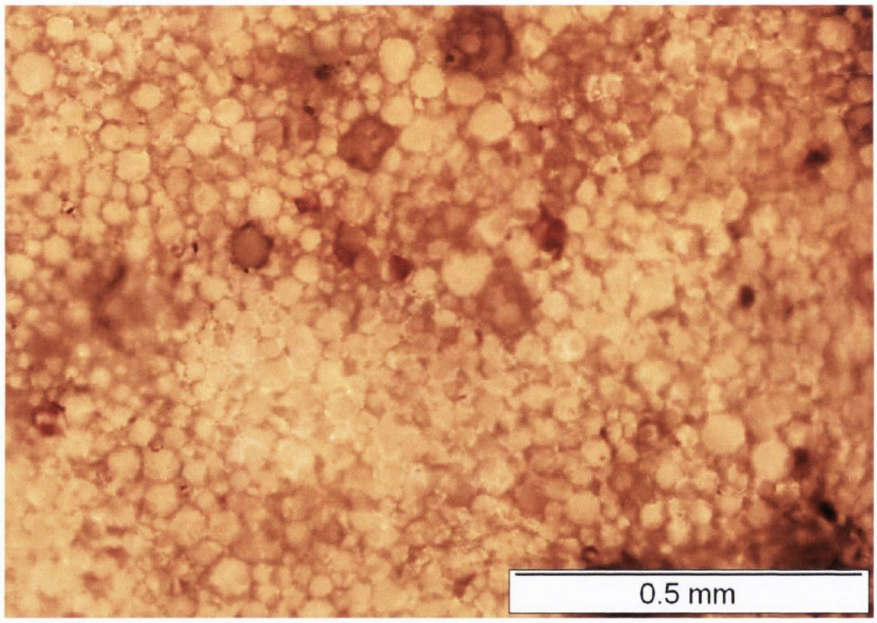

Figure 8.9: Micrograph of bone cement. The specimen is illuminated from underneath allowing visualisation of the microstructure consisting of pre-polymerised beads.

Regarding the specimens containing stress concentrations, it is clear that bone cement performed better than perspex. It is worth noting that the bone cement samples containing stress concentrations were hand-mixed and so contained high levels of porosity. It is therefore apparent that although porosity had a negative influence on the fatigue strength of the plain specimens in comparison to perspex,

the presence of porosity had no effect when the samples contained a notch or a hole. The non-effect of porosity can be attributed to the critical region surrounding the introduced stress concentration. As the defects tested were relatively sharp, the critical region, i.e. the region in which the material is going to fail, will be small. Therefore it is unlikely that a pore will be inside this region and so will not influence failure. This is corroborated by the fact that the critical stress range $\Delta\sigma_o$ for this material, which was found to be 25MPa, is very similar to the fatigue strength of the pore-free bone cement. This finding is interesting when considering the effort put into removing porosity from the cement mantle which does contain sharp stress concentrations in the form of protruding bone and the design features of artificial implants. This conclusion further verifies the findings from chapter 5 and strengthens the hypothesis that this non-effect of porosity may be responsible for lack of clinical improvement when using modern mixing techniques to reduce porosity.

This chapter has demonstrated the capability of the TCD to predict the effect of stress concentrations on the fatigue strength of two forms of PMMA. It was interesting to find that the critical stress range $\Delta\sigma_0$ was higher than the plain fatigue strength $\Delta\sigma_u$ for both perspex ($\Delta\sigma_0/\Delta\sigma_u = 1.43$) and bone cement ($\Delta\sigma_0/\Delta\sigma_u = 1.74$). A factor of 2 was found by Taylor *et al* when using the TCD to predict static failure in both perspex and bone cement. This factor has interesting implications. For an example, take a notch which has a K_t value less than this factor. In this sample the stress at the critical distance will be very similar to that at the notch root, due to the low stress gradient. Therefore the TCD, which uses a critical stress larger than that of the plain fatigue strength, would predict a fatigue strength which is greater than the plain strength of the material. As this is clearly impossible, it implies that the notch in question would be non-damaging. An alternative prediction can still be achieved by assuming that the effect of the notch is only in the reduction of the load-bearing area. The incidence of these non-damaging notches has been reported elsewhere (Taylor 2004a).

The explanation for this factor differs for each form of PMMA. Regarding the bone cement, this factor can be attributed to the presence of porosity in the HM cement as

the pore-free fatigue strength was very similar to the critical stress range (within 12%), as noted above. Therefore, a stress concentration with a K_t less than 1.74 would be non-damaging as a specimen would fail from a pore and not the notch. However, as perspex is inherently pore-free, this does not explain the factor in perspex. It is worth noting that once the critical parameters are known it is assumed that the TCD is capable of predicting failure over a complete range of K_t factors (i.e. K_t: $1 \rightarrow \infty$), the underlying assumption being that the mechanism of failure is the same over the range of K_t. However, the presence of this factor in perspex implies that the mechanism of failure is different for plain specimens and specimens containing defects with K_t factors less than approximately 1.4. Although the change in mechanism is unclear, two possible explanations were put forward by Taylor *et al* to explain this factor in PMMA under static loading (Taylor 2004a). They hypothesised that a stress gradient at a notch would allow a craze to form but not propagate; the craze could not propagate until the stress over the entire craze reached some higher value. Secondly, crazing at the notch root would result in a redistribution of stress, however as the specimens were under plane strain conditions this could suppress craze formation allowing the stresses at the notch root to reach higher levels.

Although the critical stress most likely possesses no real physical meaning it is interesting to note that the critical stress for the two forms of PMMA are very similar. This stress level may correspond to the stress required to instigate craze formation in PMMA under fatigue, i.e. the craze stress (Lang 1984). Despite the similarities in the critical stress it is clear from the comparison of the fatigue strengths and the critical distances that the two forms of PMMA tested here are fundamentally different materials. In perspex, the critical distance of 0.035mm is very similar to the length of a craze in PMMA (0.035-0.045mm). The critical distance of bone cement was 0.1mm; this is very similar to the size of the pre-polymerised beads. The larger critical distance implies that bone cement will be less notch-sensitive than perspex, as is indeed the case. This can be further demonstrated by predicting the resistance of the two materials to further cracking assuming it is already damaged. Assuming a crack of 2mm in length the TCD can be used to predict the resulting fatigue strength; this analysis predicts that bone cement would

have a higher fatigue strength than perspex, by a factor of 1.8, clearly demonstrating its greater resistance to crack growth.

8.8. Conclusion

1) Perspex performed better in fatigue than the hand-mixed bone cement but was significantly weaker when compared to the pore-free bone cement. This is an interesting finding as perspex is considered as a 'perfect' form of bone cement and has been shown to have superior fracture strength to bone cement.

2) The greater fatigue strength of pore-free bone cement can be attributed to its microstructure. The pre-polymerised beads found in bone cement may act as barriers to crack growth, resulting in a longer fatigue life.

3) On comparing the samples containing stress concentrations, bone cement once again demonstrated superior strength. This was somewhat surprising, as the bone cement containing stress concentrations was hand-mixed and so contained the same porosity as that of the plain samples.

4) Although porosity had a negative influence on the fatigue strength of the plain specimens in comparison to perspex, the presence of porosity had no effect when the samples contained a notch or a hole. This is due to the fact that failure is determined by stresses in the critical notch-root region which is unlikely to contain any pores.

5) These various effects are reflected by changes in the material constants used in the TCD (the critical distance and critical stress). The TCD proves to be a powerful tool, predicting fatigue failure over a range of stress concentrations in the two forms of PMMA.

Chapter 9

The effect of stem geometry in a bone cement mantle

9.1. Introduction

The damaging role of stress concentrations has been demonstrated in earlier chapters, in which introduced stress concentrations in the form of notches and circular holes significantly reduced the fatigue strength of tensile specimens of bone cement. One of the main sources of stress concentration *in vivo* arises from the stem, where contact between the stem and the cement can result in high localised regions of stress. Also the loading conditions *in vivo* are more complicated than that found in a simple tensile specimen.

Therefore this chapter had the following aims:

a) Develop a more realistic experimental model of the cement mantle to better approximate that found *in vivo*.

b) Using this model, investigate the role of stress concentrations in the form of design features such as the stem.

c) Investigate the effect of porosity in this more complex stress field and determine its role, if any, in the fatigue failure of a cement mantle.

d) Investigate the effect of a temperature gradient from the bone to the stem on pore formation and distribution in the cement mantle.

e) Attempt to use the TCD to predict the experimental results.

9.2. Experimental details

An experimental model was developed representing a 2D cross section through the cement mantle of an artificial hip joint. This was subjected to cyclic torsional loading, to study the effect of the torsional component of hip-joint loading, which is known to have a significant effect (Mann 1995). Torque was applied under load

control using an Instron testing machine (Model 8874). The cyclic stress employed was sinusoidal at a frequency of 1Hz and the ratio of minimum stress to maximum stress (R) was kept at a constant value of 0.1. Since the material is sensitive to temperature, samples were also tested in a water bath at body temperature (37°C).

Three different stem cross sections were developed and incorporated into the torsional fatigue specimens described in chapter 4, including some which are similar to those used in artificial hip joints (see figure 4.4). The dimensions are given in Table 9.1.

Stem Type	Dimensions	Root radius	Min Mantle Thickness
Square	10x10 mm	1.0 mm	3.0 mm
Square	10x10 mm	0.1 mm	3.0 mm
Charnley	Circle Ø = 15 mm Flat sides = 10.6 mm Width = 10.6 mm		2.5 mm

Table 9.1: Description of each of the three stem geometries tested.

In the case of the experimental model described above the definition of "failure" is not so obvious as there is no catastrophic failure such as is found in a tensile sample. In this more realistic specimen, a crack will initiate and will grow at a relatively slow rate for the duration of its life. Therefore, failure was declared when a crack had grown to a length of 1mm. The reasons for this are discussed later.

As failure is declared when a crack has grown to a certain length, it is essential that accurate monitoring of the crack length was possible throughout the test. Each test was temporarily stopped every 20,000 cycles and the crack length was measured using an inverted microscope (Olympus IX51, PA, USA). An inverted microscope was used as the crack front tends to be elliptical in shape and so the true crack tip cannot be measured on the surface. An inverted microscope illuminates the

specimen from below allowing visualization of the true crack tip. Once the crack had reached a length of 1mm, the test was terminated.

As a temperature gradient, resulting in polymerisation shrinkage away from the stem, has been highlighted as a source of porosity at the stem/cement interface, three samples were prepared using a heated outer ring (see section 4.4.3). These samples along with samples prepared at room temperature were scanned using a Scanco μ-CT 40 system to measure and visualise the distribution of porosity in the cement mantle.

9.3. Results

9.3.1. Experimental results

The aim of the experimental testing was to determine the applied torsional load that resulted in fatigue failure after 10^5 cycles, where failure corresponded to a crack of 1mm in the cement mantle. Initially, testing was conducted at higher loads in an attempt to achieve a typical stress-life (SN) curve, as it had been previously for tensile specimens. However large amounts of plastic deformation occurred at the higher loads which would result in a change in the failure mechanism of the cement. Therefore, to achieve the required load, numerous specimens were tested at varying loads in order to achieve the correct failure parameters i.e. a crack of 1mm after 10^5 cycles. If a specimen was found to exhibit large regions of plastic deformation or was found to run out i.e. test ran for over 250,000 cycles, the test was abandoned. Approximately 10 specimens were discarded for each stem investigated. Once an applied load was found to fit the parameter, a total of 21 additional stem/cement constructs (7 for each stem type) were tested to verify this load. The experimental results are given in figure 9.1. Although the experimental results fall close to the failure parameter of 10^5 cycles, in order to find the correct fatigue limit the data was extrapolated using the gradient of the plain stress/life curve in figure 5.1. The extrapolated fatigue limits are given in table 9.2.

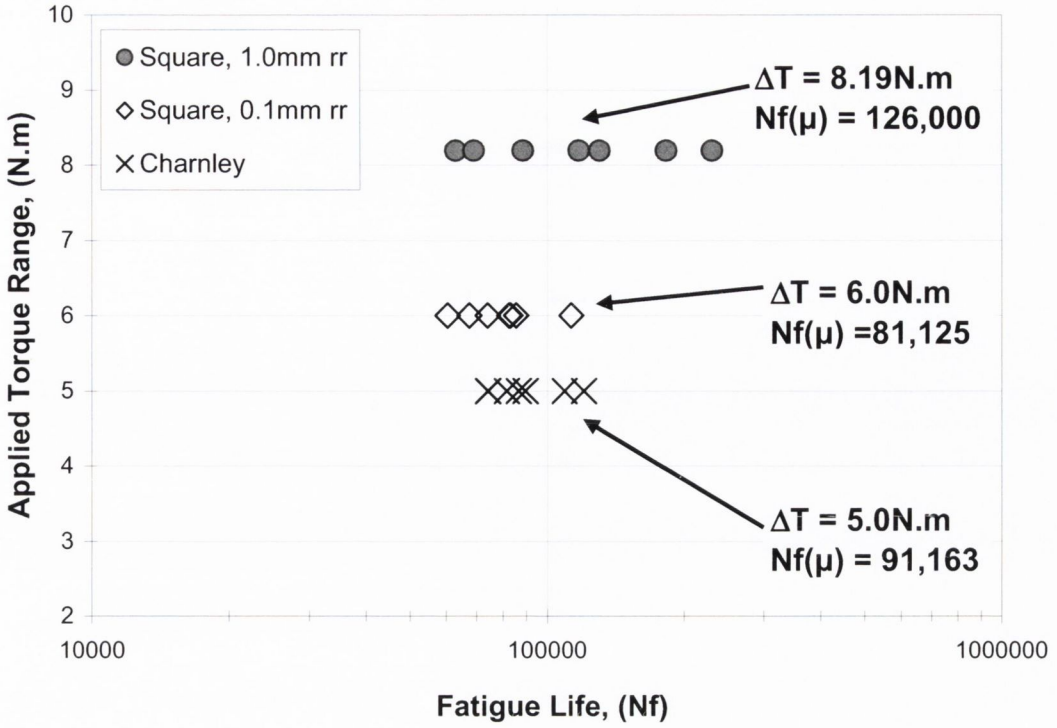

Figure 9.1: Experimental fatigue results for the three stem types tested. Also shown is the average recorded fatigue life.

Stem Type	Dimensions	Root radius	Extrap Fat Lim	
Square	10x10 mm	1.0 mm	8.42	N.m
Square	10x10 mm	0.1 mm	5.78	N.m
Charnley	Circle Ø = 15 mm Flat sides = 10.6 mm Width = 10.6 mm		4.90	N.m

Table 9.2: Fatigue limits extrapolated to 100,000 cycles for each specimen tested

9.3.2. Crack Growth Analysis

An extensive examination was conducted on cracks found within the cement. Figure 9.2 illustrates the crack growth on the surface of the cement using an inverted microscope. This technique allows all pores and defects to be visible throughout the specimen. All cracks were found to initiate at the corner of the stem. No cracks were found growing from any pore throughout the mantle. Figure 9.3(left) illustrates an

interesting phenomenon in which a crack initiated at the corner of the stem, propagated along the expected path before hitting a large pore and then terminating. A closer inspection of the cracks revealed crack growth through the interbead matrix (see figure 9.2(right)).

Figure 9.3 illustrates the location of crack initiation and the crack tip approximately half way through the specimen. Due to the highly polished surface the beads are no longer visible. The crack was found to initiate and propagate around the first bead but then began to follow a straight line, indicating the crack was growing through the beads. This finding clearly conflicts with the observations above; the reasons for this are discussed later. A region of micro-cracking was found to occur ahead of the crack tip. This region always consisted of 2-4 micro-cracks.

Figure 9.4 represents an SEM analysis of the fracture surface. This image resembles the SEM analysis from the tensile sample presented in chapter 8. The pre-polymerised beads can be seen protruding along the inside surface of the pores. The flat nature of the fracture surface indicates that the crack grew through the beads. Despite the general flat surface of the specimen, numerous cavities left from pulled out beads or full beads were witnessed on the surface (see figure 9.4(right)).

9.3.3. Porosity analysis (effect of temperature gradient)

The 3D percentage porosity was determined for the heated cement mantle and the non-heated cement mantle using μ-CT imaging. The average porosity level for the heated mantle was found to be 5.66%, while the average porosity of the non-heated mantle was found to be only 2.29%. The difference in the extent of porosity is clearly illustrated in figure 9.5 and 9.6. The distribution of porosity was also found to differ. In the non-heated mantle, the distribution of porosity was relatively even. There was also no indication of preferential pore formation at the stem/cement interface. However in the heated mantle, there was significant pore formation at the stem/cement interface. This is clearly evident in figure 9.6(right). The preferential pore formation in this area would not only decrease the strength of this interface but also increase the likelihood of pore clustering.

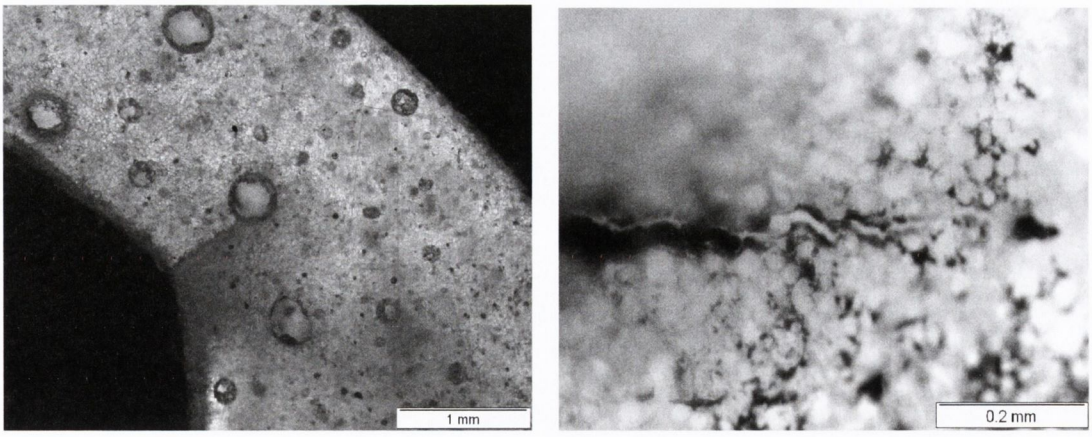

Figure 9.2: (Left) Micrograph illustrating a crack growing into and terminating at a pore. (Right) Micrograph illustrating crack growth through the interbead matrix. Both images are taken from the surface of the specimen.

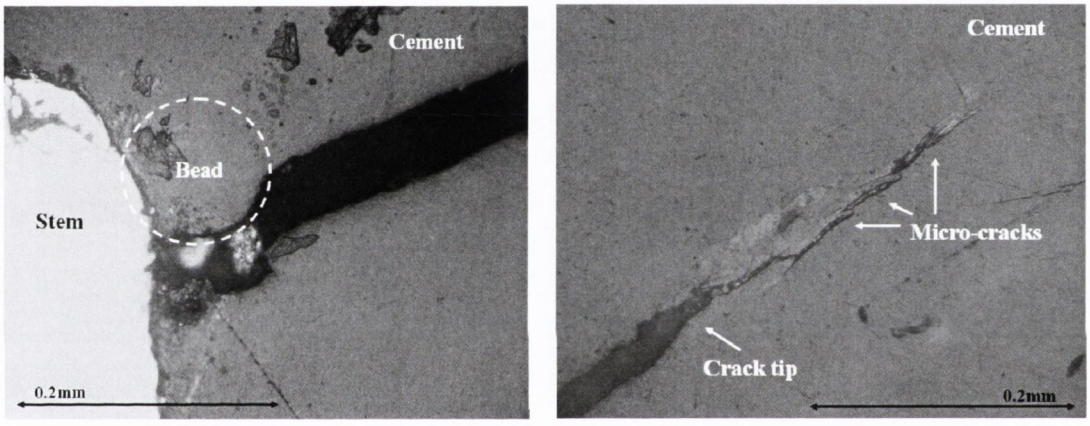

Figure 9.3: (Left) Micrograph illustrating crack initiation around a pre-polymerised bead. (Right) Micrograph illustrating the region of micro-cracks ahead of the crack tip.

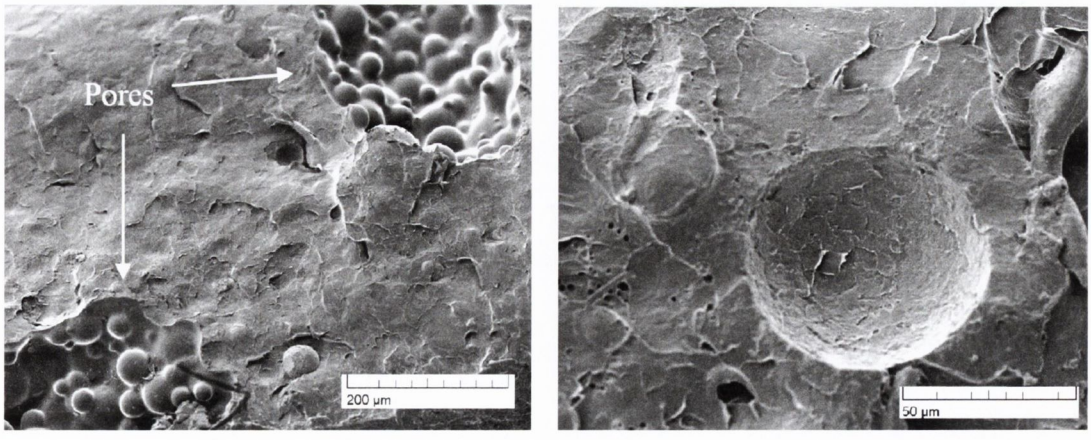

Figure 9.4: (Left) SEM of the fracture surface illustrating crack growth through the beads. (Right) Micrograph illustrating a cavity left after the pull out of a bead.

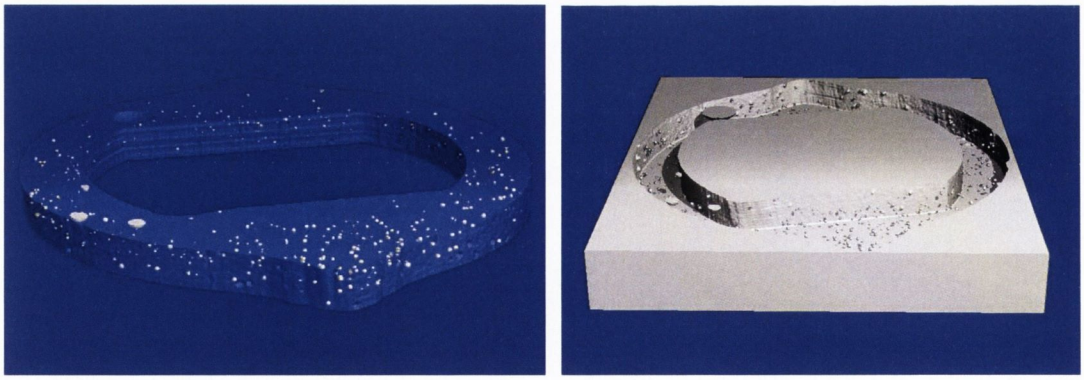

Figure 9.5: (Left) μ-CT image of the cement mantle surrounding a Charnley stem prepared at room temperature. (Right) Inverted image of the same sample, illustrating the extent of porosity at the stem/cement interface.

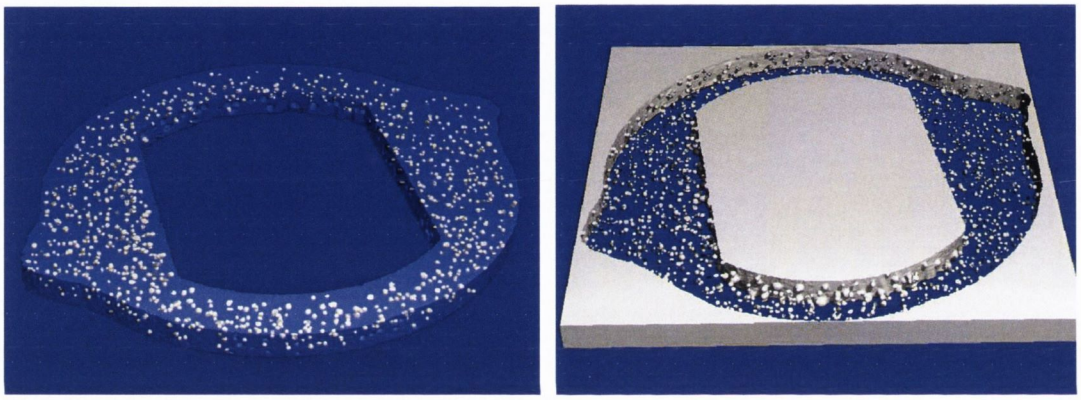

Figure 9.6: (Left) μ-CT image of the cement mantle surrounding a Charnley stem prepared with the outer ring heated to body temperature. (Right) Inverted image of the same sample, illustrating the extent of porosity at the stem/cement interface.

9.4. Computational details

Finite element analysis (FEA) was conducted using Ansys (10.0). 2D, plane strain models were created for each for the three geometries tested. The stem was modelled as both bonded and debonded from the cement mantle. A linear elastic stress analysis was conducted for each of the six scenarios allowing the stresses around the stem to be determined. Each model consisted of on average 50,000 6-node triangular elements

9.4.1. Bonded Model

For the bonded model, only the cement mantle was modeled (E = 2.38GPa; ν = 0.4). The inner surface of the mantle was constrained in all directions and the torque was applied to the outer ring of the cement. The torque was applied to the model in the following manner; a master node was created at the centre of the specimen (i.e. the origin). A moment applied to the master node was then transmitted through a set of constraint equations to slave nodes on the outer ring. The stress distribution for square 1.0mm rr bonded model is illustrated in figure 9.7(left).

9.4.2. Debonded Model

For the debonded model, the cement mantle (E = 2.38GPa; ν = 0.4) and stem (E = 207GPa; ν = 0.3) were modeled. As the aluminium ring did not slip or become debonded in the test, this ring was not modeled and the outer surface of the cement was constrained in all directions. The stem was modeled containing a circular hole through its centre. The torque was then applied through a master node to this inner surface of the stem as described above. Contact between the stem and the cement was modelled with a surface-to-surface contact algorithm (ANSYS Inc, Canonsburg, PA, USA). Friction was assumed to be present with a friction coefficient of 0.1. Changing the coefficient of friction did not result in a significant change in the stress at the critical distance. The stress distribution for square 1.0mmrr debonded model is illustrated in figure 9.8(right).

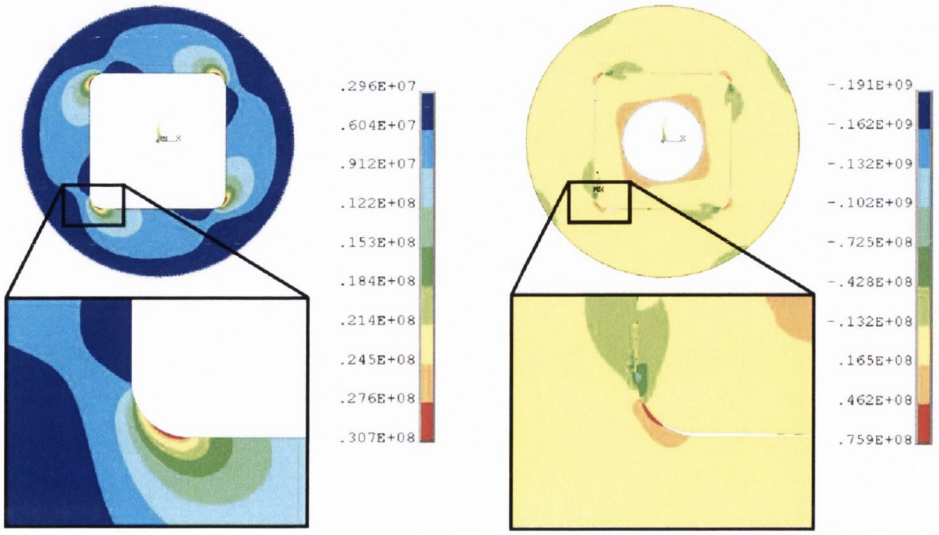

Figure 9.7: Illustration of the stress distribution for the bonded (left) and debonded (right) square 1.0mm rr stem. Units of stress are in Pa.

9.5. Predictions

Using the models described above, predictions were then made for the effect of the stem using the theory of critical distances. However, the critical parameters previously determined for bone cement were for fatigue failure in a tensile specimen. Fatigue failure in a tensile specimen consists of initiation, followed by a period of slow crack growth, followed by catastrophic failure. Therefore the majority of a tensile specimen's life is taken up in the period of slow crack growth. This period corresponds to approximately 1mm as evident from the fracture surface of tensile specimens (smooth, flat region). As the experimental model developed in this chapter involves extended periods of slow crack growth, fatigue failure in this model was defined as a crack which had grown to a length of 1mm.

Predictions of the fatigue strength could then be made using the theory of critical distances as before, by examining the stress at the critical distance from the point perpendicular to that of maximum stress concentration ('hotspot'). The hotspot in each specimen coincided with the corner of the stem. This is illustrated in figure 9.8.

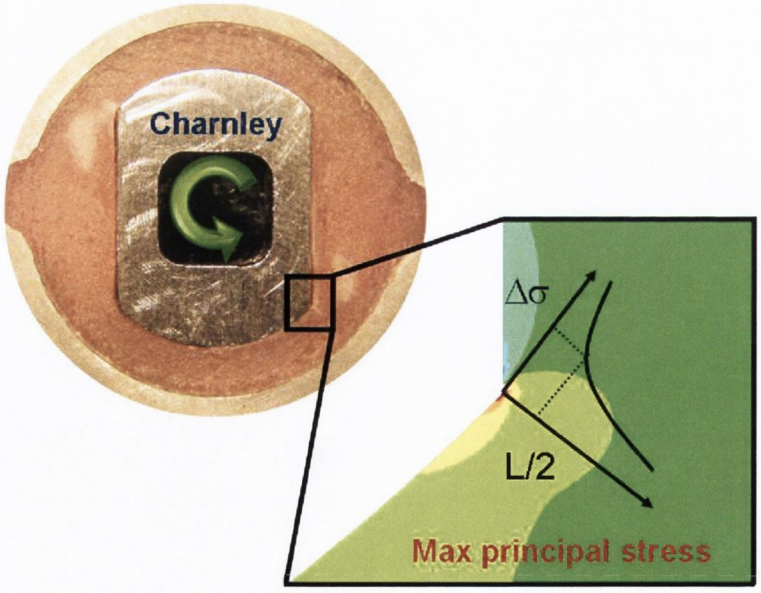

Figure 9.8: Illustration of Charnley type test specimen and a schematic showing the principle of the TCD.

Figure 9.9 reproduces the experimental fatigue strength along with the TCD prediction of the fatigue strength for a bonded and a debonded stem. For each of the three stems there is a significant difference in the fatigue strength predicted for the bonded and debonded scenarios. For the square stems the experimental fatigue strength agrees very closely with the bonded prediction. However, this is not the case with the Charnley type stem where an error of 180% is found. Comparing the debonded prediction to the experimental fatigue strength, errors of approximately 30% are found in each case. This similar trend in error in the three specimens indicates that this is the correct prediction. Also, experimentally the three stems were found to debond from the cement within the first few cycles of each test. Reasons for this 30% error are explored in the discussion.

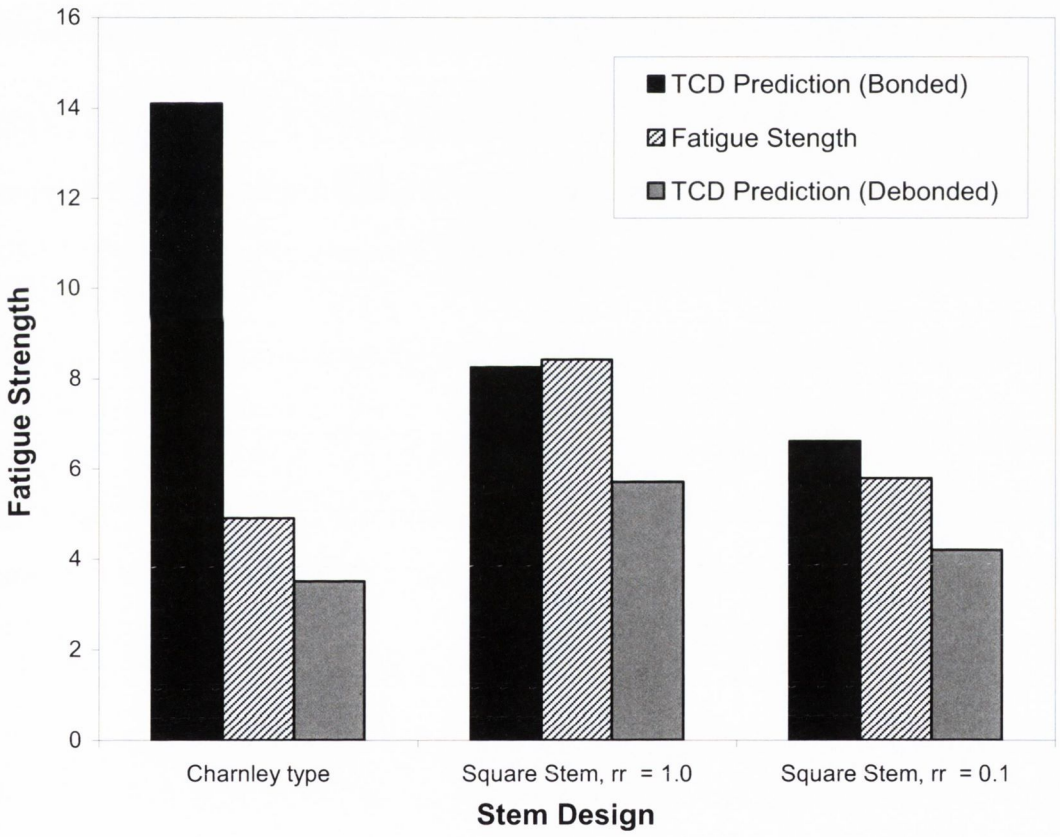

Figure 9.9: TCD predictions for the bonded and debonded stems. Also shown is the experimental fatigue strength.

9.6. Discussion

The results obtained from this chapter indicate that the TCD can be used to predict fatigue failure in this model, which reproduces some of the features of a real cement mantle. This implies that the method should prove to be a useful tool in the future design and development of cemented artificial implants. In principle it is possible to apply the same analysis to a full three-dimensional FE model of an artificial joint, taking account of multiaxial loading conditions. The TCD has previously been used to predict fatigue failure in metallic components of complex shape (Taylor 2000b; Susmel 2003b).

It was evident from the FE stress analysis that the cement mantle in this model did experience a degree of multiaxiality. This increase in the complexity of the stress field raises concerns over the applicability of the critical parameters determined under a simple uniaxial load. It was determined by Susmel and Taylor (Susmel 2006; Susmel 2008) that the critical distance determined under different modes tends to differ slightly. However despite this difference, using the critical distance determined under mode I (i.e. uniaxial load) achieved acceptable results regardless of the degree of multiaxiality. Socie (Socie 1987) determined that the relevant stress parameter depends on the primary mode of crack growth in the material. As bone cement is a brittle polymer, crack growth is primarily mode I dominated. In order to verify this, the shear stresses along the focus path were determined using FE and were found to be negligible in comparison to the normal stresses at the critical distance. Therefore the maximum principal stress was found to be applicable as the relevant stress parameter.

The TCD predictions based on a debonded stem were found to closely follow the trend set by experimental observations. However, the TCD slightly underestimates the fatigue strength in the three specimens by approximately 30%. Three possible explanations for this underestimation are discussed below. Firstly, on inspection of the failed specimens, several regions of non-elastic behaviour were witnessed close to the contact point between the stem and the cement. This damage would act to disperse the energy at the crack tip resulting in longer fatigue lives than predicted by

the TCD which assumes linear elastic behaviour. This plastic deformation was more pronounced at higher applied loads which is evident from the increased scatter from the square 1.0mm rr stem in comparison to the other stems which were tested at lower loads (see figure 9.1). It is also the rationale for not creating an SN for each stem type as the mechanism of failure changes at higher loads. Secondly, the TCD predicts failure within a given number of cycles, based on material constants derived from simple test specimens. In the case of the cement mantle the definition of "failure" is not so obvious. It was proposed that failure corresponded to a crack of the order of 1mm, given that in the tensile test specimens the great majority of the life was taken up in growing cracks up to this length. However, this length of 1mm is only an approximate as the true length of a critical crack is unknown and is bound to vary depending on the test conditions. Therefore, changing this failure criterion would change the resulting experimental fatigue strength of this more realistic model. For example, if the crack length was changed to 0.5mm, the experimental fatigue strengths would be lower and may fall closer to that predicted by the TCD. Thirdly, it was proposed in previous chapters that a crack in bone cement grows through the beads, with the beads acting as temporary obstacles and not complete barriers to crack growth. This was concluded from examining the fracture surfaces of tensile samples. In this chapter, cracks on the surface were found to grow around the beads (see figure 9.2(right)). A crack propagating through the interbead matrix would lose energy in crack deflection, the longer crack path would increase the fatigue life over that predicted by the TCD.

It is interesting to compare the TCD prediction for the bonded and debonded stem. It is well established that debonding of the stem from the cement is undesirable and is commonly recognized as the first sign of failure in a cemented joint. This outcome is well predicted by the TCD with the debonded stem predicted to demonstrate lower fatigue strength to that of the bonded. The difference in the fatigue strength is strongly dependant on stem geometry. For the bonded case, the load is being transmitted from the entire surface of the stem to the cement. However, once the stem becomes debonded the same load can only be transmitted across the points of contact. Given that the load stays the same, but the area decreases, the stresses in the cement will increase increasing the likelihood of failure. This is very much evident when comparing the square shaped stems to that

of the rectangular shaped Charnley stem. When a square stem becomes debonded, there are still four points of contact, therefore the difference between bonded and debonded is not great. Once the rectangular shaped Charnley stem becomes debonded, there are only two points of contact. This significantly reduces the load bearing area of the cement resulting in a large difference in the debonded and bonded scenarios.

Despite figure 9.2 it is apparent from figures 9.3 and 9.4 that crack growth tends to grow through the beads, as was found with the tensile samples in the previous chapter. The specimens in this chapter were 3mm in thickness to ensure plane strain conditions. However plane strain conditions may not occur at the surface of the specimen. This may result in a more complex stress field which may cause the crack to grow around the beads. This may also be an explanation for the elliptical crack front found in most specimens. However, examination of the fracture surface using SEM did not find many complete beads close to the edge of the specimen.

Cracks were found to initiate and propagate from the corners of the stem and not from any pore found within the cement mantle, despite some pores being greater than 2mm in diameter. It seems that porosity does not have a great deal of influence on the fatigue failure of bone cement when the material contains stress concentrations which are greater than those of the porosity. This conclusion agrees with the findings in chapters 5 and 8 regarding the effect of stress concentrations in tensile specimens. Also, despite a large pore being in close proximity to the stem corner in one sample, the crack did not deviate dramatically towards the pore. In addition, this crack was found to be half the size of the corresponding crack (see figure 9.10), indicating that the pore in fact acted to blunt the crack. This finding agrees with a computational study by Janssen *et al* (Janssen 2005a) in which they found that even when they placed a large pore within 1mm of the normal crack path, the crack did not preferentially deviate into the pore and in actual fact acted to decelerate the crack growth. This conclusion gains significance when you consider the effort put into removing porosity *in vivo* using modern mixing techniques and once again verifies the explanation put forward in chapter 5 for the findings from hip-register study which suggest that the fatigue life of artificial joints *in vivo* are

not improved when porosity is reduced using these modern mixing techniques (Malchau 1993; Hernigou 1999; Geiger 2001).

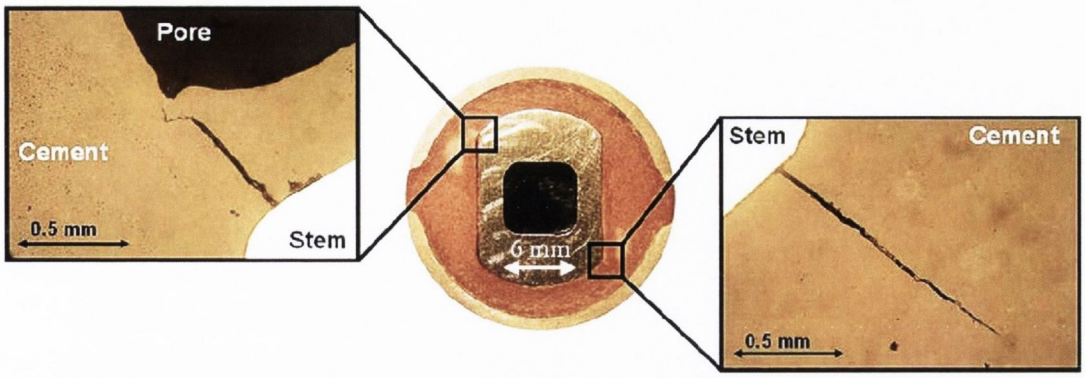

Figure 9.10: Micrograph illustrating cracks growing from opposite corners of the stem.

Several samples were mounted in epoxy and ground down to examine crack growth in the material (see figure 9.3(left)). Crack initiation was found to tend to the interbead matrix with the crack growing around the first bead and then seemingly taking a straight path thereafter. This initial region of crack growth was always very similar in length to that of the critical distance for bone cement and may actually be a physical realisation of the theory. Also examining the crack tip revealed a damage zone similar to that described by Topoleski *et al* (Topoleski 1993) where a region of micro-cracks proceeded the crack tip (see figure 9.4(b)). The length of the micro-cracks was also very similar to the critical distance and may be another possible realisation of the theory.

The heating of the outer ring to body temperature was found to have a significant effect on pore formation and distribution in the cement mantle. It is shown in figure 9.7 (right) that the number of pores on average increased along with significant pore formation at the stem/cement interface. The pore formation at the interface is most likely due to polymerisation shrinkage. Due to the heated outer ring, the cement initially cures at ring/cement interface and then cures towards the stem. However, due to shrinkage of the cement as a result of polymerisation, pores form in the cement at the cement/stem interface to counteract the shrinkage. Pore formation at this interface is a great concern, as this interface has been highlighted as a problem

region in cemented hip replacements. Also the formation of pores in close proximity increases the likelihood of a cluster occurring which could prove to be detrimental to the fatigue strength of the cement mantle as highlighted in chapter 6. The overall increase in pore formation throughout the mantle may be due to increased monomer evaporation as a result of the increased temperature. No mechanical testing was conducted on the specimens prepared at elevated temperatures. This is certainly an area worthy of further research.

Some limitations of the present chapter should be mentioned. The present study examined the torsional component of hip joint loading but the cement mantle *in vivo* experiences other types of loading such as bending. However it has been shown that the torsional component is the most damaging type of loading *in vivo*. The TCD makes predictions based on a linear elastic analysis. However non-elastic behaviour was common in this experimental model, particularly at higher loads. Therefore the TCD may struggle to predict fatigue failure in stems with higher fatigue strengths than tested in this study. This study examined the failure of a cemented implant, where failure was associated with crack initiation and growth. However a stem can also fail through torsional instability. This aspect was not studied in this chapter.

9.7. Conclusion

1) The experimental results agree very closely with that predicted by the TCD. This implies the TCD can be used to predict the effect of stem geometry in this more realistic model and should prove to be a simple yet powerful tool in the future design and development of cemented artificial implants.

2) Stem geometry played a critical role in the fatigue strength of the bone cement mantle with stems with sharp corners and rectangular cross sections demonstrating the poorest fatigue strength.

3) Porosity does not seem to contribute to the fatigue failure of the cement mantle in this model and in fact actually acted to blunt propagating cracks in various samples.

4) The non-damaging effect of porosity raises concerns over the use of expensive modern mixing techniques which would reduce porosity, reducing its beneficial effects.

5) The initial region of crack-growth around a bead and the length of the micro-cracks at the crack tip are very similar to the length of the critical distance i.e. 0.1mm. These may be a physical realisation of the critical distance.

6) Heating of the outer ring resulted in an increase in the overall porosity level of the cement and also resulted in preferential pore formation at the stem/cement interface.

Chapter 10

Discussion

10.1. Introduction

In the introduction chapter of this thesis several gaps and inconsistencies in the literature were highlighted regarding the effect of stress concentrations on the fatigue behaviour of bone cement. Several questions were posed and it was proposed that the answers to these questions would fundamentally advance the understanding of the fatigue behaviour of bone cement. A series of experimental tests and computational models were designed to answer the questions and the results were stated and discussed in the previous five chapters. This chapter presents an examination of the results with regard to their implications.

Before the results of this study are discussed, the main limitations of the study need to be mentioned. Firstly the complex *in vivo* loading cycle is approximated by a constant amplitude sine wave. Secondly the effect of additives such as radiopacifiers and antibiotics are neglected in this study, although they may influence the fatigue strength *in* vivo. Thirdly the effect of residual stresses is also ignored. Therefore the experiments simplify the clinical situation to some extent.

10.2. The role of stress concentrations

The main focus of this thesis was to investigate the role of stress concentrations in the fatigue behaviour of bone cement. This was achieved through extensive experimental testing. It was evident that an increase in the stress concentration factor (K_t) reduced the fatigue strength, but it was also clear that the reduction factor was not as large as K_t. This implies that bone cement is less susceptible to stress concentrations than might have been expected given its brittle nature.

The effect of stress concentrations in high-cycle fatigue is generally expected to follow the behaviour described by Smith and Miller (Smith 1978). This behaviour was briefly introduced in chapter 3 (see section 3.4). The principle is illustrated in figure 10.1(a), which shows schematically the effect of the notch stress concentration factor K_t on the nominal fatigue limit $\Delta\sigma_{on}$ for a series of notches in

which K_t is varied by changing the notch root radius, ρ, whilst keeping the notch depth, D, constant. Two regimes of behaviour are apparent. If $K_t<K_t^*$ then the fatigue limit (or fatigue strength in the high-cycle regime) can be adequately described by:

$$\Delta\sigma_{on} = \frac{\Delta\sigma_o}{K_t} \tag{10.1}$$

Here the effect of the notch is simply to reduce the fatigue limit of the material $\Delta\sigma_o$ (measured using plain specimens) by the factor K_t. However, if $K_t>K_t^*$ the fatigue limit becomes constant, equal to that of a sharp crack of the same length, therefore the standard fracture mechanics equation applies:

$$\Delta\sigma_{on} = \frac{\Delta K_{th}}{F\sqrt{\pi D}} \tag{10.2}$$

Here F is the crack geometry factor. These two regimes can conveniently be referred to as "Blunt Notch" and "Sharp Notch" respectively.

Reanalysing the data collected in chapter 5, the behaviour of stress concentrations in bone cement is illustrated schematically in figure 10.1(b). Instead of two regions, there were three. For very low values of K_t, the measured fatigue strength (at 10^5 cycles to failure) remained constant, equal to $\Delta\sigma_o$ (when any reduction in cross-section due to the notch was taken into account), i.e. the notch itself had no effect on fatigue behaviour. This regime can be referred to as "Safe Notch": in addition the data showed evidence of the Blunt and Sharp regions, as normal. The two transition values between these regions can be referred to as K_{t1} and K_{t2} as shown on figure 10.1(b).

The existence of this third unexpected region (i.e. safe) can be attributed to porosity. It was shown that porosity only had an effect if the notch K_t factor is less than a certain value, K_{t1}. For notches with higher K_t factors the material behaviour could be predicted using the TCD with a critical stress equal to the true fatigue strength of

the material, i.e. by assuming that there was no porosity present. In general, complex interactions between notches and porosity might be expected, but it was shown, at least for bone cement that this is not the case. In fact, the behaviour in all cases can be described by one of two failure mechanisms.

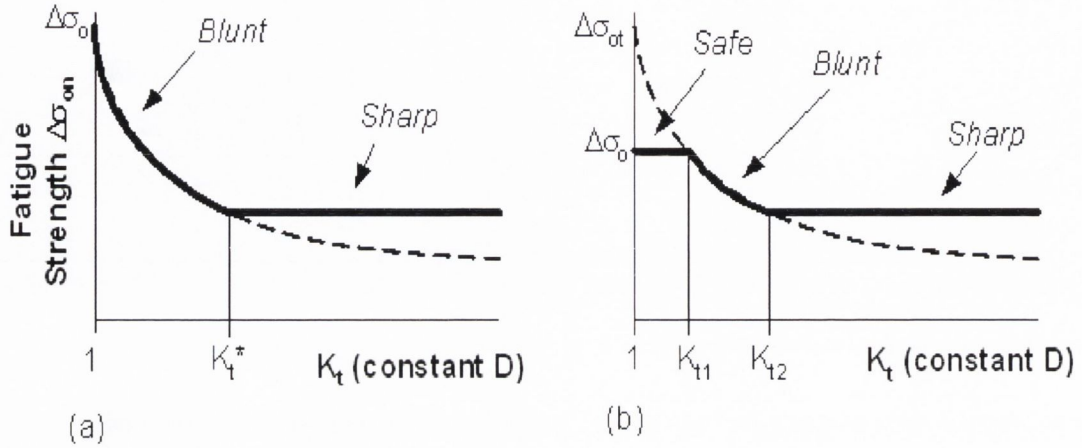

Figure 10.1: Schematics showing (a) typical notch fatigue behaviour as described by Smith & Miller; (b) behaviour demonstrated by porous bone cement.

10.2.1. Mechanism I ($K_t > K_{t1}$)

If bone cement contains a notch or stress concentration which is sufficiently sharp i.e. $K_t > K_{t1}$, then porosity will have no effect, because failure will be dictated by cracking in a small region close to the notch. Normally this region will not contain any pores, but even if it does, the only effect of a pore will be to slightly change the local geometry of the notch (its root radius or length). This will have no effect if $K_t > K_{t2}$, and even if K_t lies between K_{t2} and K_{t1} its effect will be small unless the notch itself is very small.

The conclusion that porosity does not influence failure once the cement contains a stress concentration with a $K_t > K_{t1}$ has significant implications. In order to determine if the cement mantle *in vivo* does indeed contain such a stress concentration, a full 3D finite element reconstruction of a cemented joint replacement would be required. However, there are indications in the literature, along with findings from this study that suggest that such a stress concentration does occur *in vivo*. Numerous studies have reported no increase in the fatigue life of the cement mantle despite the porosity being removed. This would imply that porosity was not influencing failure;

hence the cement mantle must contain a stress concentration greater than K_{t1}. Also, the results from chapter 9 verified that the stem was the main cause of failure despite the mantle as a whole being quite porous, therefore indicating that the stem generated a stress concentration with a $K_t > K_{t1}$. The findings from chapter 9 are in agreement with retrieval studies demonstrating fatigue cracks propagating from the corners of the stem (Jasty 1991). Apart from the stem, there are various other sources of stress concentration which could result in a $K_t > K_{t1}$. These include large casting defects such as the defects reported by Culleton *et al* (Culleton 1993) and struts of trabecular bone, particularly at the proximal end of the femur.

10.2.2. Mechanism II ($K_t < K_{t1}$)

The second failure mechanism occurs if bone cement only contains a notch or stress concentration which is sufficiently blunt i.e. $K_t < K_{t1}$. If this is the case then this stress concentration will have no effect, simply because failure will occur from pores located elsewhere in the specimen. As stated above, the cement mantle most likely contains a stress concentration with a $K_t > K_{t1}$. Therefore, theoretically the effect of porosity in the cement mantle should be negligible.

It is clear that the most important parameter is the value of K_{t1}, as this value states the transition between the two mechanisms. The results from chapter 5 indicate "Safe Notch" behaviour in notches with K_t factors up to 2.4. Therefore a K_t value of 2.4 may a reasonable approximation of the transition. This value will not be exact and will also be dependant on the stressed volume in question. This issue is discussed in more detail in chapter 5.

10.3. The optimal cement mantle

Given the damaging effects of stress concentrations demonstrated in this thesis, it is fair to assume that an optimal cement mantle should contain no forms of stress concentration. As ideal as this scenario may be, it is impossible as sites of stress concentration will always arise at the two interfaces. At the bone/cement interface, sites of stress concentration will arise from struts of trabecular bone protruding into

the cement. This is required to achieve acceptable interface strength through interdigitation. At the cement/stem interface, sites of stress concentration will arise from the corners of the stem. The stem is required to provide rotational stability in the mantle, particularly once debonded. It is therefore clear that in order to achieve an optimal cement mantle, these sites of stress concentration need to be optimised, i.e. reduce their stress concentration capability while maximising their role in increasing interface strength. The TCD should prove to be a simple, yet powerful tool in optimising these sites of stress concentration. Although designing an optimal cement mantle is beyond the scope of this thesis, some general ideas regarding stress concentration can be put forward.

10.3.1. The bone/cement interface

Regarding stress concentration at this interface, the most favourable solution would involve the removal of all trabecular bone. This would eradicate all sites of stress concentration, however, consequently would significantly decrease the shear strength of this interface. Therefore in order to optimise this interface, a compromise is required. The effect of protruding trabeculae would be very similar to that of the notches demonstrated in chapter 5. Recent developments in bone bed preparation have resulted in a significant improvement in the strength of this interface (Majkowski 1993) along with a decrease in the number a cracks emanating from this surface indicating that this interface is close to an acceptable compromise.

10.3.2. The cement/stem interface

As the stem is clearly an essential component of a hip reconstruction, it is worrying that the stem may be a major source of stress concentration in the cement mantle. The damaging effect of the stem was demonstrated in chapter 9, where three different stem designs were found to initiate fatigue cracks in the mantle. It is apparent from these results that future stem designs should try to minimise this stress concentration. For example, a circular stem would generate very little, if any stress concentration, especially in the torsional specimens tested in chapter 9. However this is unrealistic as the stem is required to provide torsional stability. Once again, in order to optimise this interface a compromise is required.

Regarding stem design, the cross-sectional shape is predicted to play a major role in the fatigue strength of the cement mantle, particularly when the stem becomes debonded from the cement. For example, in chapter 9 the Charnley type stem was predicted to demonstrate significantly lower fatigue strength when the stem became debonded from the cement. This was attributed to the rectangular cross section of stem, which results in only two points of contact post-debonding. However the square shaped designs have four points of contact which results in only a minor difference between the bonded and debonded scenarios. The rationale behind a rectangular stem is rotational stability. Therefore given the findings from this thesis, possible stem cross-sections could consist of a rectangular shaped design with additional flanges on each side. This would provide acceptable rotational stability while increasing the number of contact points once the stem becomes debonded.

Despite the potential future improvement in stem design, a review of the literature along with the findings from this study indicate that currently the stem is the major source of stress concentration in the cement mantle and as a consequence is the major cause of failure *in vivo*. As stated in section 10.2.1, it is reasonable to assume that the stem creates a stress concentration in the cement mantle greater than K_{t1}. Therefore it can be concluded that the cement mantle fails through mechanism I (see section 10.2.1)

10.3.3. Casting defects

The effect of casting defects such as incomplete filling of the bone cavity, premature solidification and trapped debris would once again be very similar to that demonstrated by the notches in chapter 5. Given the detrimental effects of such a stress concentration and the fact that this form of stress concentration has no beneficial effect in the cement mantle, this form of defect should be removed from the cement mantle. It is therefore encouraging that surgeons are now using modern surgical techniques to try and reduce these types of stress concentration.

10.3.4. Porosity

Regarding the effect of porosity, this thesis has demonstrated the damaging effects of porosity in uniaxial test specimens, where large pores and pores in close proximity can play a major role in the fatigue failure of the material (chapter 6).

Also the extent of porosity plays a major role in failure, as an increased level of porosity increases the probability of getting a large pore or cluster (chapter 7). Despite the damaging effects of porosity, it was hypothesised above that the cement mantle most likely fails through mechanism I, hence theoretically the effect of porosity in the cement mantle should be negligible. Therefore, given the beneficial effects of porosity (i.e. improved drug dispersion, bone ingrowth and as a method of blunting cracks), it is proposed that porosity should not be removed from the cement mantle.

Despite the potential negligible effect of porosity, it is important that the damaging effects of porosity are not ignored. It was therefore proposed in chapter 6 that an even distribution of small pores might be an acceptable compromise. This would allow sufficient porosity to achieve the beneficial effects but at the same time minimising the risk associated with pore size and pore clustering. Hand-mixing of the cement would seem the most likely technique for achieving this type of distribution as the hand-mixed cement has a pore size distribution consisting of relatively small pores.

A return to hand-mixing of the cement has many desirable qualities. First of all, hand-mixing results in a relatively even distribution of pores which is the ideal distribution needed for the three beneficial effects of porosity to have full effect. Therefore hand-mixing would reintroduce the beneficial effects which are lost when using modern mixing techniques. Secondly, there are considerable economic benefits associated with a return to hand-mixing. For example if the surgeon was to use vacuum-mixing, a machine is needed to provide the vacuum and disposable vacuum mixing chambers are needed for each mix. This raises the cost of each surgery appreciably. Also, mixing the cement under a vacuum requires more time in comparison to simple hand-mixing, as a result the surgery takes longer which in turn increases the price of the surgery. A study by Macaulay *et al* (Macaulay 2002) suggested that a return to hand-mixing would result in a saving of $2.7 million per year in the US (assuming 100,000 cemented THAs per year).

Despite the economic and medical benefits associated with a return to hand-mixing, there are risks involved. For example, despite the pores arising from hand-mixing

on average being relatively small, due to the number of pores present the probability of finding at least one large pore is very high. It was determined in chapter 7, that in order to achieve a distribution of porosity in hand-mixed cement where the maximum pore or cluster diameter was not greater than 1mm in diameter, a porosity of 1.8% was required. An illustration of a hand-mixed bone cement sample containing 1.8% porosity is presented in figure 10.2. In addition, achieving this porosity level only resulted in a 50% chance of achieving the above parameters. A 50% chance of obtaining the required distribution is unacceptable. Therefore in reality, an even lower level of porosity would be required. There are two things wrong with this. First of all, a very low porosity level will consist of very few pores and so will limit the connectivity of the pores which is required to allow penetration of dissolution fluids for antibiotic release. Secondly, achieving a porosity level this low consistently is very difficult to achieve. This finding indicates that hand-mixing the cement is not an appropriate technique to achieve an even distribution of pores that would result in a safe compromise. Therefore, further work is needed to develop a mixing technique capable of achieving this.

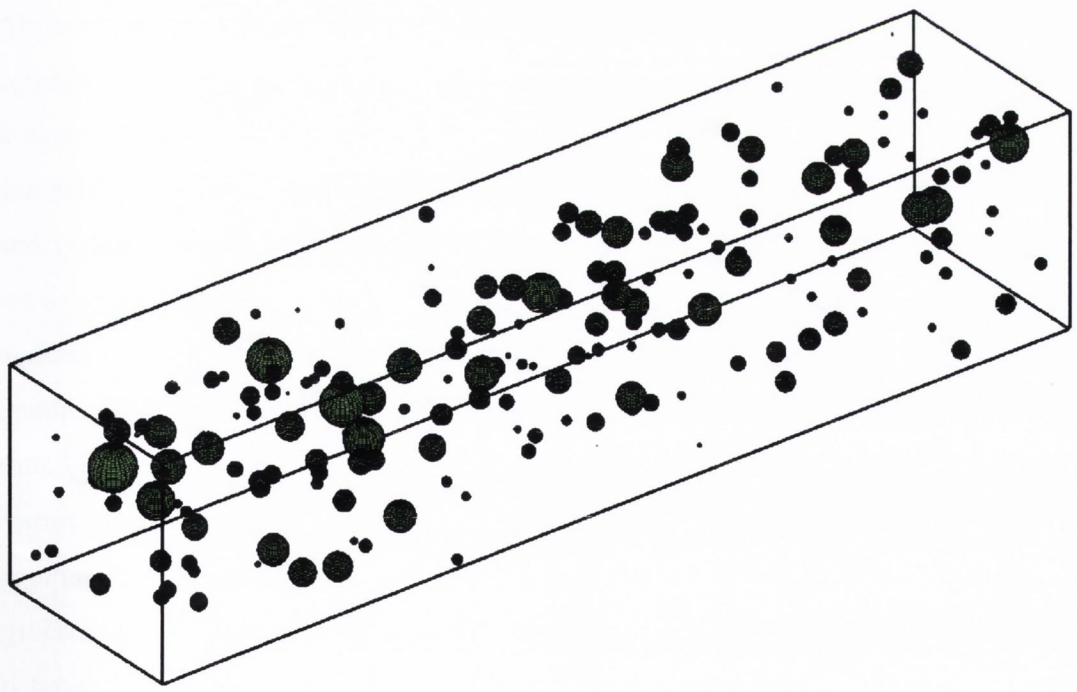

Figure 10.2: Illustration of hand-mixed bone cement sample containing 1.8% porosity. Dimensions of specimen are 16x3.5x3.5mm.

Various attempts have been made to develop such a preparation technique. Both Tunney *et al* (Tunney 2008) and Shi *et al* (Shi 2006) incorporated nanoparticles of chitosan into the cement. Chitosan is a copolymer of glucosamine and *N*-acetyl glucosamine deacetylated from the natural polymer chitin and in its crystalline form it is biodegradable and biocompatible. The idea behind this technique was to mix the cement under a vacuum, eradicating the pores. The nanoparticles would then degrade *in vivo*, resulting in a uniform distribution of small cavities or pores which would facilitate the release of antibiotics. Shi *et al* found this technique to be a great success, with improved drug release and only a marginal decrease in the mechanical properties of the material. However the study by Tunney *et al* reported conflicting results with decreased drug release and significantly reduced mechanical properties. Either way, it can be concluded that this technique has promise but further work is needed to fully verify this approach.

Another approach may involve mixing the cement at atmospheric pressure but developing a mixing technique that will result in a relatively low level of porosity, such as the 1.8% mentioned above. Various mixing bowls are available commercially but these tend to be incorporated into vacuum-mixing systems. The effect of mixer design has been shown to be very influential on the resulting fatigue life of the cement. For example, cement prepared using the HiVac system has been found to demonstrate superior fatigue strength to that prepared by the Ultramix system (Eveleigh 2002). This was a result of HiVac using a rotating axis system, where the mixing paddle continually rotates around the circumference of the bowl. This ensures that even when the cement is in the doughy state, the paddle continues to mix the cement. The Ultramix system uses a fixed axis and as a consequence tends to push the cement rather than mix it once it has reached the doughy state. Also numerous studies have reported large variations in the quality of cement prepared by different scrub technicians. Macaulay *et al* (Macaulay 2002) reported large variations in mean porosity and mean pore size while Eveleigh *et al* (Eveleigh 2002) reported a significant difference in the fatigue life of samples prepared by scrub staff to that prepared by the authors in the laboratory. Significant variance was found in all results. Therefore, a possible design to achieve a consistent uniform distribution of small pores may involve operator independent mechanical mixing of the cement using a rotating axis system at atmospheric pressure.

Other studies have attempted to use a whisk like device to mix the cement with the aim of increasing porosity to increase drug elution. Using a whisk to mix the cement resulted in porosity of approximately 8% and significantly improved drug elution (Shiramizu 2008). However, using a whisk would aim to incorporate porosity through air entrapment. This type of porosity formation tends to result in very large pores which are something that should be avoided. The study by Shiramizu *et al* did not record pore sizes and did not conduct any mechanical tests.

A common technique which was not investigated in this study was mixing at atmospheric pressure followed by centrifugation. This technique has been shown to reduce porosity levels and also reduce the average size of pores. This technique may provide an acceptable distribution of porosity. Regarding all the possible techniques discussed above, the distribution of porosity could be determined and incorporated into the virtual models developed in chapter 7. This would allow an investigation into the suitability of each technique at producing the required cement porosity distribution.

Another issue regarding the effect of porosity needs to be mentioned. It was demonstrated in chapter 9 that a heat gradient can result in preferential pore formation at the cement/stem interface as a result of polymerisation shrinkage. This is a major concern as this interface has been highlighted as weak region in cemented joint replacements. Also it was proposed in this study that porosity would not influence failure as it was unlikely that a pore would be in the critical region close to the corner of the stem. This may not be the case if large numbers of pores are forming at this interface. Further work is needed to investigate this phenomenon.

10.4. Approximate rules

In order to discover the exact effect of any stress concentration feature in bone cement, it is necessary to carry out an elastic stress analysis using finite element modelling and to utilize the TCD as described in chapter 5-9. However, some

simple approximate rules can be derived as follows. For the purpose of further analysis the equation to determine the critical distance is reproduced below.

$$L = \frac{1}{\pi}\left(\frac{\Delta K_{th}}{\Delta \sigma_0}\right)^2 \tag{10.3}$$

Assuming that the Smith/Miller approach applies for all notches greater than K_{t1}, then equations 10.1-10.3 above can be used, but taking the fatigue strength to be $\Delta\sigma_{ot}$ rather than $\Delta\sigma_o$. Values for the two critical K_t values can then be derived, as follows:

$$K_{t1} = \frac{\Delta \sigma_{ot}}{\Delta \sigma_o} \tag{10.4}$$

$$K_{t2} = F\sqrt{\frac{D}{L}} \tag{10.5}$$

The value of K_{t1} is useful because it defines the transition from the safe to blunt regime in figure 10.1(b) i.e. the transition from porosity influencing failure to porosity having no effect in the cement. Using equation 10.4 a value of 25/14.4 = 1.74 could be predicted. Experimentally, "Safe" behaviour was found in all notches with a $K_t<1.74$ and also for some other notches with K_t up to 2.4. This suggests that equation 10.4 gives a conservative estimate of the limits of this region. The value of K_{t2} is also useful because it defines the worst possible stress concentration. So if the mantle already contains such a stress concentration, there is nothing to be lost by increasing its K_t factor even more, because this will not reduce the fatigue strength any further.

K_{t2} is dependant on three factors, D, ρ and F; however it is worth noting that the K_t factors of many notches can be approximated by the well-known formula derived by Neuber, which is exact for elliptical notches:

$$K_t = 1 + 2\sqrt{\frac{D}{\rho}} \qquad (10.6)$$

Comparing equations 10.5 and 10.6 it can be seen that K_{t2} is characterised by a notch root radius which is of the same order of magnitude as the critical distance, L, so this will be a useful approximate guide for the transition between the Blunt Notch and Sharp Notch regimes.

Chapter 11

Conclusions

11.1. Conclusions

11.1.1. Stress concentrations in Bone Cement

11.1.2. Theory of Critical Distances (TCD)

11.2. Future work (Suggestions)

11.2.1. Stem geometry

11.2.2. Mixing technique

11.2.3. Heat gradient on pore formation

11.2.4. Pre-polymerised beads

11.1. Conclusions

11.1.1. Stress concentrations in Bone Cement

- This thesis has presented the most comprehensive study of the effect of stress concentrations on the fatigue behaviour of bone cement. Stress concentrations in the form of sharp notches and circular holes were found to significantly reduce the fatigue strength of bone cement, particularly when their stress concentration factor (K_t) was greater than approximately 2.4. This type of defect would be similar to casting defects or protruding bone in the cement mantle.

- Stress concentrations in the form of the corners of the stem were found to initiate fatigue failure in an experimental model representing a 2D cross section of a cemented hip replacement. This indicates the stem as a major source of failure *in vivo*.

- Porosity was found to significantly reduce the fatigue strength of plain uniaxial test specimens. Key factors regarding porosity were pore size and pore distribution, where pores in close proximity would link together to form a pore of more complex shape. Also the extent of porosity was very influential, with high levels of porosity increasing the probability of a large pore or cluster of pores occurring.

- Despite the damaging effects of porosity it was demonstrated that once bone cement contains a stress concentration with a Kt>2.4 i.e. more damaging than porosity, the porosity did not influence fatigue failure in any form. This non-effect of porosity provides an explanation for why removing porosity from the cement mantle is not resulting in an increased fatigue life in cemented implants, as high stress concentrations do arise *in vivo* in the form of the stem.

- Given the potential non-effect of porosity and taking into account its beneficial effects, it is proposed that porosity should not be removed from

the cement mantle. However, in order to minimise the damaging effect of porosity, a possible solution may be a compromise of small evenly distributed pores throughout the cement mantle.

- Pore-free bone cement demonstrated superior fatigue strength to pure PMMA in the form of perspex. The greater fatigue strength of pore-free bone cement can be attributed to its microstructure. The pre-polymerised beads found in bone cement may act as barriers to crack growth, resulting in a longer fatigue life.

11.1.2. Theory of Critical Distances (TCD)

- The Theory of Critical Distances (TCD) in the form of the Point Method (PM) was successfully developed to predict the role of stress concentrations in the form of introduced notches and design features such as the stem. This is the first time this theory has been used to predict fatigue failure in any polymer and should prove to be a simple yet powerful tool in the future design and development of cemented arthroplasties.

- The TCD was developed to predict the role of pore size and pore clustering and was incorporated into a virtual model of bone cement allowing the scatter associated with porous specimens to be predicted.

- The non effect of porosity was verified theoretically using the TCD, as the TCD successfully predicted the effect of stress concentrations using a critical stress equal to the true strength of bone cement i.e. assuming that porosity was not present in the material.

- The initial region of crack-growth around a bead and the length of the micro-cracks at the crack tip in bone cement are very similar to the length of the critical distance i.e. 0.1mm. These may be a physical realisation of the critical distance.

11.2. Future Work (Suggestions)

11.2.1. Stem geometry

It was demonstrated in chapter 9 that the geometry of the cross-section of the stem plays a major role in fatigue failure of the cement mantle. Further testing could be conducted on different cross sections to determine the optimal rotational stability while minimising the stress concentration. A computational study by Kim *et al* (Kim 2008) concluded that an oval shaped stem with corners of 2mm root radius would prove to be an optimal design. This could be verified using the experimental rig designed for this study. Other factors regarding stem design are the cross section in the longitudinal direction. This would investigate the flexural loads transmitted by the stem on the cement mantle. This type of rig has been developed by other authors such as Jeffers *et al* (Jeffers 2007) (see figure 11.1). The effectiveness of the TCD in predicting fatigue failure in such a specimen could be investigated.

Ultimately the final step would involve the application of the TCD to a full 3-dimensional reconstruction of the cement mantle.

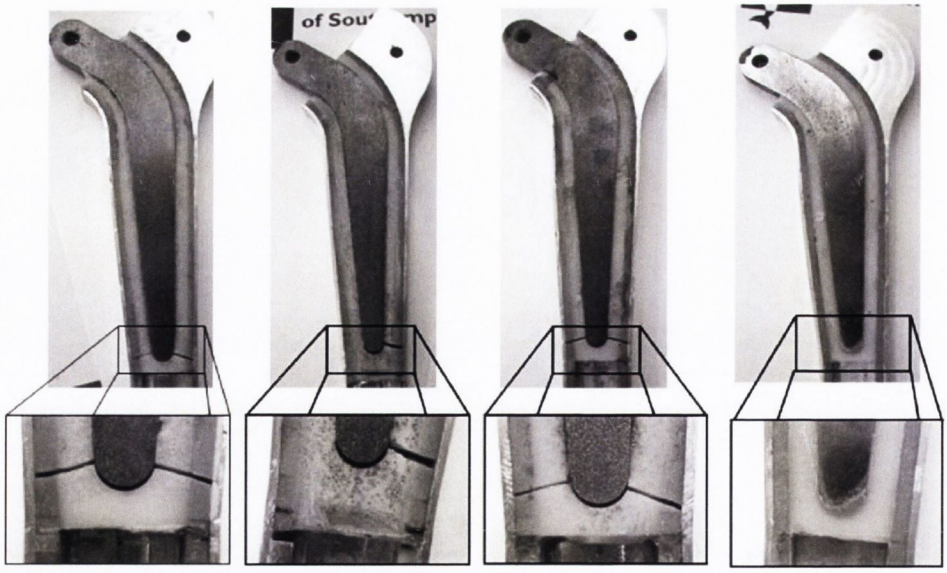

(a) (b) (c) (d)

Figure 11.1: Cement mantle fractures in the four different specimens after 2 million load cycles for the polished stem finish (a–c) and grit blasted stem finish (d). Taken from (Jeffers 2007)

11.2.2. Mixing technique

The effect of mixing technique on the porosity level and distribution was discussed in chapter 10 and several possible future designs were proposed. An investigation into future mixing techniques that may result in an optimal pore distribution could be investigated. The pore size distribution resulting from each mixing technique could be determined and incorporated into the virtual models created in chapter 7. This would allow an investigation into each techniques capability of achieving a safe distribution of porosity.

11.2.3. Heat gradient on pore formation

A preliminary study on the effect of a heat gradient on pore formation was conducted as part of this thesis and the results were presented in chapter 9. The results proved to be interesting, with significantly increased porosity levels and pore formation at the stem/cement interface. Further work is needed to verify and explain these initial findings. Mechanical testing of the heated samples should be conducted to investigate the effect of this pore formation at the interface. Also the effect of heating the stem should also be investigated. This would eradicate the heat gradient and so theoretically prevent preferential pore formation. This would also allow an investigation into the increased overall level of porosity. Is this increase a result of the increased heat (i.e. increased monomer evaporation) or was it a result of the polymerisation shrinkage?

11.2.4. Pre-polymerised beads

The role of pre-polymerised beads on the mechanical properties of bone cement has recently become a topic of discussion. Lewis and co-authors have suggested that pre-polymerised beads should be eliminated from the cement while other authors have suggested that may act to blunt propagating cracks. This thesis has proposed a relationship between the size of the pre-polymerised bead and length of the critical distance for fatigue in bone cement. If this relationship exists then an increase in the size of the beads may result in an increase in the critical distance. An increase in the critical distance would imply an increase in the resistance to crack propagation, hence increasing the fatigue strength of the material. Therefore an investigation into the effect of pre-polymerised bead size on the fatigue behaviour of bone cement may a worthwhile direction for future research.

References

Ashby, F. A., Jones, D.R.H. (1980). Engineering Materials 1, Elsevier Science.

Baker, A. S., Greenham, L.W. (1988). "Release of gentamicin from acrylic bone cement. Elution and diffusion studies." J. Bone Joint Surg. **70**: 1551-1557.

Bhambri, S. K., Gilbertson, L.N. (1995). "Micromechanisms of fatigue crack initiation and propagation in bone cements." Journal of Biomedical Materials Research **29**: 233-237.

Breusch, S., Malchau, H. (2005). The Well-Cemented Total Hip Arthroplasty, Springer Berlin Heidelberg.

Bruens, M. L., Pieterman, H., de Wijn, J.R., Vaandrager, J.M. (2003). "Porous polymethylmethacrylate as bone substitute in the craniofacial area." Journal of Craniofacial Surgery **14**(4): 596-598.

Burke, D. W., Gates, E.I., Harris, W.H. (1984). "Centrifugation as a method of improving tensile and fatigue properties of acrylic bone cement." Journal of bone and joint surgery **66**(A): 1265-1273.

Burns, A. W. R., Bourne, R.B. (2006). "Economics of revision total hip arthroplasty." Current Orthopaedics **20**: 203-207.

Carter, D. R., Gates, E.I., Harris, W.H. (1982). "Strain controlled fatigue of acrylic bone cement." Journal of Biomedical Materials Research **16**: 647-657.

Charnley, J. (1960). "Anchorage of the femoral head prosthesis to the shaft of the femur." Journal of Bone and Joint Surgery, Br **42**: 28-30.

Cox, B. D., Wilcox, R.K., Levesley, M.C., Hall, R.M. (2006). "Assessment of a three-dimensional measurement technique for the porosity evaluation of PMMA bone cement." Journal of Material Science: Materials in Medicine **17**: 553-557.

Crawford, R. J., Klewpatinond, V., Benham, P.P. (1978). "Effect of moulded and machined notches upon the fatigue strength of an acetal copolymer." Polymer **20**(5): 649-652.

Cristofolini, L., Erani, P., Savigni, P., Bordini, B., Viceconti, M. (2007). "Preclinical assessment of the long-term endurance of cemented hip stems. Part 2: *in vitro* and *ex-vivo* fatigue damage of the cement mantle." Proc Inst Mech Eng [H] J, Journal of engineering in medicine **221**: 585-599.

Cristofolini, L., Minari, C., Viceconti, M. (2000). "A methodology and criterion for acrylic bone cement fatigue tests." Fatigue and Fracture of Engineering Materials and Structures **23**: 953-957.

Culleton, T. P., Prendergast, P.J., Taylor, D. (1993). "Fatigue failure in the cement mantle of an artificial hip joint." Clinical Materials **12**: 95-102.

Davies, J. P., Harris, W.H. (1988). "Optimization and Comparison of Three Vacuum Mixing Syetems for Porosity Reduction of Simplex P Cement." Clinical Orthopaedics and Related Research **254**: 261-269.

Davies, J. P., O'Connor, D.O., Burke, D.W., Harris, W.H. (1989). "Influence of antibiotic impregnation on the fatigue life of Simplex P and Palacos R acrylic bone cements, with and without centrifugation." Journal of Biomedical Material Research **23**(4): 379-397.

Demarest, V. A., Lautensclager, E.P., Wixson, R.L. (1983). Vacuum mixing of acrylic bone cement. 9th Annual Meeting of the Society for Biomaterials, Birmingham, Alabama.

Dunne, N. J., Hill, J., McAfee, P., Kirkpatrick, R., Patrick, S., Tunney, M. (2008). "Incorporation of large amounts of gentamicin sulphate into acrylic bone cement: effect on handling and mechanical properties, antibiotic release, and biofilm formation." Proc Inst Mech Eng [H] J, Journal of engineering in medicine **222**(3): 355-366.

Dunne, N. J., Orr, J.F., Beverland, D.E. (2004). "Assessment of cement introduction and pressurization techniques." Proc Inst Mech Eng [H], Journal of engineering in medicine **218**(1): 11-25.

Dunne, N. J., Orr, J.F., Mushipe. M.T., Eveleigh. R.J. (2003). "The relationship between porosity and fatigue characteristics of bone cements." Biomaterials **24**: 239-245.

Ebramzadeh, E., Sarmiento, A., McKellop, H.A., Llinaf, A., Gogan, W. (1994). "The cement mantle in total hip arthroplasty. Analysis of long-term radiographic results." Journal of Bone and Joint Surgery, Am **76**: 77-87.

El Haddad, M. H., Smith, K.N., Topper, T.H. (1979). "Fatigue crack propagation of short cracks." Journal of Engineering Materials and Technology (Trans ASME) **101**: 42-46.

Evans, S. L. (2006). "Effects of porosity on the fatigue performance of polymethyl methacrylate bone cement: an analytical investigation." Proceedings of the institution of Mechanical Engineers, Part H: Journal of Engineering in Medicine **220**(1): 1-10.

Eveleigh, R. J., Dunne, N.J., Mushipe, M.T., Orr, J.F., Beverland, D.E. (2002). "The fatigue life of bone cement: how is it affected by mixer design, vacuum level and user technique." Journal of Advanced Perioperative Care **1**(1): 13-17.

Freitag, T. A., Cannon, S.L. (1977). "Fracture and fatigue characteristics of bone cements." Journal of Biomedical Materials Research **11**: 609-624.

Frost, N. E., Marsh, K.J., Pook, L.P. (1974). Metal fatigue. London, Oxford University Press.

Gardiner, R. C., Hozack, W.J. (1994). "Failure of the cement-bone interface. A consequence of strengthening the cement-prosthesis interface?" Journal of bone and Joint Surgery - Series B **76**(1): 49-52.

Geiger, M. H. M. K., E. Michael MD; Ritter, Merrill A. MD; Ginther, Jeffrey A. MD; Faris, Philip M. MD; Meding, John B. MD (2001). "The Clinical

Significance of Vacuum Mixing Bone Cement." Clin Orthop Relat Res **382**: 258-266.

Gilbert, J. L., Hasenwinkel, J.M., Wixson, R.L., Lautenschlager, E.P. (2000). "A theoretical and experimental analysis of polymerization shrinkage of bone cement: A potential major source of porosity." Journal of Biomedical Materials Research **52**: 210-218.

Ginebra, M. P., Albuixech, L., Fernandez-Barragan, E., Aparicio, C., Gil, F.J., San Roman, J., Vazquez, B., Planell, J.A. (2002). "Mechanical performance of acrylic bone cements containing different radiopacifying agents." Biomaterials **23**: 1873-1882.

Gotham, K. V. (1973). Plastics and Polymers.

Harrigan, T. P., kareh, J.A., O'Connor, D.O., Burke, D.W., Harris, W.H., (1992). "A finite element study of the initiation of failure of fixation in cemented femoral total hip replacements." Journal of Orthopaedic Research **10**: 134-144.

Havelin, L. I., Engesaeter, L.B., Espehaug, B., Furnes, O., Lie, S.A., Vollset, S.E (2000). "The Norwegian arthroplasty register - 11 years and 73,000 artheoplasties." Acta Orthopaedica Scandinavica **71**(4): 337-353.

Heisel, C., Norman, T., Rupp, R., Pritsch, M., Ewerbeck, V., Breusch, S.J. (2003). "In vitro performance of intramedullary cement restrictors in total hip arthroplasty." Journal of Biomechanics **36**(6): 835-843.

Hernigou, P., Le Mouel, S. (1999). "Do voids on a femoral cement mantle affect the outcome?" The Journal of Arthroplasty **14**(8): 1005-1010.

Hertzberg, R. W., Manson, J.A. (1980). Fatigue of engineering plastics, London: Academic Press.

Hertzler, J., Miller, M.A., Mann, K.A. (2002). "Fatigue crack growth rate does not depend on mantle thickness: an idealized cemented stem construct under torsional loading." Journal of Orthopaedic Research **20**: 676-682.

Ishihara, S., McEvily, A.J., Goshima, T., Kanekasus, K., Nara, T. (2000). "On fatigue lifetimes and fatigue crack growth behaviour of bone cement." Journal of materials science: materials in medicine **11**: 661-666.

Jacobs, J., J., Roebuck, K,A., Archibeck, M., Hallab, N,J., Glant, T.T. (2001). "Osteolysis: basic science." Clinical Orthopaedics and Related Research **393**: 71-77.

James, S. P., Jasty, M., Davies, J., Piehler. H, Harris, W.H. (1992a). "A fractographic investigation of PMMA bone cement focusing on the relationship between porosity reduction and increased fatigue life." Journal of biomedical materials research **26**: 651-662.

Janssen, D., Aquarius, R., Stolk, J., Verdonschot, N. (2005a). "The contradictory effects of pores on fatigue cracking of bone cement." Journal of biomedical materials research **74B**(Applied Biomaterials): 747-753.

Janssen, D., Stolk, J., Verdonschot, M. (2005b). "Why would cement porosity reduction be clinically irrelevant, while experimental data show the contrary." Journal of Orthopaedic Research **23**: 691-697.

Jasty, M., Davies, J.P., O'Connor, D.O., Burke, D.W., Harrigan, T.P., Harris, W.H. (1990). "Porosity of various preparations of acrylic bone cements." Clinical Orthopaedics and Related Research **259**: 122-129.

Jasty, M., Maloney, W.J., Bragdon, C.R., O'Connor, D.O., Haire, T., Harris, W.H. (1991). "The initiation of failure in cemented femoral components of hip arthroplasties " The Journal of Bone and Joint Surgery **73-B**(4): 551-558.

Jeffers, J. R. T., Browne, M., Lennon, A.B., Prendergast, P.J., Taylor, M. (2007). "Cement mantle fatigue failure in total hip replacement: Experimental and computational testing." Journal of Biomechanics **40** 1525-1533.

Jeffers, J. R. T., Browne, M., Roques, A., Taylor, M. (2005). "On the importance of considering porosity when simulating the fatigue of bone cement." Journal of Biomechanical Engineering **127**: 563-570.

Johnson, J. A., Provan, J.W., Krygier, J.J., Chan, K.H., Miller, J. (1989). "Fatigue of acrylic bone cement - effect of frequency and environment." Journal of Biomedical Material Research **23**(8): 819-31.

Karageorgiou, V., Kaplan, D. (2005). "Porosity of 3D biomaterial scaffolds and osteogenesis." Biomaterials **26**: 5474-5491.

Karrholm, J., Garellick, G., Herberts, P. (2006). Swedish Hip Arthroplasty Register.

Kedgley, A. E., Takaki, S.E., Lang, P., Dunning, C.E. (2007). "The effect of cross-sectional stem shape on the torsional stability of cemented implant components." Journal of Biomechanical Engineering **129**: 310-314.

Kim, B., Moon, B., Mann, K.A., Kim, H., Boo, K. (2008). "Simulated crack propagation in cemented total hip replacements." Materials Science and Engineering **doi:10.1016/j.msea.2007.01.171**.

Kinloch, A. J., Williams, J.G. (1980). "Crack blunting mechanisms in polymers." Journal of Material Science **15**: 987-996.

Kinloch, A. J., Young, R.J. (1983). Fracture behaviour of polymers. London, Applied Science Publishers.

Kjellson, F. (2005). Non-ionic contrast media in acrylic bone cement. Lund, Lund University Hospital. **Phd**.

Krause, W., Mathis, R.S. (1988). "Fatigue properties of acrylic bone cement: Review of the literature." Journal of biomedical Material Research **22**(A1): 37-53.

Kühn, K.-D. (2000). Bone Cements: Up-to-date comparison of physical and mechanical properties of commercial materials, Springer Verlag New York.

Kurtz, S. M., Villarraga, M.L., Zhao, K., Edidin, A.A. (2005). "Static and fatigue mechanical behavior of bone cement with elevated barium sulphate content for treatment of vertebral compression fractures." Biomaterials **26**: 3699-3712.

Lang, R. W., Manson, J.A., Hertzberg, R.W. (1984). "Craze development in Poly(Methyl Methacrylate) during stable fatigue crack propagation." Polymer engineering and science **24**(10): 833-842.

Lazzarin, P., Tovo, R., Meneghetti, G. (1997). "Fatigue crack initiation and propagation phases near notches in metals with low notch sensitivity." International Journal of Fatigue **19**: 647-657.

Lewis, G. (1997). "Properties of acrylic bone cement: state of the art review." Journal of biomedical materials research **38**: 155-182.

Lewis, G. (2002). "Fatigue testing and performance of acrylic bone cement materials: State of the art review." Journal of Biomedical Materials Research Part B: Applied Biomaterials **66B**: 457-486.

Lewis, G., Janna, S., Carroll, M. (2003). "Effect of test frequency on the *in vitro* fatigue life of acrylic bone cement." Biomaterials **24**: 1111-1117.

Lewis, G., Xu, J., Madigan, S., Towler, M.R. (2007). "Influence of two changes in the composition of an acrylic bone cement on its handling, thermal, physical, and mechanical properties." Journal of Material Science: Materials in Medicine **18**: 1649-1658.

Linden, U., Gillquist, J. (1989). "Air inclusion in bone cement. Importance of the mixing technique." Clin Orthop Relat Res **247**: 148-151.

Ling, R. S., Lee, A.J. (1998). "Porosity reduction in acrylic cement is clinically irrelevant." Clinical Orthopaedics and Related Research **355**: 249-53.

Lucht, U. (2000). "The Danish hip arthroplasty register." Acta Orthopaedica Scandinavica **71**(5): 433-439.

Macaulay, W., DiGiovanni, C.W., Restrepo, A., Saleh, K.J., Walsh, H., Crossett, L.S., Peterson, M.G.E., Li, S., Salvati, E.A. (2002). "Differences in Bone-Cement Porosity by Vacuum Mixing, Centrifugation, and Hand-Mixing." The Journal of Arthroplasty **17**(5): 569-575.

Majkowski, R. S., Miles, A.W., Bannister, G.C., Perkins, J., Taylor, G.J.S. (1993). "Bone surface preparation in cemented joint replacement." Journal of Bone and Joint Surgery, Br **75**: 459-463.

Malchau, H., Herberts, P., Ahnfelt, L. (1993). "Prognosis of total hip replacement in Sweden. Follow-up of 92,675 operations performed 1978-1990." Acta Orthop Scand **64**(5): 497-506.

Malchau, H., Herberts, P., Ahnfelt, L.E., Johnell, O. (1994). "Prognosis of total hip replacement. Results from a national register of revised failures 1979-1990 in Sweden - a 10 year follow up of 92,675 total hip replacements." Scientific exhibition presented at the 61st American Academy of Orthopaedic Surgeons.

Maloney, W. J., Jasty, M., Rosenberg, A., Harris, W.H. (1990). "Bone lysis in well fixed cemented femoral components." Journal of Bone and Joint Surgery **72-B**: 966-970.

Mann, K. A., Bartel, D.L., Wright, T.M., Burstein, A.H. (1995). "Coulomb frictional interfaces in modeling cemented total hip replacements: a more realistic model." Journal of Biomechanics **28**: 1067-1078.

McCaskie, A. W., Barnes, M.R., Lin, E., Harper, W.M., Gregg, P.J. (1997). "Cement pressurisation during hip replacement " Journal of Bone and Joint Surgery, Br **79**: 379-384.

McCormack, B. A. O., Prendergast, P.J. (1999a). "Microdamage accumulation in the cement layer of hip replacements under flexural loading." journal of biomechanics **32**: 467-475.

McCormack, B. A. O., Prendergast, P.J., O'Dwyer, B. (1999b). "Fatigue of cemented hip replacements under torsional loads." Fatigue and Fracture of Engineering Materials and Structures **22**: 33-40.

Messick, K. J., Miller, M.A., Damron, L.A., Race, A., Clarke, M.T., Mann, K.A. (2007). "Vacuum-mixing cement does not decrease overall porosity in cemented femoral stems." Journal of Bone and Joint Surgery **89-B**(8): 1115-1121.

Muller, R. T., Heger, I., Oldenburg, M. (1997). "The mechanism of loosening in cemented hip prostheses determined from long term results." Arch Orthrop Trauma Surg **116**(41-45).

Murphy, B. (2001b). Aspects of the fatigue behaviour of acrylic bone cement. Dublin, Trinity College. **Phd**.

Murphy, B. P., Prendergast, P.J. (2000). "On the magnitude and variability of the fatigue strength of bone cement." International Journal of Fatigue **22**: 855-864.

Murphy, B. P., Prendergast, P.J. (2001a). "The relationship between stress, porosity, and non-linear damage accumulation in acrylic bone cement." Journal of Biomedical Materials Research **59**(4): 646-654.

Neuber, H. (1958). Theory of notch stresses: principles for exact calculation of strength with reference to structural form and material. Berlin, Springer Verlag.

Oparaugo, P., C., Clarke, I,C., Malchau, H., Herberts, P. (2001). "Correlation of wear debris induced osteolysis and revision with volumetric wear rates of polyethylene: a survey of 8 reports in the literature." Acta Orthopaedica Scandinavica **72**: 22-28.

Paravic, V., Noble, P.C., Alexander, J.W., Liebs, T.R., Elliot, A. (1999). Effect of specimen preparation on porosity and fatigue life, a study of centrifuged and hand-mixed cement. 45th Orthopaedic Research Society Meeting, Anaheim, CA.

Peterson, R. E. (1959). Notch sensitvity. In *Metal Fatigue*. New York, McGraw Hill.

Prendergast, P. J., Monaghan, J., Taylor, D. (1989). "Materials selection in the artificial hip joint using finite element stress analysis." Clinical Materials **4**: 361-376.

Scheerlinck, T., Casteleyn, P.P. (2006). "The design features of cemented femoral hip implants." Journal of Bone and Joint Surgery, Br **88**: 1409-1418.

Shi, Z., Neoh, K.G., Kang, E.T., Eang, W. (2006). "Antibacterial and mechanical properties of bone cement impregnated with chitosan nanoparticles." Biomaterials **27**: 2440-2449.

Shiramizu, K., Lovric, V., Leung, A., Walsh, W.R. (2008). "How do porosity-inducing techniques affect antibiotic elution from bone cement? An in vitro

comparison between hydrogen peroxide and a mechanical mixer." Journal of Orthopaedics and Traumatology **9**: 17-22.

Sinnett-Jones, P. E., Browne, M., Ludwig, W., Buffiere, J.-Y., Sinclair, I. (2005). "Microtomography assessment of failure in acrylic bone cement." Biomaterials **26**: 6460-6466.

Smith, R. A., Miller, K.J. (1978). "Prediction of fatigue regimes in notched components " International Journal of Mechanical Science **20**: 201-206.

Socie, D. (1987). "Multiaxial fatigue damage models." Journal of Engineering Materials and Technology, Trans ASME **109**(4): 293-298.

Soltesz, U. (1994). "The influence of loading conditions on the lifetimes in fatigue testing of bone cements." Journal of Material Science: Materials in Medicine **5**: 654-656.

Susmel, L. (2003b). "A unifying approach to estimate the high cycle fatigue strength of notched components subjected to both uniaxial and multiaxial cyclic loadings." Fatigue and Fracture of Engineering Materials and Structures **27**: 391-411.

Susmel, L. (2008). "The theory of critical distances: a review of its applications in fatigue." Engineering Fracture Mechanics **75**(7): 1706-1724.

Susmel, L., Taylor, D. (2003). "Fatigue design in the presence of stress concentrations." The Journal of Strain Analysis for Engineering Design **38**(5): 443 - 452

Susmel, L., Taylor, D. (2003a). "Two methods for predicting the multiaxial fatigue limits of sharp notches." Fatigue and Fracture of Engineering Materials and Structures **26**: 821-833.

Susmel, L., Taylor, D. (2005). The theory of critical distances to predict fatigue lifetime of notched components. Advances in Fracture and Damage Mechanics IV, Eastleigh, UK, EC Publications.

Susmel, L., Taylor, D. (2006). "A simplified approach to apply the theory of critical distances to notched components under torsional fatigue loading." International Journal of Fatigue **28**: 417-430.

Tanaka, K. (1983). "Engineering formulae for fatigue strength reduction due to crack-like notches." International Journal of Fracture **22**(2): R39 - R46

Taylor, D. (1999). "Geometrical effects in fatigue: a unifying theoretical model." International journal of fatigue **21**: 413-420.

Taylor, D. (2005a). "Analysis of fatigue failures in components using the theory of critical distances." Engineering failure analysis **12**: 906-914.

Taylor, D. (2007). The Theory of Critical Distances: A New Perspective in Fracture Mechanics, Elsevier.

Taylor, D., Bologna, P., Bel Knani, K. (2000b). "Prediction of fatigue failure location on a component using a critical distance method." International Journal of Fatigue **22**: 735-742.

Taylor, D., Cornetti, P., Pugno, N. (2005b). "The fracture mechanics of finite crack extension." Engineering Fracture Mechanics **72**: 1021-1038.

Taylor, D., Hoey, D. (2008). "High cycle fatigue of welded joints: The TCD experience." International Journal of Fatigue **doi:10.1016/j.ijfatigue.2008.01.011**.

Taylor, D., Merlo, M., Pegley, R., Cavatorta, M.P. (2004a). "The effect of stress concentrations on the fracture strength of polymethylmethacrylate " Material Science and Engineering **382**(A): 288-294.

Taylor, D., Wang, G (2000a). "The validation of some methods of notch fatigue analysis." Fatigue and Fracture of Engineering Materials and Structures **23**: 387-294.

Topoleski, T. L. D., Ducheyne, P., Cuckler, J.M. (1990). "A fractographic anaylsis of in vivo poly(methyl methacrylate) bone cement failure mechanisms." Journal of biomedical materials research **24**: 135-154.

Topoleski, T. L. D., Ducheyne, P., Cuckler, J.M. (1993). "Microstructural pathway of fracture in poly(methyl methacrylate) bone cement." Biomaterials **14**: 1165-1172.

Tunney, M., M., Brady, A, J., Buchanan, F., Newe, C., Dunne, N, J. (2008). "Incorporation of chitosan in acrylic bone cement: Effect on antibiotic release, bacterial biofilm formation and mechanical properties." Journal of Material Science: Materials in Medicine **19**: 1609-1615.

van de Belt, H., Neut, D., Uges, D.R.A., Schenk, W., van Horn, J.R., van der Mei, H.C., Busscher, H.J. (2000). "Surface roughness, porosity and wettability of gentamicin-loaded bone cements and their antibiotic release." Biomaterials **21**: 1981-1987.

Verdonschot, N., Huiskes, R. (1996). "mechanical effects of stem cement interface characteristics in total hip replacement." Clin Orthop Relat Res **329**: 326-36.

Waddoups, M. E., Eisenamnn, J.R., Kaminski, B.E. (1971). "Macroscopic fracture mechanics od advanced composite materials." Journal of Composite Materials **5**: 446-454.

Whitney, J. M., Nuismer, R. J. (1974). "Stress fracture criteria for laminated composites containing stress concentrations." Journal of Composite Materials **8**: 253-265.

www.ansys.com. (2008).

www.enotes.com. (2008). "How Products are Made: Acrylic Glass."

www.jointreplacement.com (2005).

www.orthoteers.co.uk (2005).

www.stryker.com (2008).

Yousef, A., Wallace, A. (2006). "The effectiveness of the proximal femoral stem centraliser on the stem alignment in total hip replacement." European Journal of Orthopaedic Surgery and traumatology **16**(3): 223-227.

Appendix I

AI.1. Uniaxial fatigue results

AI.1.1. Bone cement

AI.1.2. Polymethylmethacrylate

AI.1.3. Porosity data

AI.2. Torsional fatigue results

AI.1. Uniaxial fatigue results

AI.1.1. Bone cement

Plain	**(Hand Mixed)**			
Stress Level	**N_f**			
20.7 MPa	610,	80		
18.9 MPa	33495,	6490,	14144,	5286,
	2789,	2653,	956	
17.1 MPa	6116,	4299,	3633,	6731,
15.3 MPa	26872,	54715,	11735,	
13.5 MPa	241225,	47271,	22309,	16490

Table A1.1: Number of cycles to failure for a plain specimen at four different stress levels.

Plain	**(Vacuum Mixed)**			
Stress Level	**N_f**			
20.7 MPa	3469,	2913,	6549,	165
18.9 MPa	3250,	3206,	9338,	12128
17.1 MPa	63544,	146531,	7007,	17989
15.3 MPa	120177,	18648,	41457,	300311

Table A1.2: Number of cycles to failure for a vacuum mixed plain specimen at four different stress levels.

Plain	**(Pore free)**			
Stress Level	**N_f**			
24.3 MPa	23291,	42530,	27731,	66073
22.5 MPa	66900,	29284,	69027,	107088
21.6 MPa	73669,	127581,	36959,	83600

Table A1.3: Number of cycles to failure for a pore free plain specimen at three different stress levels.

Notch	(0.1mm rr, 2mm depth)			
Stress Level	**N_f**			
15.3 MPa	126,	22		
10.8 MPa	457,	387		
8.1 MPa	62418,	10967		
7.2 MPa	10217			
6.3 MPa	273214,	32998		

Table A1.4: Number of cycles to failure for a notched specimen (rr = 0.1mm) at five different stress levels.

Notch	(0.75mm rr, 2mm depth)			
Stress Level	**N_f**			
10.8 MPa	4495,	1792,	2691,	2477,
	3041			
9 MPa	22537,	8409,	6916	
7.2 MPa	40067,	97000,	21933,	18618
6.75 MPa	271925 (S),	244667 (S)		
6.3 MPa	237155 (S),	175951,	250056 (S)	

Table A1.5: Number of cycles to failure for a notched specimen (rr = 0.75mm) at five different stress levels. (S) implies sample was stopped.

Notch	(1.5mm rr, 2.2mm depth)			
Stress Level	**N_f**			
13.5 MPa	2311,	1812,	1497,	1382
11.7 MPa	15083,	8512,	7126,	6692
9.9 MPa	233983,	38894,	9231,	9115
9 MPa	477801,	208756,	152424,	69486

Table A1.6: Number of cycles to failure for a notched specimen (rr = 1.5mm) at four different stress levels.

Notch	(4mm rr, 2mm depth)			
Stress Level	**N_f**			
15 MPa	156, 88	2371,	2200,	991,
13 MPa	9988,	2071,	18165,	41
11 MPa	13731,	83843,	122729	
10 MPa	82055,	95687,	130389	

Table A1.7: Number of cycles to failure for a notched specimen (rr = 4mm) at four different stress levels.

Notch	(7mm rr, 2mm depth)			
Stress Level	**N_f**			
15 MPa	3681,	1578,	175,	2340
13 MPa	3265,	14327,	31479,	4721
11 MPa	2245,	23673,	43152,	6158
10 MPa	66353,	44466		
9 MPa	9704,	198972,	192789	

Table A1.8: Number of cycles to failure for a notched specimen (rr = 7mm) at five different stress levels.

Notch	(50mm rr, 2mm depth)			
Stress Level	**N_f**			
16.2 MPa	4508,	3087,	3016,	2591
14.4 MPa	26787,	15220,	13328,	10980
13.05 MPa	59514,	46680,	5340	
11.7 MPa	172874,	98252,	73612,	43821

Table A1.9: Number of cycles to failure for a notched specimen (rr = 50mm) at four different stress levels.

Hole	(2.2mm diameter)			
Stress Level	**N_f**			
12.6 MPa	4399			
11.7 MPa	31523,	17635		
9.9 MPa	103913,	72192		
8.1 MPa	627402			

Table A1.10: Number of cycles to failure for a specimen containing a hole at four different stress levels.

Hemisphere	(1mm diameter)			
Stress Level	**N_f**			
18.9 MPa	6490,	2713,	5664,	
17.1 MPa	17911,	6456,	6835,	
15.3 MPa	21189,	33164,	21797,	30438
13.5 MPa	102653,	489259,	250046,	

Table A1.11: Number of cycles to failure for a specimen containing a hemisphere at four different stress levels.

AI.1.2. Polymethylmethacrylate

Plain			
Stress Level	**N_f**		
28 MPa	2066,	1356,	
26 MPa	6614,	12984,	2157
24 MPa	5176,	4054,	10039,
22 MPa	14855,	5096,	17884
20 MPa	29951,	10138	
18 MPa	35960,	16007	
16 MPa	88713,	61510	
15 MPa	133386		

Table A1.12: Number of cycles to failure for a plain specimen at eight different stress levels.

Notch	**(0.1mm rr, 2mm depth)**		
Stress Level	**N_f**		
7 MPa	4062,	3766,	5749
6 MPa	5019,	4205,	3859
5 MPa	11419,	14475,	7058
4 MPa	120048,	50356,	34370

Table A1.13: Number of cycles to failure for a notched specimen (rr = 0.1mm) at four different stress levels.

Notch	(1.5mm rr, 2.2mm depth)		
Stress Level	**N_f**		
11 MPa	2446,	1643,	1613
10 MPa	1723,	3727,	19412
9 MPa	6145,	56177,	50392
8 MPa	132321,	131522,	39475
7 MPa	194716		
5 MPa	214693 (S)		

Table A1.14: Number of cycles to failure for a notched specimen (rr = 1.5mm) at six different stress levels. (S) implies sample was stopped.

Hole	(2.2mm diameter)			
Stress Level	**N_f**			
14 MPa	5533,	5350,	3540,	3199
12 MPa	16132,	16634,	12648,	17141
10 MPa	17740,	27489,	13590,	24337
9 MPa	45843,	70433,	70171	
8 MPa	180855,	54320,	114374,	211510 (S)

Table A1.15: Number of cycles to failure for a specimen containing a hole at four different stress levels. (S) implies sample was stopped.

AI.1.3. Porosity data

Plain	(Hand Mixed)		
Stress Level	**N_f**	**%Porosity**	
		(3D)	**(2D)**
15.3 MPa	20130	8.43	7.4
	12706	9	3.6
	77695	12.51	7.1
	12887	5.65	10.5
	6812	8.53	10
	68512	5.58	2.7
	9726	14.57	6.8
	11910	12.84	9.5
	66372	3.57	5.6
	1519	9.13	9.2

Table A1.16: N_f for HM plain specimens containing different porosity levels

Plain	(Vacuum Mixed)		
Stress Level	**N_f**	**%Porosity**	
		(3D)	**(2D)**
15.3 MPa	18648	1.66	7.52
	1933	5.03	12.17
	41457	1.33	1.02
	7792	2.15	9.73
	120177	1.39	4.42
	814	3.7	8.87
	27919	4.26	13.67
	100170	1.96	2.3
	23340	2.34	5.36
	300311	1.45	0.4

Table A1.17: N_f for VM plain specimens containing different porosity levels

AI.2. Torsional fatigue results

Stem	(Charnley)		
Torque Level	**N**		
	No Failure	**Failure**	**Average**
5 Nm	51023	87412	74218
	81423	97784	89604
	82671	90537	86604
	96605	121941	109273
	71783	91315	81549
	113730	127625	120678
	68445	79900	74173

Table A1.18: Number of cycles to failure for a charnley type stem design

Stem	(Square, 0.1mm rr)		
Torque Level	**N**		
	No Failure	**Failure**	**Average**
6 Nm	68000	97000	82500
	71000	95000	83000
	73000	98000	85500
	54000	81000	67500
	63000	85000	74000
	71000	95000	83000
	104000	122000	113000
	49000	72000	60500

Table A1.18: Number of cycles to failure for a square shaped stem with corners of radius 0.1mm.

Stem		(Square, 1.0mm rr)		
Torque Level		**N**		
		No Failure	**Failure**	**Average**
8.19	Nm	75000	102000	88500
		171000	195000	183000
		120000	141000	130500
		51000	75000	63000
		211000	250000	230500
		102000	133000	117500
		55000	83000	69000

Table A1.18: Number of cycles to failure for a square shaped stem with corners of radius 1.0mm.

Appendix II

AII.1. Matlab Coding

AII.1.1. 2D Fatigue life prediction of HM bone cement

AII.1.2. 3D Fatigue life prediction of HM bone cement

AII.1. Matlab Coding

AII.1.1. 2D Fatigue life prediction of HM bone cement

The Matlab function created to predict the fatigue life of a single 2D hand-mixed specimen is shown below. In order to make a prediction for a vacuum-mixed 2D specimen, the highlighted line below would be changed to incorporate the pore size distribution for vacuum-mixed bone cement. A Master script was then created which called the function as many times as required. The master script is also shown below.

Cluster2DHM Function

```
function [porosity, FL] = cluster2DHM(k)

for i=1:k;
   x(i)=16*rand(1,1);                          % Location of pore centre on x-axis
   y(i)=3.5*rand(1,1);                         % Location of pore centre on y-axis
   r(i)=(lognrnd(-1.53737,0.562528)/2);        % Radius of pore for a hand-mixed cement

   porearea(i) = pi*r(i)^2;                    % 2D x-sectional area of pore
end

b=1;
for j=1:k;
   for i=1:k;
      radii = r(i)+r(j);
      if ((abs(x(i) - x(j))-radii) > 0.2) && ((abs(y(i) - y(j))-radii) > 0.2)  % The distance between the
                                                                               % surface of two pores in the
                                                                               % x and y direction
          continue
      end

      dist = sqrt((x(i)-x(j))^2+(y(i)-y(j))^2);   % The dist between the centre of two pores
      continue

      distall = dist-radii;                       % The dist between the surface of two pores
      if(distall>0 && distall<0.2)                % If dist between the surface of pores >0 but
         case1(b) = dist+radii;                   % <0.2 then new pore Ø = dist+radii.
      else case1(b) = 0;
      end

      if(distall<0 && (r(i)+dist) > r(j))         % If two pores overlap then new pore Ø =
         case2(b) = dist+radii;                   % dist+radii
      else case2(b) = 0;
      end
     b=b+1;
   end
end
```

```
PoreSize = 2*max(r);
PoreSize1 = max(case1);
PoreSize2 = max(case2);
y = [PoreSize PoreSize1 PoreSize2];
CriticalPore = max(y);                          % Maximum pore or cluster Ø


% Percent porosity of specimen
surfacearea = 16*3.4;
a=1;
totalporearea = 0;
for a = 1:k;
   totalporearea = totalporearea + porearea(a);
end
porosity = (totalporearea/surfacearea)*100;


FLarea = 9.074 - (- 0.00002*porosity^3 - 0.0002*porosity^2 - 0.0595*porosity + 9.0766);
% Effect of porosity (reduction in load bearing area) on fatigue life of specimen loaded at 15.3MPa

FLsc = 0.087*CriticalPore^4 - 0.8806*CriticalPore^3 + 3.2973*CriticalPore^2 -
6.3946*CriticalPore+ 9.5198;
% Effect of porosity (stress concentration) on fatigue life of specimen loaded at 15.3MPa

FL = FLsc - FLarea;                             % Predicted fatigue life of 2D specimen
```

Master script 2D Hand-Mixed

```
clc
clear
close all

for i=1:10000;                                  % No. of specimens
   i
   k = randint(1,1,[1,100]);                    % No. of pores
   [por(i), FL(i)] = cluster2DHM(k);            % Call the function cluster2DHM

end


plot(FL,por,'r.')                               % Plot the predicted results
xlabel('Fatigue Life')
ylabel('% Porosity')
hold on
xdata = [4.303843775 4.104008851 4.110151829    % Nf of HM exp specimens
         3.833274639 4.835766646 3.987934265
         4.075911761 4.821984905 3.181557774
         4.890393071];
ydata = [7.4 3.6 10.5 10 2.7 6.8 9.5 5.6 9.2 7.1];   % Percent porosity of exp specimens
plot(xdata,ydata,'+')                           % Plot the experimental results
axis([1 8 0 18])
```

AII.1.2. 3D Fatigue life prediction of HM bone cement

The Matlab function created to predict the fatigue life of a single 3D hand-mixed specimen is shown below. In order to make a prediction for a vacuum-mixed 3D specimen, the highlighted line below would be changed to incorporate the pore size distribution for vacuum-mixed bone cement. A Master script was then created which called the function as many times as required. The master script is also shown below.

Cluster3DHM Function

```
function [porosity, FL] = cluster3DHM(k)


for i=1:k;
   x(i)=16*rand(1,1);                          % Location of pore centre on x-axis
   y(i)=3.4*rand(1,1);                         % Location of pore centre on y-axis
   z(i)=3.5*rand(1,1);                         % Location of pore centre on z-axis
   r(i)=(lognrnd(-1.53737,0.562528)/2);        % Radius of pore for a hand-mixed cement

   volume(i) =(4/3)*pi*r(i)^3;                 % Volume of  pore
end



b=1;
for j=1:k;
   for i=1:k;
      radii = r(i)+r(j);
      if ((abs(x(i) - x(j))-radii) > 0.2) || ((abs(z(i) - z(j))-radii) > 0.1259) || ((abs(y(i) - y(j))-radii) >0.2)
      % The distance between the surface of two pores in the x, y and z direction
         continue
      end

      dist = sqrt((x(i)-x(j))^2+(y(i)-y(j))^2+(z(i)-z(j))^2);   % The dist between the centre of two pores
      zdist = sqrt((z(i)-z(j))^2);          % The dist between the centre of two pores in the Z direction
      distall = dist-radii;                 % The dist between the surface of two pores

      if(distall>0 && distall<0.2 && zdist < 0.1259)  % If dist between the surface of pores >0 but
         case1(b) = dist+radii;                       % <0.2  and dist in Z direction <0.1259 then
                                                      % new pore Ø = dist+radii.
      else case1(b) = 0;
      end

      if(distall<0 && (r(i)+dist) > r(j) && zdist < 0.1259)  % If two pores overlap and dist in Z
                                                             % direction <0.1259 then new pore Ø
                                                             % = dist+radii.
         case2(b) = dist+radii;
      else case2(b) = 0;
      end
```

```
    b=b+1;
  end
end

PoreSize = 2*max(r);
PoreSize1 = max(case1);
PoreSize2 = max(case2);
y = [PoreSize PoreSize1 PoreSize2];
CriticalPore = max(y);                          % Maximum pore or cluster Ø


% Percentage porosity of specimen
a=1;
totalvolume = 0;
for a = 1:k;
  totalvolume = totalvolume + volume(a);
end
porosity = (totalvolume/190.4)*100;


FLarea = 9.074- (- 0.00002*porosity^3 - 0.0002*porosity^2 - 0.0595*porosity + 9.0766);
% Effect of porosity (reduction in load bearing area) on fatigue life of specimen loaded at 15.3MPa


FLsc = 0.087*CriticalPore^4 - 0.8806*CriticalPore^3 + 3.2973*CriticalPore^2 -
6.3946*CriticalPore+ 9.5198;
% Effect of porosity (stress concentration) on fatigue life of specimen loaded at 15.3MPa

FL = FLsc - FLarea;
```

Master script 3D Hand-Mixed

```
clc
clear
close all

for i=1:10000;                                  % No. of specimens
  i
  k = randint(1,1,[1,1200]);                    % No. of pores
  [por(i), fatlim(i)] = cluster3DHM(k);         % Call the function cluster3DHM
end


plot(fatlim,por,'r.')                           % Plot the predicted results
xlabel('Fatigue Life')
ylabel('% Porosity')
hold on
xdata = [4.303843775 4.104008851 4.110151829    % Nf of HM exp specimens
         3.833274639 4.835766646 3.987934265
         4.075911761 4.821984905 3.181557774
         4.890393071];
ydata = [8.43 9 5.65 8.53 5.58 14.57 12.84 3.57 9.   % Percent porosity of exp specimens
         13 12.51];
plot(xdata,ydata,'+')                           % Plot the experimental results
axis([1 7 0 20])
```